Measurement and mathematical modeling of hyperthermia induced bioeffects in pancreatic cancer cells

By

Faraz Chamani

M.S., Kansas State University, 2019

An ABSTRACT OF DISSERTATION

submitted in partial fulfillment of the requirements for the degree

DOCTOR OF PHILOSOPHY

Department of Electrical and Computer EngineeringCarl R. Ice College of Engineering

KANSAS STATE UNIVERSITY
Manhattan, Kansas

2023

Abstract

Surgical resection is the standard of care for pancreatic cancer, although treatment outcomes remain poor, and a large fraction of the patient population are not surgical candidates. Minimally invasive interventions employing non-ionizing energy, such as image-guided thermal ablation, are under investigation for treatment of unresectable tumors and potentially for debulking and downstaging tumors. Tissue regions at the periphery of an ablation zone are exposed to sub-ablative thermal profiles (referred to as "mild hyperthermia"), which may induce a range of bioeffects including change in perfusion, immune modulation, and others. Bioeffects induced by heating are a function of intensity of heating and duration of thermal exposure. This dissertation presents a suite of tools for integrated *in vitro* experimental studies and modeling for characterizing bioeffects following thermal exposure to pancreatic cancer cells.

An instrumentation platform was developed for exposing monolayer cell cultures to temperatures in the range 42–50°C for 3–60 minutes. The platform was employed to determine the Arrhenius kinetic parameters of thermal injury to pancreatic cancer cells (i.e. loss in viability) following heating. When coupled with bioheat transfer models, these parameters facilitate investigations of thermal injury profiles in pancreatic tumors following thermal exposure with practical devices.

There has been growing interest in exploring the potential of thermal therapies for modulating tumor—immune system interactions, due in part to release of damage associated molecular patterns (DAMPs) from stressed tumor cells

and their role in recruiting and activating antigen presenting cells. The *in vitro* thermal exposure platform was further expanded to allow for experimental measurement of extracellular DAMPs released from murine pancreatic cancer cells following heating to temperatures in the range 42 – 50°C for 3-60 mins. A model predicting the dynamics of heat-induced DAMPs release was developed and may inform the design of experiments investigating the role of heat in modulating the anti-tumor immune response.

While *in vitro* experiments on monolayers are informative, 3D cell cultures (e.g., spheroid, organoids) provide an experimental platform accommodating multiple cell types in an environment that may be more representative of tumors *in vivo*. Furthermore, while the water-bath based *in vitro* platform applied for monolayers is well suited to achieving near-uniform temperature profiles, *in vivo* delivery of hyperthermia often yields a gradient of temperatures that is not achieved through water-bath based heating. Thus, an *in vitro* platform for exposing cells in 3D culture (co-culture of multiple cell populations) to 2.45 GHz microwave hyperthermia was developed. The platform includes a printed patch antenna and associated thermal management elements and was applied to study changes in gene expression profile of a 3D culture of pancreatic cancer cells and fibroblasts. This non-contact microwave heating approach may help enable additional studies for exploring the bioeffects of heat on cancer cells.

Measurement and mathematical modeling of hyperthermia induced bioeffects in pancreatic cancer cells

By

Faraz Chamani

M.S., Kansas State University, 2019

A DISSERTATION

submitted in partial fulfillment of the requirements for the degree

DOCTOR OF PHILOSOPHY

Department of Electrical and Computer EngineeringCarl R. Ice College of Engineering

KANSAS STATE UNIVERSITY
Manhattan, Kansas

2023

Approved by:
Major Professor
Dr. Punit Prakash

Copyright

Abstract

Surgical resection is the standard of care for pancreatic cancer, although treatment outcomes remain poor, and a large fraction of the patient population are not surgical candidates. Minimally invasive interventions employing non-ionizing energy, such as image-guided thermal ablation, are under investigation for treatment of unresectable tumors and potentially for debulking and downstaging tumors. Tissue regions at the periphery of an ablation zone are exposed to sub-ablative thermal profiles (referred to as "mild hyperthermia"), which may induce a range of bioeffects including change in perfusion, immune modulation, and others. Bioeffects induced by heating are a function of intensity of heating and duration of thermal exposure. This dissertation presents a suite of tools for integrated *in vitro* experimental studies and modeling for characterizing bioeffects following thermal exposure to pancreatic cancer cells.

An instrumentation platform was developed for exposing monolayer cell cultures to temperatures in the range 42–50°C for 3–60 minutes. The platform was employed to determine the Arrhenius kinetic parameters of thermal injury to pancreatic cancer cells (i.e. loss in viability) following heating. When coupled with bioheat transfer models, these parameters facilitate investigations of thermal injury profiles in pancreatic tumors following thermal exposure with practical devices.

There has been growing interest in exploring the potential of thermal therapies for modulating tumor—immune system interactions, due in part to release of damage associated molecular patterns (DAMPs) from stressed tumor cells

and their role in recruiting and activating antigen presenting cells. The *in vitro* thermal exposure platform was further expanded to allow for experimental measurement of extracellular DAMPs released from murine pancreatic cancer cells following heating to temperatures in the range 42 – 50°C for 3-60 mins. A model predicting the dynamics of heat-induced DAMPs release was developed and may inform the design of experiments investigating the role of heat in modulating the anti-tumor immune response.

While *in vitro* experiments on monolayers are informative, 3D cell cultures (e.g., spheroid, organoids) provide an experimental platform accommodating multiple cell types in an environment that may be more representative of tumors *in vivo*. Furthermore, while the water-bath based *in vitro* platform applied for monolayers is well suited to achieving near-uniform temperature profiles, *in vivo* delivery of hyperthermia often yields a gradient of temperatures that is not achieved through water-bath based heating. Thus, an *in vitro* platform for exposing cells in 3D culture (co-culture of multiple cell populations) to 2.45 GHz microwave hyperthermia was developed. The platform includes a printed patch antenna and associated thermal management elements and was applied to study changes in gene expression profile of a 3D culture of pancreatic cancer cells and fibroblasts. This non-contact microwave heating approach may help enable additional studies for exploring the bioeffects of heat on cancer cells.

Table of Contents

Contents

List of Figures

List of Tables

Acknowledgements

Foremost, I am grateful to my Advisor Dr. Punit Prakash for his continuous support, encouragement and mentorship during my PhD study and research years. He has guided me through his immense knowledge and has inspired me to enjoy research. It was a great pleasure to work with him.

Besides my advisor, I would like to express my appreciation to my dissertation committee: I would like to express my appreciation to my dissertation committee: Dr. Bala Natarajan, Dr. Matthew Basel, Dr. Nathan Albin, and Dr. Subhrajit Saha for their insightful comments and feedback that helped me to improve my dissertation.

I would like to thank my friends and fellow labmates in Biomedical Computing and Devices Laboratory: Jan Sebek, Nooshin Zeinali, and Anna Bottiglieri. I really enjoyed working and collaborating with them.

My deep and sincere gratitude to my mom and dad, for their forever support and unconditional love. They have always been there for me, through thick and thin. Thank you, mom, and dad, for everything you have done for me.

Last but not least, I would like to thank my emotional support companion dog, Shayler. Shayler always knows how to make me smile and feel better through her playful antics and cuddles. I am grateful for her presence in my life.

1. Introduction

1.1 Overview

According to the American Cancer Society[1], an estimated 64,000 new cases of pancreatic cancer will be diagnosed in United States in 2023. Depending on the stage of the cancer (i.e., localized, regional, distant and combined), the 5-year survival rate of patients with pancreatic cancer varies between 3% and 44%, making it the seventh leading cause of cancer related deaths for both men and women worldwide[2], [3]. Pancreatic cancer tends to not show symptoms in the early stages, and therefore it is mostly diagnosed at a late stage where the cancer has already metastasized to other organs such as liver or lungs.

There are several types of pancreatic cancer including adenosquamous carcinoma, squamous cell carcinoma and the most common type, adenocarcinoma of pancreas which occurs in the lining of the pancreatic duct[4]. Pancreatic cancer can be described in terms of the location within the pancreas where the tumor develops – the pancreas head, body or tail. Surgery remains the standard of care for patients with pancreatic cancer and can be potentially when it is possible to remove the entire tumor and a margin of surrounding normal tissue. Palliative surgery is used in patients to relieve symptoms, improve quality of life, or prevent certain complications if the tumor cannot be resected completely. Curative surgery is often possible in patients tumors arising in the head of pancreas since these tumors are more likely to be identified at an earlier stage [5]. Although surgical removal of pancreatic tumors through open or distal pancreatectomy may offer short-term benefits, poor survival and post-surgery complications remain a major concern[6], [7]. Compared to other types of cancers, the

5-year survival rate for patients with pancreatic cancer after surgery is still very low, at approximately 12%; however, a recent study showed that patients whose tumor is diagnosed at the earliest stage, may have a five-year survival of over 80%[8]. Unfortunately, far more people are diagnosed at late stages when the disease has already metastasized. Moreover, only about 15% of the patients with resectable pancreatic tumors may be eligible to undergo surgical treatment[9], [10].

After surgery, tumor recurrence is common, contributing to the low median survival of approximately 20 months. Neoadjuvant systemic therapy followed by surgery is the first-line treatment approach for patients with resectable disease[11]. Systemic therapy followed by radiation is the standard therapeutic approach for patients with locally advanced and unresectable tumors due to the dense and aggressive tumor microenvironment. On the other hand, for patients with advanced metastatic pancreatic cancer, multiagent chemotherapy regimens are often administered, resulting in patient survival of up to 6 months[11]. Several studies have highlighted the benefits of combined radio-chemotherapy in patients with locally advanced pancreatic cancer[12]–[14] compared to radiotherapy or chemotherapy alone, however the overall survival is still low (6–18 months) in treated patients. Pancreatic cancer is quite resistant to chemo/radiotherapies which is mainly due to the abundance and dense accumulation of stroma cells which hampers delivery of oxygen as well as delivery of chemotherapeutics[15], [16]. Such hypoxic microenvironment in pancreatic tumors significantly reduces the sensitivity to chemo/radiation therapies.

1.2 Thermal therapy

Thermal therapy refers to the modulation of tissue temperature for therapeutic benefits. Thermal therapies have been used as stand-alone and adjuvant treatments

for a range of tumors. In this context, the term ablation is used to refer to treatments where heat is used as a standalone modality, with tissue temperatures reaching or exceeding ~50 °C. The term hyperthermia is used to refer to treatments where heat is used as an adjuvant to other modalities, with tissue temperatures typically raised to the range ~40–44 °C. Bioeffects of heating including changes in cell viability, blood perfusion, vascular permeability, stress protein expression, and other changes are a function of the intensity and duration of heating. Heating can be induced to the target regions through a wide range of energy modalities such as non-invasive high-intensity ultrasound (HIFU)[17], minimally invasive percutaneous or endoscopically delivered microwave (MW) heating[18], lasers[19], and radiofrequency (RF) currents[20]. Figure 1-1 shows the radial temperature profile from a thermal ablation applicator, indicating that both ablative (T>50°C) and mild hyperthermic temperature range (T<50°C) are obtained following thermal ablation treatment.

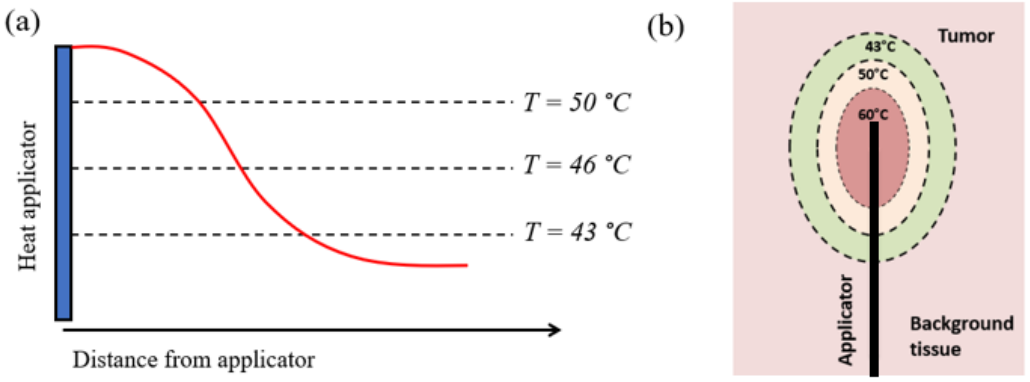

Figure 1- 1 (a) An example of a thermal device radial heating within target tissue (b) schematic view of regions of the thermal ablation zone illustrating hyperthermic regions at the periphery of the ablation zone

Figure 1-1 (b) highlights the importance of thermal dose dependency (i.e., time and temperature history) during heating resulting in different clinical outcomes such as

ablation volume due to exposure to extreme temperatures or bioeffects affected by mild hyperthermia in regions where sub-lethal tissue heating (42–50°C) occurred.

Over the last decade, minimally invasive thermal therapy either as a stand-alone ablative or as an adjuvant to chemoradiotherapy has received substantial attention for the treatment of many local malignancies[21]. Preoperative hyperthermia combined with radiation and/or chemotherapy with surgery may benefit patients with locally advanced cancer by decreasing local recurrence and improving the survival rate within patients[22]. Several clinical studies have highlighted the benefits of thermal ablation treatment in patients with pancreatic cancer by heating tumors to cytotoxic temperatures of 50°C or higher for 4 minutes or longer[23]–[26]. Thermal ablation is increasingly being used as a minimally invasive therapeutic option for surgically unresectable tumors and to provide non-toxic localized treatment through multiple mechanisms such as coagulative necrosis, protein denaturation, or mitochondrial dysfunction with improved overall survival in patients with pancreatic cancer[27]–[30]. Aside from ablative cytotoxic effects in thermal ablation modalities, it has been shown that mild hyperthermia exposure (39–42°C) for >30 min, induces many biological effects such as tumor reoxygenation[31], [32], anti-tumor immunity[33]–[35], improved drug delivery[36], [37], sensitization of cancer cells to DNA damaging agents[38], [39], and activating promoters for gene therapy[40], [41].

1.3 Tumor-immune system interactions

The release of damage associated molecular patterns (DAMPs) are recognized as contributing factor to the tumor-immune system interactions [42], [43]. Tumor specific DAMPs released during hyperthermia can activate antigen presenting cells (APCs) and thereby contribute to the adaptive immune

response. The presence of the hyperthermic zone on the periphery of ablation zones, and associated release of DAMPs in these regions, may serve to modulate the tumor immune system interaction (see Figures 1-1 and 1-2). The role of the kinetics of DAMPs expression following external intervention is recognized as an important factor in how the intervention affects the anti-tumor immune response[44].

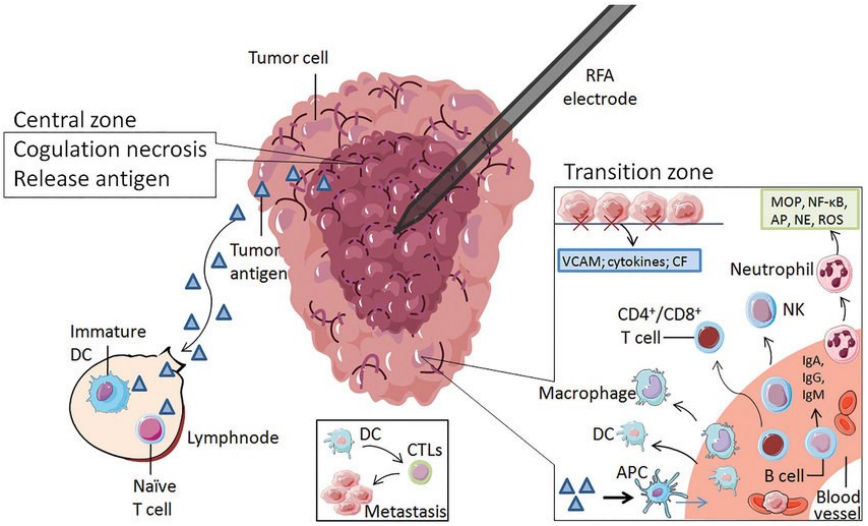

Figure 1- 2 sub sections of ablation zone (figure reproduced from [233])

1.4 Overview of hyperthermia-induced cancer immunotherapy

There is growing interest in the immunosuppressive state of the tumor microenvironment (TME), supported by the hypoxia within tumors[45], [46] that is affected by multiple dynamic factors such as tumor cell metabolism and abnormal vascular perfusion. Mild hyperthermia treatments at sub-lethal temperatures (40–45°C) do not cause direct cytotoxicity, however, tumor microenvironment (TME) is subjected to change at these thermal doses. It was reported that when tumors were

subjected to mild hyperthermic temperatures, increase in tumor oxygenation was observed which correlates with the radiation sensitivity of the tumor as well as enhanced drug delivery[47]–[49]. Moreover, it was proposed that mild hyperthermia may trigger anti-tumor immunity and T cell infiltration within tumors by activating tumor specific damage-associated molecular pattern (DAMPs) such as High mobility group box protein 1 (HMGB1) and heat shock proteins (HSPs) family[42], [50]–[52] that promote recruitment and activation of antigen presenting cells. Multiple cancer-related studies have reported the application of mild hyperthermia as an immunotherapeutic agent. The understanding of the use of mild hyperthermia as an adjuvant therapy, and its effects on the immune cells activation and infiltration, are limited. Hibma *et al.*[53] investigated the effects of mild hyperthermia at 43°C on tumor regression and on the immune cells and molecules in inoculated murine breast tumors. Results from their study showed that local hyperthermia can reduce tumor progression and may significantly increase the median survival of tumor-bearing mice. Moreover, immunohistochemical analysis revealed a significant reduction in cells proliferation in treated tumor, which was accompanied by an abundance of HSP70.

1.5 Bioeffects of heating as a function of time and temperature profile

Computational models of thermal therapies solve the differential equations describing external power deposition and bioheat transfer within tissue and aim to predict transient temperature profiles in tissue following a thermal intervention. The bioeffects induced by heating are a function of the time–temperature profile during heating and may vary across cell types. Mathematical models relating changes in cell viability, stress protein expression, and other biomarkers to the time–temperature history during heating have been reported, and when coupled with models of bioheat

transfer, provide a means for understanding the spatio-temporal profiles of bioeffects induced by thermal therapies [54]. Cell/tissue-specific parameters for these models can be determined from experiments on cells *in vitro*. One of the most widely used models is the Arrhenius thermal injury model[55], which describes cell death following heating as a first-order exponential relationship between temperature and duration of heating, and has been applied to assess thermal damage in various cell types, including liver cancer cells[56], prostate tumor cells[57], and breast cancer cells[58]. The thermal isoeffective dose model (CEM43)[59] which relates an arbitrary transient temperature profile to equivalent minutes of heating at a reference temperature, typically taken to be 43°C, is derived from the Arrhenius model. While thermal injury parameters for a range of cell types have been reported, there are few published data reporting on the viability of pancreatic cancer cells following heating. Hence, identification of thermal injury parameters is important to inform the design of thermal therapy devices and systems, select treatment doses, and to inform interpretation of experimental and clinical studies involving heat as a therapeutic modality[60].

1.6 Research approach and contributions of this dissertation

This dissertation reports on the development and application of integrated *in vitro* experimental and computer modeling tools to enable studies investigating the bioeffects of heating.

Chapter 2 provides a literature review for *in vitro* heating apparatus to explore the bioeffects of heating in experimental cell culture models. *In vitro* thermal dosimetry studies have provided a strong basis for characterizing biological responses of cells to heat. We conducted a review of hyperthermia instrumentation platforms and surveyed a variety of different approaches for heating cells *in vitro*, including CO2

incubators, circulating water baths, microheaters, electromagnetic sources, acoustic sources, and microfluidic devices. We discuss critical heating parameters including spatio-temporal thermal profiles, complexity, peak temperature, and technical limitations of each heating modality. The application of these *in vitro* platforms for identifying kinetics of thermal injury processes is discussed.

In **chapter 3**, we report on experiments in monolayer cell culture *in vitro* to assess the kinetics of thermal injury (i.e. loss of cell viability) in two murine pancreatic cancer cell lines, and one normal fibroblast cell line following heating to temperatures in the range 42.5–60°C for up to 60 min. While thermal injury parameters for a range of cell types have been reported, there are few published data reporting on the viability of pancreatic cancer cells following heating. Identification of thermal injury parameters is important to inform the design of thermal therapy devices and systems, selection of treatment doses, and to inform interpretation of experimental and clinical studies involving heat as a therapeutic modality. Experimental data were used to identify parameters of thermal injury for three established models of thermally-induced cell death, and the models were comparatively assessed against experimental measurements where cells were subjected to time–temperature profiles similar to those anticipated at the periphery of an ablation zone.

Chapter 4 reports on measurement and modeling of heat-induced DAMPs release from murine pancreatic cancer cells with application to informing strategies for anti-tumor immune stimulation. Several *in vitro* studies have shown the role of heat stress in inducing DAMPs release from cancer cells, thereby promoting recruitment of activation of antigen presenting cells to tumor sites. Although these studies demonstrated increased levels of extracellular DAMPs in cancer cells following heat exposure, there are few studies reporting on quantitative characterization of the

heat-induced release of DAMPs from pancreatic cancer cells. We assessed the extent of the heat-induced release of HMGB1, HSP70 and HSP90, release from two murine pancreatic cancer cell lines. The experimental data were modeled as dependent on the thermal isoeffective dose and coupled with computational models of bioheat transfer. This may enable development of thermal dosimetry guidelines and predictive models for DAMPs release and cell injury as a function of thermal stress (CEM43) to introduce and design thermal therapies in the context of potentiating immunotherapy approaches.

In **chapter 5**, we present the design and characterization of a microwave (MW) device for delivering hyperthermia to 3D cell culture models. The *in vitro* experiments for studying changes in cell viability and DAMPs release following hyperthermia reported in Chapters 3 and 4 were conducted on monolayer cell cultures with a water-bath based heating apparatus. While water baths present a practical method for uniform delivery of thermal doses, inhomogeneous thermal profiles are expected during *in vivo* and in the clinical scenario. Further, 3D cell culture models, including those that support co-culture of multiple cell populations may provide an *in vitro* experimental platform more representative of *in vivo* tumor architectures than monolayers. A microstrip antenna operating at 2.45 GHz was developed to expose cells in culture to temperatures up to 60°C, thereby providing a platform for studying the bioeffects of hyperthermia and thermal ablation. Computational models of electromagnetic power absorption and heat transfer were used to optimize the antenna geometry and feedpoint. Optimized antenna designs were fabricated, and their electromagnetic and thermal performance was characterized. The developed platform was employed in pilot studies to assess changes in gene profiles of pancreatic cancer

cells and normal fibroblasts in co-culture after exposure to temperatures in the range 42–46 °C.

List of published works and presentations resulting from this dissertation

Publications in peer-reviewed journals

F. Chamani, I. Barnett, M. Pyle, T. Shrestha, and P. Prakash, "A Review of *In Vitro* Instrumentation Platforms for Evaluating Thermal Therapies in Experimental Cell Culture Models," *Critical Reviews™ in Biomedical Engineering*, vol. 50, 2022, doi: 10.1615/CritRevBiomedEng.2022043455. [This work is presented in Chapter 2].

F. Chamani, M. Pyle, T. Shrestha, J. Sebek, S. Bossmann, M. Basel, R. Sheth, and P. Prakash., "In Vitro Measurement and Mathematical Modeling of Thermally Induced Injury in Pancreatic Cancer Cells," *Cancers*, vol. 15, no. 3, Art. no. 3, Jan. 2023, doi: 10.3390/cancers15030655. [This work is presented in Chapter 3].

The work presented in Chapter 4 and Chapter 5 is in preparation for submission to peer-reviewed journals.

Conference abstracts

F. Chamani, M. Pyle, T. Shrestha, J. Sebek, I. Barnett, S. Bossman, R. Sheth, P. Prakash, "In vitro measurements and mathematical modeling of hyperthermia induced injury in pancreatic cancer cell lines," Accepted abstract for poster presentation at SIO 2022 Annual Scientific Meeting, 24–28 March 2022. San Francisco, CA, USA.

F. Chamani, M. Pyle, T. Shrestha, A. Bottiglieri, S. Bossman, S. Saha, R. Sheth, P. Prakash, " Modeling of temperature dependent release of HSP70, HSP90, and HMGB1 from

pancreatic cancer cells," Accepted abstract for oral presentation at Society for Thermal Medicine (STM) 2023 Annual Scientific Meeting, 23–27 April 2023. San Diego, CA, USA.

2. Background: a literature review[1]

2.1 Hyperthermia

Hyperthermia refers to heating the target cells or biological tissues to temperatures exceeding physiologic temperature. Heating induces a number of local and systemic effects, from the macroscopic tissue level down to the sub-cellular molecular level, which may be harnessed for cancer therapy. The specific changes induced by heating are a function of the spatio-temporal temperature profiles induced in tissue during treatment. In addition to cytotoxicity[55], mild hyperthermia, 39–42°C delivered for > 30 min, induces tumor reoxygenation[31], [32], improves drug delivery[61], [62], activates promoters for gene therapy[63], [64], augments anti-tumor immunity[65]–[67], and sensitizes cancer cells to DNA damaging agents by inhibiting DNA repair, supporting the hypothesis that repair pathways can be affected by heat[38], [39]. Multiple phase II/III clinical trials have demonstrated the benefit of combining hyperthermia with chemo/radiation therapies in patients with different types of cancer, showing a significant enhancement in treatment effectivity without significant toxicity effects[38], [68]–[70]. Compared to mild hyperthermia as an adjuvant therapeutic option, high temperature thermal ablation (T > 50°C) is increasingly being used for *in situ* destruction of unresectable localized tumors[71]. Elevated temperatures can affect cells in different ways, but the primary means of cell death during thermal ablation is acute coagulative necrosis. While irreversible cell damage, microvascular thrombosis and hypoxia can occur at cytotoxic temperatures

[1] This chapter has been published as: F. Chamani, I. Barnett, M. Pyle, T. Shrestha and P. Prakash, "A Review of In Vitro Instrumentation Platforms for Evaluating Thermal Therapies in Experimental Cell Culture Models," Crit. Rev. Biomed. Eng., vol. 50, Issue. 2, 2022. (DOI10.1615/CritRevBiomedEng.2022043455) by Begell House, Inc. www.begellhouse.com

(T > 50°C), coagulative necrosis (i.e. thermal ablation boundary) would be visible at temperatures near 60°C[72], [73] where rapid protein denaturation occurs[74].

With the development and ongoing clinical translation of several thermal therapy delivery modalities (e.g., magnetic resonance guided high intensity focused ultrasound, nanoparticle mediated laser therapy, probe-based radiofrequency (RF) and microwave (MW) hyperthermia/ablation), combining heat with other cancer therapeutic strategies, including immunotherapy and gene therapy, has remained an area of research investigation. For instance, thermally-sensitive microbubbles and nanoparticles are being explored for highly selective delivery of drugs and other therapeutic agents to targeted tissue[62], [75]. The augmented immune response elicited by thermal ablation is being investigated to boost the efficacy of immunotherapy strategies, thereby enabling local control of tumors and inducing sustained anti-tumor immunity[76], [77]. However, there are few standardized quantitative assessment tools linking heating profiles to local and systemic effects of heat in combination with other therapeutic modalities. The availability of such tools would pave the way for the design of customized patient-specific heating strategies that optimize specific physiological responses to heat for synergy with other treatments.

The local effects induced by a thermal therapy procedure are strongly dependent on the spatio-temporal temperature profiles achieved during treatment[78], [79]. Mathematical models provide a powerful tool for quantitatively assessing the physiological responses to heat treatment across multiple spatial and temporal scales. These models rely on underlying experimental data characterizing bioeffects (e.g., cell viability, stress protein expression) as a function of intensity and duration of heating. *In vitro* platforms of cells in culture (2D and 3D), provide a

powerful experimental approach for investigating bioeffects of heating across a variety of cell lines. These experimental platforms rely on isothermal heating of cells for known duration of times to facilitate development of quantitative models of the bioeffects of heating.

2.2 Rational in selecting *in vitro* heating platforms

In vitro heating can be delivered using different strategies; the vast majority of studies employed conductive and convective processes using circulating water baths and CO_2 incubators[80]–[84]. Recently, other modalities have been developed to deliver *in vitro* heating, including: Joule heating[85], [86], microwaves[87]–[90], lasers[91]–[94], alternating magnetic fields[95], [96] and ultrasound mediated heating[97]–[99]. Achieved peak temperature, accuracy of heating, and technical limitations may vary significantly depending on the selected heating approach. Traditional heating modalities such as water baths and incubators facilitate uniform temperature regulation with a high degree of accuracy and simplicity; however heating rate is slow, limiting the opportunity to study the mechanisms of heat-induced cellular response. Accurate control of cell culture temperature provides several opportunities to study the temperature-dependent cellular responses. For example, it enables one to characterize transient response of cells during heating and cooling phases, or to determine a thermal dose threshold necessary for the heat-induced cell death[100]–[102]. Characteristics of *in vitro* hyperthermia exposure apparatus include:

- High temperature ramp rate (the time to reach the target temperature) and/or short heat-up phase
- Precise control of temperature with high degree of accuracy
- Homogeneous heating pattern throughout the sample area

- Simple design and easy to use

The objective of the present review is to provide an overview of currently available *in vitro* heating modalities and recent advances in the field. All reported techniques along with the corresponding specifications (heat-up phase, heating accuracy, level of integration, peak temperature and heating limitations), are summarized in Table 2-1 where "T_{Output}" denotes obtained sample temperature, "$T_{Initial}$" is the initial temperature of the sample prior to heating, "Input" is the input signal (e.g. power, temperature, voltage), "Accuracy" is the accuracy of temperature control during heating, "Uniformity" is temperature distribution homogeneity during heating, "$T_{Sensors}$" describes number of temperature sensors that was used in each heating system, and finally, level of integration was subjectively assessed based on complexity of each hyperthermia system in order to systematically assemble higher-level systems from lower-level ones considering the number of implemented elements.

2.3 Overview of *in vitro* heating methods

2.3.1 CO_2 incubators

Temperature-controlled CO_2 incubators, which are routinely used for providing a controlled environment for culturing cells, have been adapted as a primary heating source for *in vitro* hyperthermia studies[81], [103], [104]. Convective heat exchange between cells in culture and the air in the incubator provides a means for heating; however, the air temperature within the incubator may not be stable when the incubator door is opened to move the plates in or out of the incubator, taking extended periods of time to stabilize. Consequently, this may lead to poor control of temperature during transient hyperthermia exposures. The incubator's specifications with respect to uniformity and temperature control fluctuation are normally within 0.25˚C and

0.1˚C, respectively. In order to record the sample temperature directly, thermocouples can be inserted inside the cell culture dish during hyperthermia treatments. Nytko *et al.*[103] described such a system using a 5% CO_2 incubator, and reported that it took approximately 40 min for cells to achieve the hyperthermic temperature (42°C). Figure 2-1 illustrates the temperature profiles inside the culture dish that was measured in different runs.

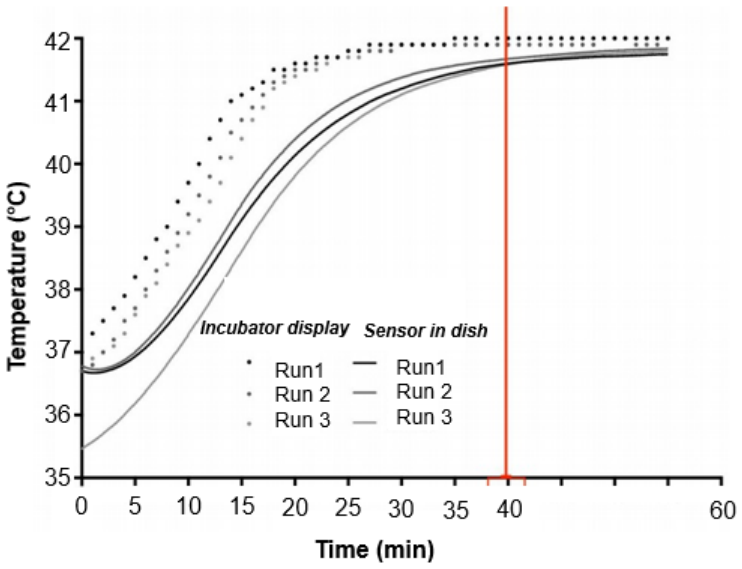

Figure 2- 1 temperature profile of the incubator during heating from 37°C to 42˚C steady-state with three different runs. Dot makers show the temperature displayed by the incubator while the solid lines describe actual measured temperature of the sample based on three different runs inside cell culture dish (figure adapted from [103])

Shellman *et al.*[81] also used a conventional CO_2 incubator to perform *in vitro* heating. They developed a heating system using multiple thermocouples (T-type) and measured the temperatures in multiple wells (Figure 2-2). Temperature of sample that was controlled in their study was reported with 0.2°C of accuracy.

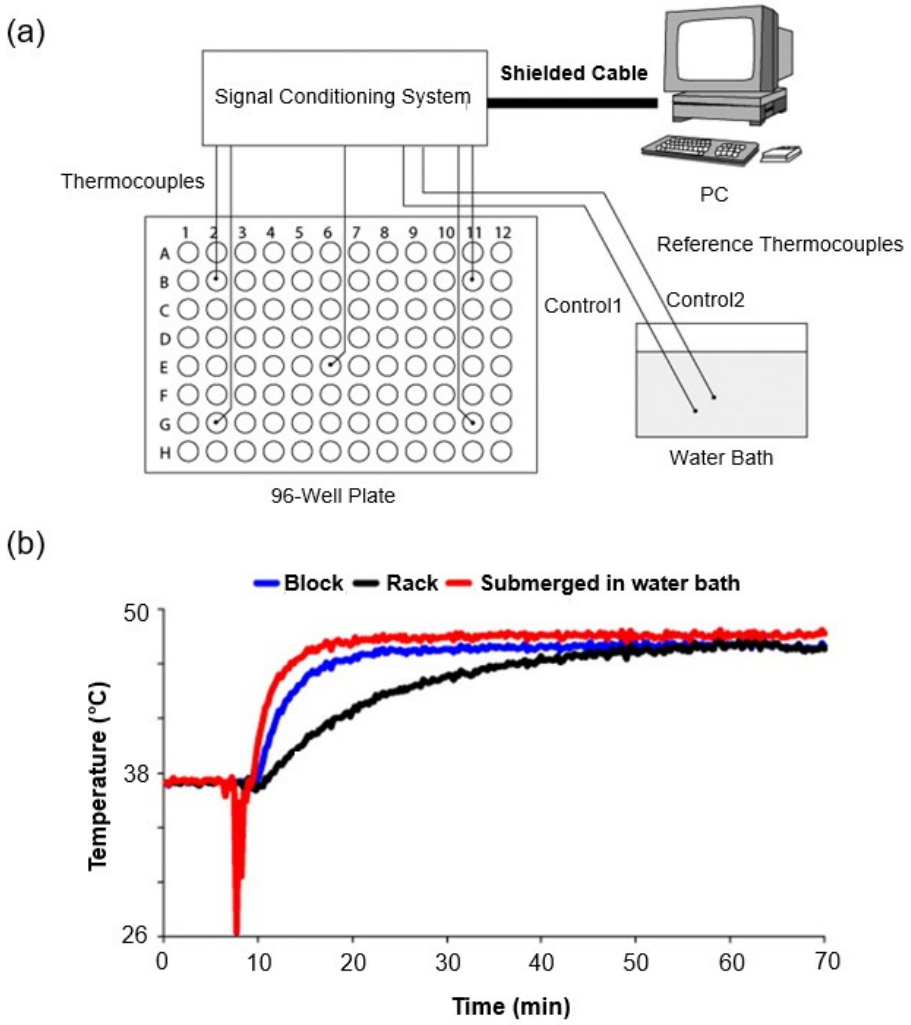

Figure 2- 2 (a) Equipment setup for temperature measurement of media in a 96-well plate consisting of five sealed thermocouples in different wells of the culture plate to monitor the actual sample temperature during hyperthermia exposure, (b) average measured temperature based on five temperature probes sealed in different wells of a culture plate at each time point for different heating techniques (i.e. submerged in water bath, placed in incubator rack with no copper blocks and with copper blocks) (figure adapted from [81])

As shown in Figure 2-2, using custom made copper blocks in contact with the 96-well plate inside the incubator provided a significantly fast ramping rate with a heat-up phase of ~20 min to achieve desired hyperthermic temperature (in this case 48°C) while using no copper blocks during incubation led to a significantly longer heat-

up phase (40 min). A technical obstacle in their study was that heating the cells with copper blocks in the incubator achieved 0.8°C less than of the desired hyperthermic temperature which can be resolved by adjusting the temperature setting in the incubator.

2.3.2 Water bath

Many studies have used temperature-controlled water baths to heat cells *in vitro*[80], [105]–[109]. Briefly, this method involves immersing the cells within the culture container into a water bath set at the desired hyperthermic temperature. An electronic interface in most water baths allows users to set a desired temperature.

However, to prevent contamination of the cells in culture, the plates need to be sealed. The effects of lower CO_2 levels in the media accompanying long incubation time can affect cell viability in some cell types as previously described by Shellman *et al.*[81]. Another challenge with the water bath heating technique is that the cell culture plates heated in a water bath tend to have condensation on their lid that may cause inconsistency in the volume of the media of each well after heating. This can decrease the reproducibility of certain biological assays. It is recommended for the cell culture plates to be placed on a stand in the preheated water bath to avoid direct contact with the metal bottom of the water bath upon the immersion. This is to avoid adhesion of deposited chemical substances to the culture plates at the bottom of the water bath.

Massey *et al.*[84] presented a method for measuring target engagement in adherent cells. In their study, a preheated water bath was used as the heat source for cells at the target temperature of 55°C. Meanwhile, the temperature changes inside the cell culture plates were determined by using two different thermocouples. The ramping rate to desired hyperthermic temperature was determined in both thin-

walled PCR tube and 96-well plates, either floating or submerged in the preheated water bath (Figure 2-3). The PBS in the PCR tube heated up rapidly reaching 54°C within 45 s. The heat-up phase to achieve a temperature of 54°C was 3 and 5.5 fold slower in a cell culture plate that was submerged and floating in a preheated water bath, respectively.

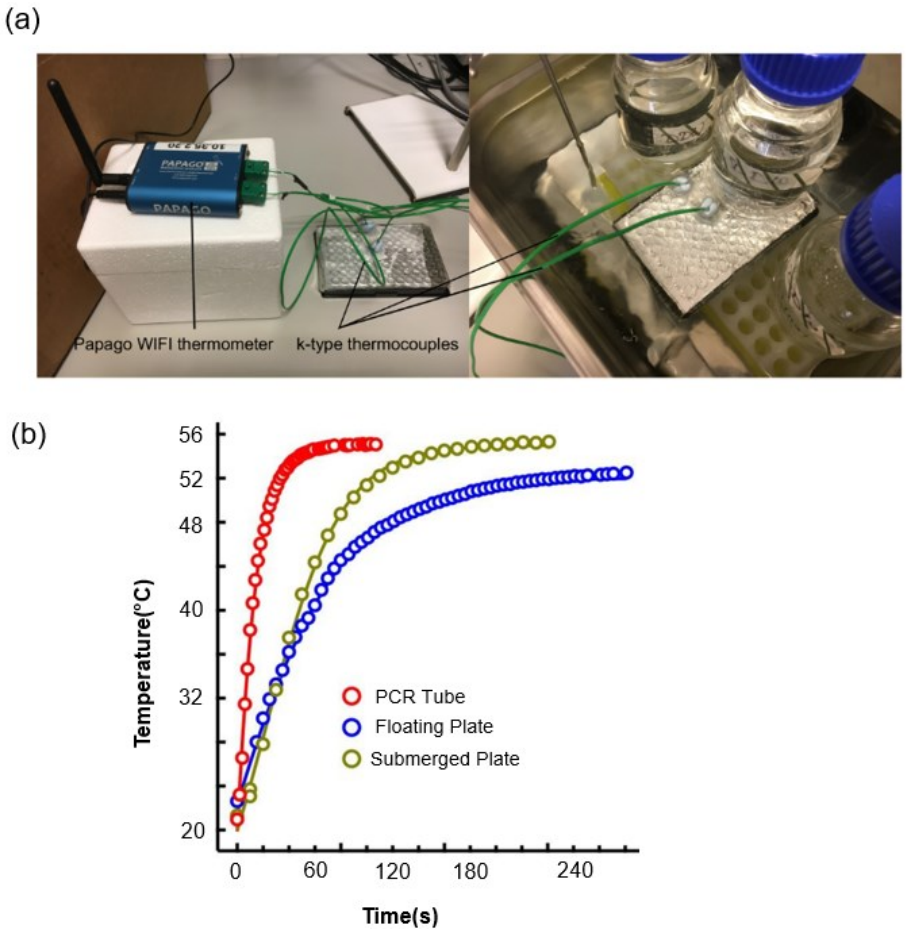

Figure 2- 3 (a) Thermometer set up with two k-type thermocouples placed in a cell carrier-96 plate that was sealed with an aluminum plate sealer and was heated by immersion in the water bath, (b) measured sample temperature following floating and submerged cell carrier-96 plate in a preheated water bath at 55°C, shown by blue color and green color, respectively (figure adapted from [84])

Similarly, Rylander *et al.*[110] used a constant temperature circulating water bath as a heat source to identify elevated levels of heat shock proteins following hyperthermia exposures. Two K-type thermocouples were used on 25 cm^2 phenolic flask containing cell culture medium and recorded the temperature during heat exposure in the bottom and inside the culture medium. The flask was then filled with 70 ml of heating medium (0.1°C equilibrium) and immersed in the water bath for different durations (1–30 min). Samples were subjected to temperatures of 44, 46, 48, and 50°C with six samples for each time increments. A relatively fast temperature ramping rate (~4 s) was obtained, achieving ~63% of the desired hyperthermic temperature. Temperature of cells was estimated as the average of bottom wall and culture medium values and reached within 0.5°C and 0.2°C of desired hyperthermic temperature in 12 s and 60 s, respectively.

2.3.3 Electromagnetic radiation

Conventional incubators, such as dry air ovens, heating blocks and water baths, rely on conductive and convective processes for heat transfer. The techniques described in this section involve active heating of cells in culture with the use of electromagnetic radiation.

2.3.3.1 Microwave hyperthermia systems

Microwaves non-ionizing electromagnetic radiation at 30 MHz–300 GHz frequency range can efficiently generate heat by rapid changes in the electric field within lossy media, such as cell culture samples. Recently, different types of MW applicators have been reported for *in vitro* hyperthermia assessment of cells in culture[111]–[113].

Kiourti *et al.*[111] developed a MW system to heat the cell culture samples in a temperature controlled manner. Figure 2-4 shows the MW radiation system in their study that was equipped with a 2.4 GHz antenna, a 50 Ω coaxial cable to feed the antenna from the MW generator, a culture dish with copper tape to contain 2.75 mL of medium, an amplifier, and a K-type thermocouple inside the dish to record the temperature. Also, use of a 2.4 GHz sleeve balun was reported that was placed between the power amplifier output and the MW antenna input to minimize cable radiation and achieve a balanced operation.

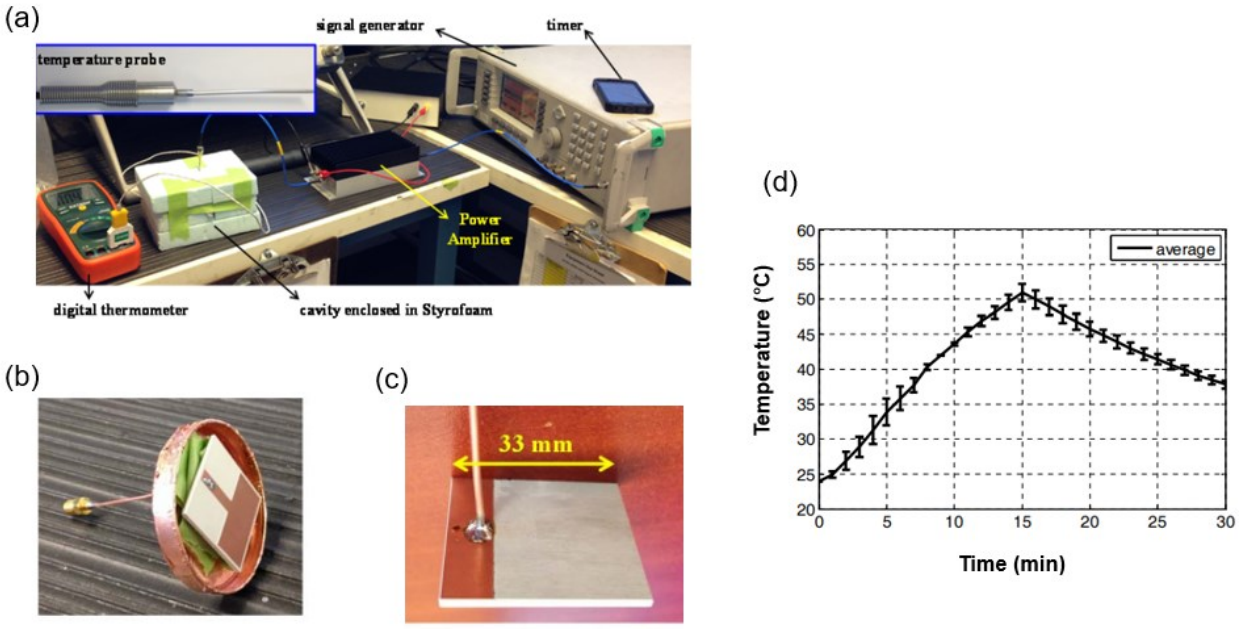

Figure 2- 4 MW radiation system (a) Experimental set-up including power amplifier and a thermocouple probe connected to a thermometer for monitoring the temperature during heat exposure, (b) proposed MW cavity for in vitro heating of 2.75 mL culture medium, (c) monopole antenna to be enclosed within the MW cavity, (d) average measured temperature of three samples with standard deviation (SD) error bars (figure adapted from [111])

Because of the surrounding metal shield, when the MW antenna is excited at 2.4 GHz, resonance will be achieved which will enhance heating, hence causing

temperature rise within the culture dish. In their study, the generator remained 'ON' for 15 min, and the heating response was recorded as a function of time. The MW source was then turned 'OFF' to allow the medium to cool as illustrated in Figure 2-4 (d). On average, temperature rise inside the culture dish rose from initial room temperature (24℃) to hyperthermic temperatures of 40℃ and 50℃ within 8 min and 15 min of MW radiation, respectively.

Temperature inside the cell culture samples can be controlled by adjusting the intensity (radiating power) and duration (exposure time) of MW radiation. Asano *et al.*[114] reported such system which can provide MW irradiation at varied output powers to maintain the temperature at 37°C. In their study, MW irradiation was applied at different output powers up to 20 W to maintain the temperature under the cell culture dish at a specific value using an IR camera. The temperature data from the IR camera was transmitted to a controller which estimates the reflected power to adjust the output power to the system radiator. According to their study, the drifting temperature over the desired temperature range was within 3°C inside the cell culture dishes (Figure 2-5). The temperature ramp rate inside the cell culture media was within 1 min to achieve 37°C from initial temperature of ~20°C, indicating a faster ramping rate during MW heating when compared to regular incubation.

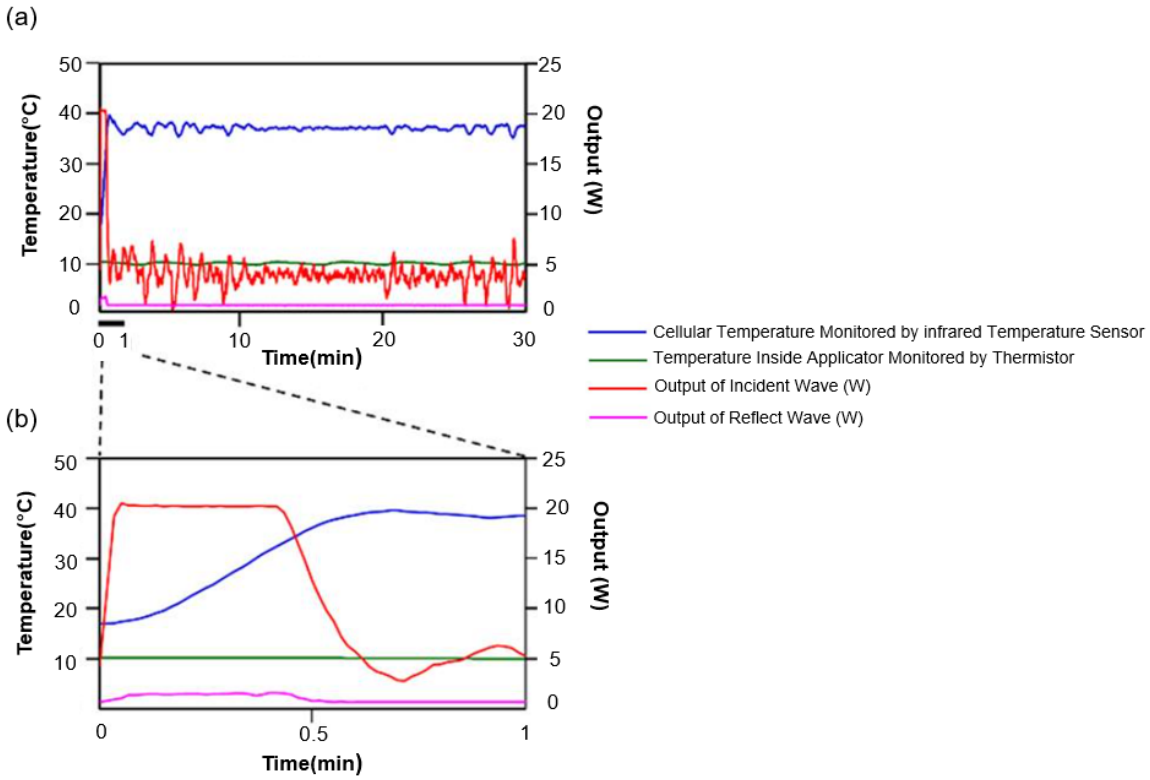

Figure 2- 5 Changes in temperature and output of microwave irradiation (a) changes in temperature and output power within 30 min of MW irradiation and (b) over 0–1 min of MW irradiation Sample temperature (shown by blue color) was monitored by an IR camera and reached the target temperature of 40°C from initial room temperature within ~30 s of MW irradiation, indicating a fast ramp rate (figure adapted from [114])

Manop *et al*[113], investigated the efficacy of MW heating at cellular levels taking into account the microwave power and heating time. In their study, *in vitro* microwave heating experiment was performed on HepG2 cells. A microwave generator was used to generate energy at the frequency of 2.45 GHz, and was connected to a coaxial triple slot antenna for transferring microwave energy to the target cells cultured in a 6-well plate. Fiber optic sensors were positioned within each well to measure the temperature uniformity across four different positions (Figure 2-6). An infrared (IR) camera was also utilized to measure the temperature at the surface of

culture samples in each well. They reported the effects of different powers and heating duration on cell viability and surface temperature uniformity.

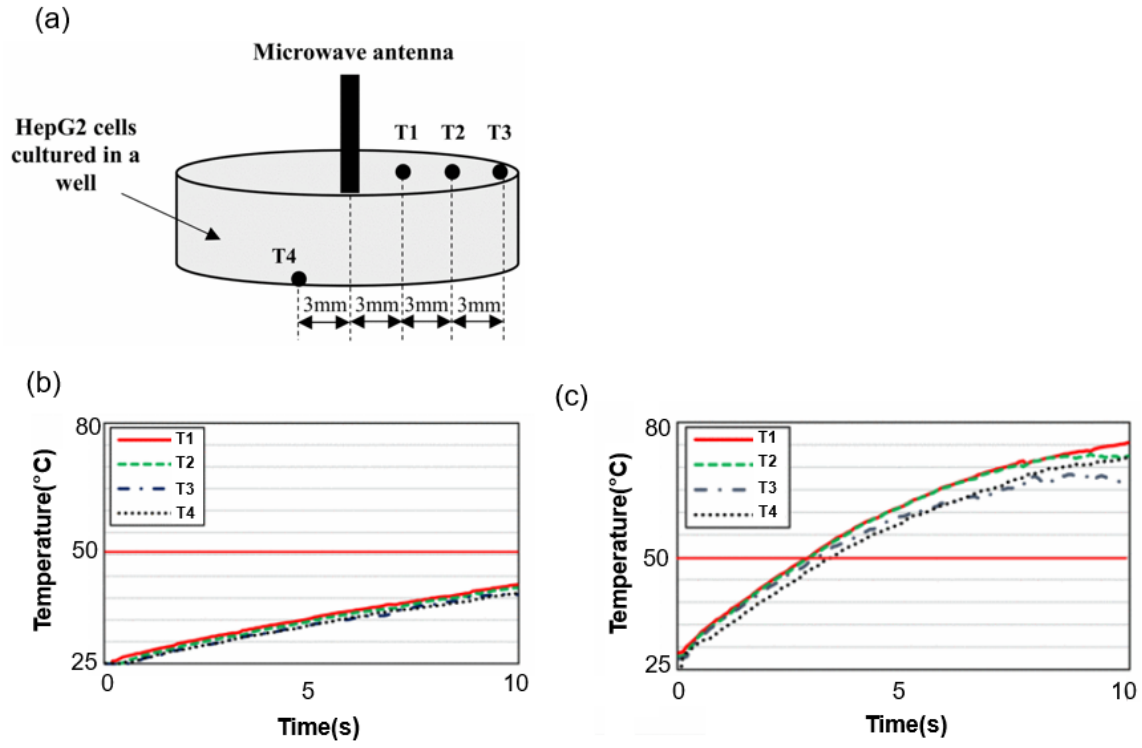

Figure 2- 6 (a) Placement of microwave antenna and fiber optic sensors during heating experiment where all temperature sensors were placed within 3 mm spacing from each other with three sensors at the surface and one sensor at the bottom of the culture well, (b) temperature distribution at four different points during MW heating based on 5 W applied power, (c) temperature distribution at four different points during MW heating based on 20 W applied power (figure adapted from [113])

Figure 2-6 demonstrates the temperature distribution at various points (T1–T4) inside each well during MW exposure. The heat-up phase from room temperature (~25°C) to target temperature was significantly reduced by increasing the power level; however, increasing the power level led to higher temperature heterogeneity (~5°C)

throughout the sample. This indicates the trade-off between the ramping rate and temperature distribution throughout the sample.

Chen *et al.*[115] also performed MW irradiation to treat cancer cells. A microwave needle fixed with a temperature measuring probe was inserted into each well of 48-well plate containing 500 µL of cell culture media. For the purpose of their study, the microwave heating device was set to 15 W power. The heating duration was considered to be at 15, 20, 25, 30, 40, 50 and 60 s while the microwave heating treatment was repeated 3 times for each duration. Finally, the sample temperature was recorded as depicted in Figure 2-7, showing a linear relationship between sample temperature and heating duration in MW heating when using a fixed power.

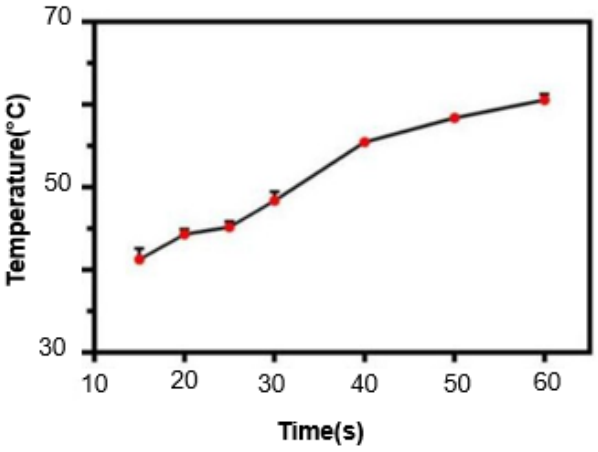

Figure 2- 7 Time-temperature curve based on 15 W microwave heating with three trials (n=3), indicating a linear relationship between heating time and obtained temperature. Data are expressed as the mean ± SD among multiple treatment groups. The time required to reach the target temperatures of 41, 48 and 60°C were 15, 30 and 60 s, respectively (figure adapted from [115])

2.3.4 Near-infrared (NIR) laser heating

In this section, we discuss laser induced hyperthermia techniques *in vitro*, where laser illumination can produce heat in nanoscale sample volumes. Near-

infrared (NIR) Laser has high penetrability and is commonly used in the treatment of lesions[116], [117]. NIR Laser is a form of electromagnetic radiation at wavelengths of 800–980 nm which converts optical energy into thermal energy through photo-thermal absorption. This phenomenon leads to a rapid and direct heating inside the samples.

Inagaki *et al.*[118] used diode laser (810 nm) irradiation to target cells in a photocoagulation treatment. In their study, epithelial cells were seeded on 32 cm^2 culture dishes and were treated by laser irradiation. Figure 2-8 demonstrates their system design which includes the laser beam passing through the dichroic mirror for irradiating the cells in a culture dish.

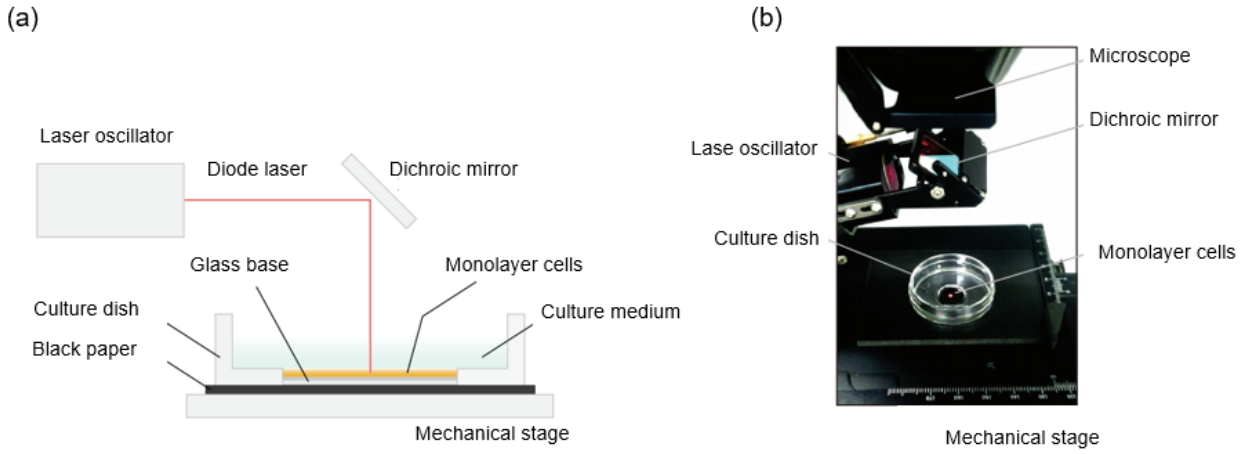

Figure 2- 8 Experimental setup for laser irradiation via a dichroic mirror and a perpendicular laser where cells were cultured on glass-bottomed dishes with (a) diagram illustration and (b) photograph of the experimental setup. A diode laser beam was passed through the dichroic mirror to irradiate a full confluent cultured cell layer perpendicularly on a glass-based dish. Use of culture medium with no phenol red was reported to avoid blocking diode laser light (figure adapted from [118])

As discussed earlier, precise control of temperature inside the samples with a uniform heating pattern and short heat-up phase are crucial to study sensitive heat-induced cellular reactions. Manderson *et al.*[91] reported a rapid and controlled optical heating via NIR laser incubation, where targeted illumination of a blood-antibody sample is converted into heat through photothermal absorption. In their study, a feedback control system was employed to accurately maintain the sample temperature. The heating platform included a laser incubation chamber, an NIR diode laser (980 nm), a mirror to illuminate sample mixture, and an IR temperature sensor to provide real-time temperature data to the feedback system program. Laser illumination increased the temperature of the sample volume (75 μL) from 24°C to 37°C within approximately 30 s, while the heat-up phase was approximately 150 s with the traditional heating block technique. The fast-ramping rate in laser-based technique is due to its independence from an external heat source; instead, it is a function of laser output power which is regulated by the sample temperature. As depicted in Figure 2-9, temperature control of sample was obtained via pulsating mechanism during laser-based heating with an accuracy of 1°C that was in agreement with the results presented by other groups[119].

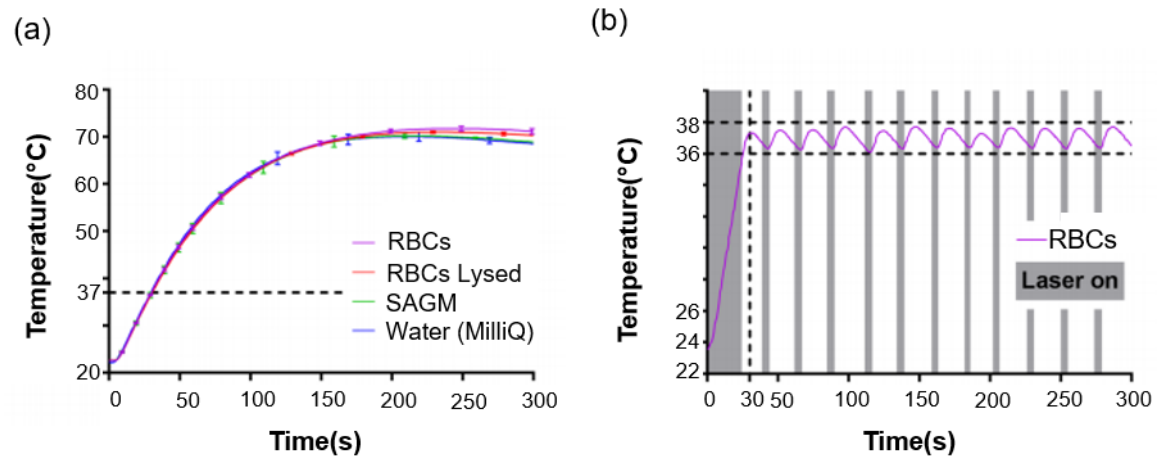

Figure 2- 9 Laser light absorption by red blood cells (RBCs) shown in pink color (a) Without pulsing, laser light absorption rapidly heats the sample (75µL) to 70°C within 150 s, (b) laser illumination with pulsed on (grey) and pulsed off (white) to maintain the sample temperature between 36°C and 38°C (figure adapted from [91])

The laser absorption can be considered as non-uniform due to different diffusions of temperature for the seeded cells in various regions inside the culture dish, even with a fixed power. Therefore, to overcome these limitations and critical points, Miura *et al.*[92] developed an alternative method that allows to measure the spatial temperature distribution inside the cell culture dish while laser irradiation is being performed. Figure 2-10 shows the schematic view of laser irradiation platform for *in vitro* heating purposes.

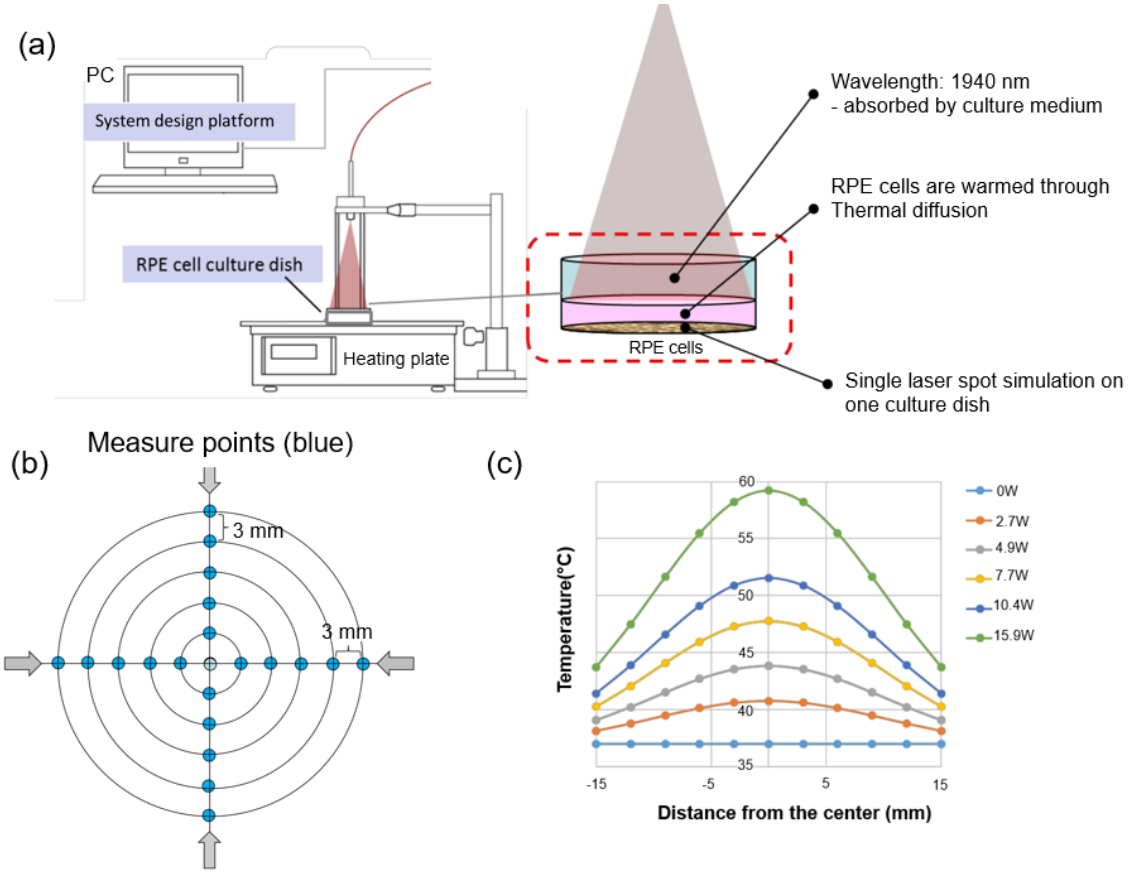

Figure 2- 10 (a) Schematic Image of laser irradiation station consisting of a culture dish that was placed on the heating plate while the cells are placed 12 cm below the laser fiber tip for providing identical beam size to the inner diameter of the dish, (b) measurement of the temperature distribution at 21 different positions (blue dots) inside the cell culture dish with 5 radial points over 4 different angles, (c) non-uniform (bell-shaped) distribution of the measured temperature across the culture dish (figure adapted from [92]

As illustrated in Figure 2-10 (a), a culture dish was placed on the heating plate to maintain 37°C prior to laser heating while the laser irradiation was being controlled by a time-controlled routine. Within seconds of laser irradiation, the temperature inside the cell culture dish increased, and led to thermal convection throughout the cells. The highlight of this study was the ability to measure the temperature distribution throughout the cell culture. The temperature distribution was created by data

interpolation based on 21 points on a culture dish where fine thermocouples were inserted (Figure 2-10 (b)). Since thermocouples are not recommended to be used in sterilized cell cultures, the authors selected the same amount of medium (1.2 mL) that was used in the cell culture experiments and finally measured the temperature uniformity at the bottom of dummy (cell-free) dishes. Figure 2-10 (c) highlights the center of the cell culture dish as the highest temperature that was measured during laser irradiation. Similar to [93], [119], maximum measured temperature was positively correlated to laser output power. The non-uniform bell-shaped heating pattern in cell culture plates during NIR laser radiation was also reported by other groups[120], [121].

In vitro heating by laser irradiation has the advantage of a fast temperature ramping rate as well as ability of temperature control, however, the drawback is that temperature is not uniformly distributed throughout the sample. One possible solution is to use lower absorption coefficient in water. However, the lasers must have high power due to the fact that only a small portion of the light can be absorbed over small regions.

2.3.5 High intensity focused ultrasound (HIFU)

High Intensity Focused Ultrasound (HIFU) has been clinically applied to non-invasively deposit energy in deep tissues and has been used for treating several types of cancer[122]–[124]. Frictional heating is generated due to acoustic absorption, causing temperature rise within the sample. HIFU systems typically operate at ~0.5–5 MHz, providing a balance between effective heating and penetration within tissue. Although cellular response to hyperthermia treatments has been widely studied[125], [126], the underlying mechanism in which HIFU induced cellular necrosis occurs is still unclear. Zhang *et al.*[127] were able to design an *in vitro* based system that

generates heat through ultrasound in a 96-well culture plate. The HIFU *in vitro* system (Figure 2-11 (a)) consists of a box where the transducer and culture dishes are placed. To avoid the formation of unwanted air bubble inside the culture dish, use of degassed deionized water was reported that was being circulated in the system through a water pump. Finally, a piezoelectric transducer was used in the water container to generate the ultrasound induced signal. As shown in Figure 2-11 (b), samples were exposed to focused ultrasound at 213 W/cm^2 for 30 min. In their study, feedback loop algorithm based on real-temperature data measured by a thermal camera was reported to maintain the mean temperature of the samples at 45°C with an accuracy of ~2°C. A ramping rate of approximately 2 min was required to achieve a hyperthermic temperature of 45°C from 34°C.

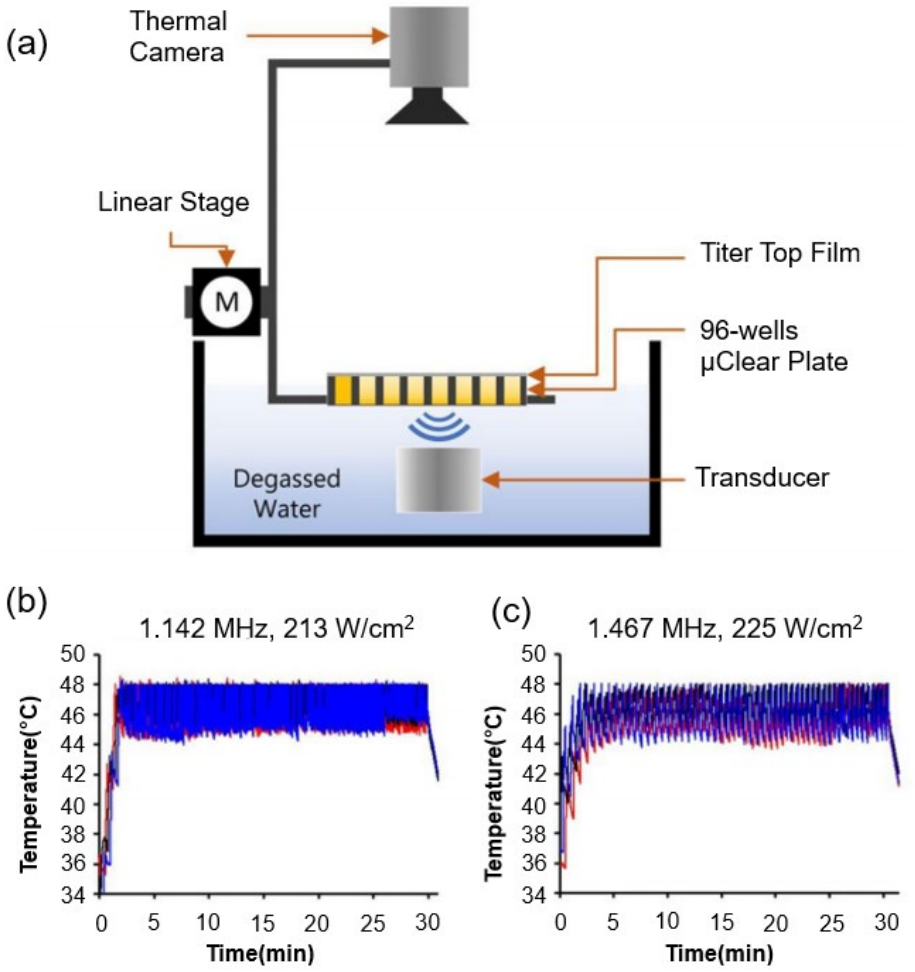

Figure 2- 11 The in vitro focused ultrasound system, (a) diagram of experimental design where ultrasound signal was generated using a piezoelectric focused transducer driven by a signal generator that was immersed at the bottom of a tank filled with degassed water, (b) measured temperature generated by the FUS transducer was measured by an IR thermal camera during focused ultrasound heating with different actuation frequencies. The red, black and blue lines represent the real-time temperatures in three in-parallel sonicated waves (figure adapted from [127])

In order to subject the cells to focused ultrasound while ideally provide a fair stability and cellular compatibility, we might need to place the cells inside tissue mimicking materials. This is because culture medium is far less attenuating than the

soft tissue, causing restricted cellular heating during ultrasound exposure. Such experimental arrangement was demonstrated by Arvanitis *et al.*[99]. In their study, the cells were embedded inside the agarose gel with glass microbeads. The cells and tissue mimicking gel were immersed in a water tank that was maintained at 37°C. A fine type-T thermocouple was inserted in the gel to record the temperature focally. The signal from the temperature sensor was recorded every 10 ms with a multiplexer, transferring the temperature data to a PC. This design however, may result in reading errors due to the possible interference between ultrasound induced beam and the thermocouple, leading to ~1°C temperature rise. A temperature rise of 10–25°C occurred in less than 2 s during HIFU exposures within high pressure ranges, indicating the fast ramping rate of ultrasound based heating modality. The temperature was not kept constant during the ultrasound exposure, and instead was followed with a continuous increase.

Another application stemming from the use of a HIFU was reported by Rivens *et al.*[97]. The authors were able to embed the cells in a compressed collagen gel sandwiched between slices of PVA gel**.** In their study, gels were exposed to ultrasound using a transducer at 1.6 MHz frequency. A sterilized fine K-type thermocouple was vertically inserted into the collagen layer to monitor the real-time temperature for 300 s treatment with a sampling rate of 0.01 s. An increase in the temperature of ~23°C was achieved within only 200 s of ultrasound exposure, confirming a fast heating rate that was in agreement with the results presented by Arvanitis *et al.*[99].

Although ideally HIFU treatment would be given as a homogeneous thermal dose distribution to all cells, this can be rarely visualized. To this end, Rivens *et al.*[97] measured and simulated the temperature inside the culture dish at different distances from center. As illustrated in Figure 2-12 (a), temperature uniformity was reported

within 2°C at 3 mm distance compared to center. Experimental measurements showed that heterogeneity of temperature distribution increased significantly (6°C) at distances further away from 3 mm of the center. Therefore, achieving a uniform heating pattern during HIFU exposures might be difficult, supporting the simulation results depicted in Figure 2-12 (b).

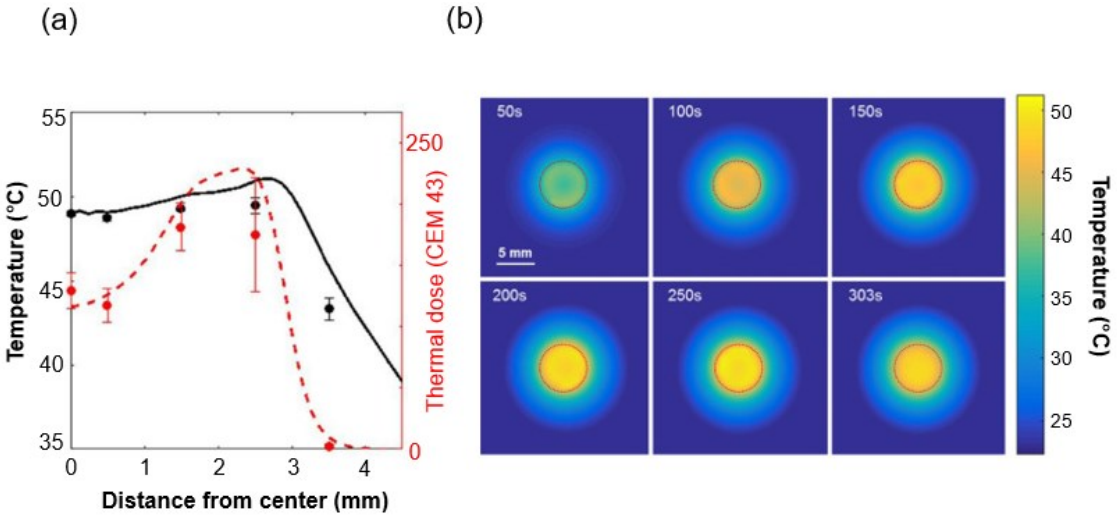

Figure 2- 12 Temperature distribution during ultrasound exposure throughout the collagen layer. (a) Comparison of simulated (solid line) and measured (markers) maximum temperature and thermal dose shown by black and red colors, respectively and (b) simulated temperature distributions at different time points ranging from 50 s to 300 s (figure adapted from [97])

To allow long-term cellular manipulation, it is necessary to maintain a stable temperature. Manneberg *et al.*[98] were able to integrate an ultrasonic heating system using a microplate. In their study, temperature dependency on applied voltage was obtained by inserting a probe in each well of the microplate as illustrated in Figure 2-13.

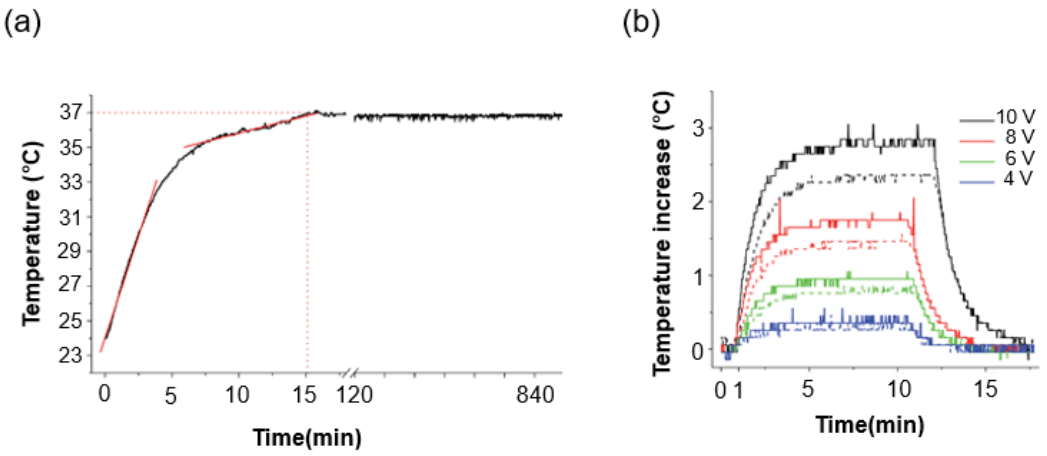

Figure 2- 13 Temperature control during ultrasound heating (a) temperature calibration and maintenance at 37°C where red lines show the approximate rates of the faster ultrasonic and slower chamber heating, (b) temperature was measured adjacent to the transducer (solid lines) that was dependent on the applied voltage (4–10 V) over the transducer and within the fluid in the micro-wells (dotted lines) (figure adapted from [98])

In their study, the heat-up phase was ~20 min to stabilize the temperature of the ultrasonic device. Following the stabilization, the temperature was maintained stable over a long period of 15 hours with a high degree of accuracy (standard deviation of 0.02°C). The uniformity of temperature was also measured over the chip surface (from the transducer to the opposite corner of the chip) that was within 1°C, estimated to cause ~0.3°C difference in temperature uniformity throughout the samples. The presented heating technique by Manneberg *et al.*[98] enables precise temperature control with high degree of accuracy and uniformity throughout the samples; however, the temperature ramp rate is very slow (0.2–2°C min^{-1}), indicating a major drawback of this heating modality.

2.3.6 Microheaters

A number of heating modalities using microheaters have been reported for cell culture studies. These methods utilize heating elements and cell culture chambers to establish a controlled heating throughout the living cells. Heating elements used in microheaters are not only electrically conductive but also optically transparent, and Joule heating can be generated when electrical power is applied. Mäki *et al.*[128] designed such microheater system with a temperature control working principle using a proportional-integral derivative (PID) controller. In their study, they utilized an indium tin oxide plate as a heating element (70 × 70 × 0.7 mm), a temperature sensor made on a glass substrate (49 × 49 × 1 mm) , a cell culture chamber, and a custom-written MATLAB (MathWorks, Inc., Natick, MA, USA) user interface software for controlling the temperature (Figure 2-14). Temperature measurement was performed by using 14 identical sensors that were attached on the heating plate**.** The set power of the controller was limited to 2 W.

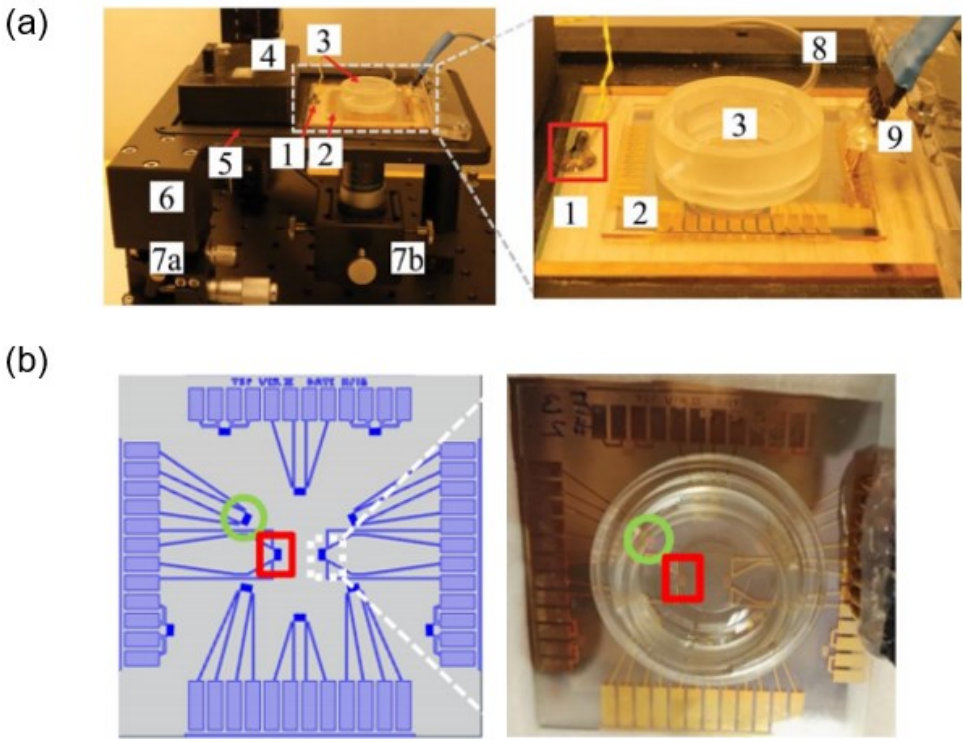

Figure 2- 14 Microscale cell culture system. (a) Experimental setup consisting of ITO plate as the main heating component, a temperature sensor plate made on glass substrate and a cell culture device, (b) temperature logging designed sensor layout and temperature sensor plate together with cell culture chamber. Sensor is marked with a green circle while resistors are marked with a red square (figure adapted from [128])

This microscale cell culture system precisely controls cell culture temperature with an accuracy of ~0.3°C during heating, as shown in Figure 2-15 (a). This was similar to that in other studies; for instance, temperature variations of ±0.2°C[129]–[131], ±0.26°C[132], ±0.3°C[133], ±0.5°C[134], and ±0.8°C[135] have been previously measured.

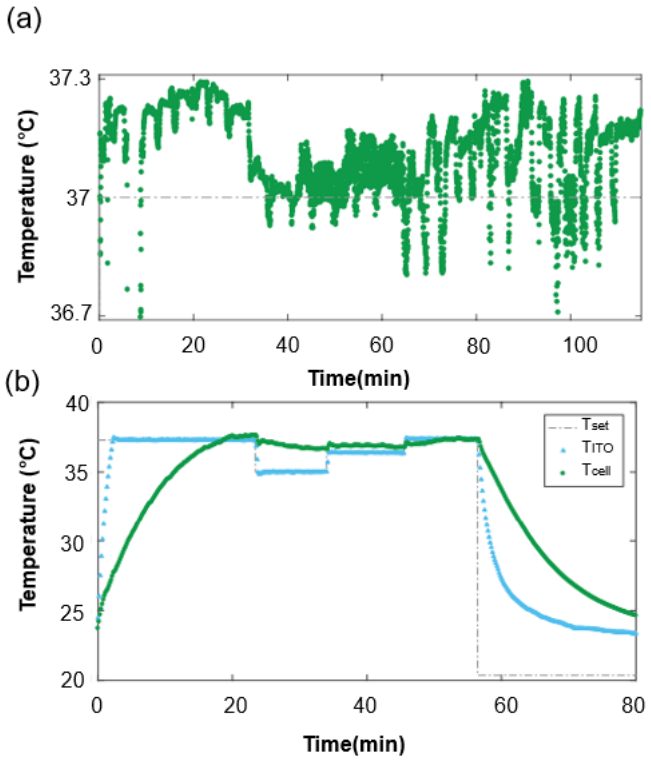

Figure 2- 15 Temperature control (a) long term maintenance of the cell culture temperature with 0.3°C accuracy for more than 4 days, (b) measured cell culture temperature during heating experiment where the set-point temperature was randomly changed, and both $T_{outside}$ and T_{cell} were recorded (figure adapted from [128])

Despite an accurate control of temperature during heating, the system still lacks some of the requirements for an ideal heating modality. The heat-up phase took ~20 min to reach to the target temperature of 37°C from initial room temperature of 24°C (Figure 2-15 (b)). Moreover, temperature uniformity was measured between the min and max values over the cell culture area by using a thermal camera, and was reported as ±2°C.

Lin *et al.*[130] developed an indium tin oxide (ITO)-based microheater chip that serves as a thermal control system for perfusion cell culture outside the incubator. The device consists of a multi-channel syringe pump for media supply, medium

feeding tubing, microcontroller, perfusion micro-bioreactor chambers with the format of a standard 96 well cell culture microplate each containing 50 µl of the mixture, ITO microheater chip, thermocouple, and medium outlet tubing. Figure 2-16 (a) shows the microcontroller module with the ITO microheater chip designed in this study.

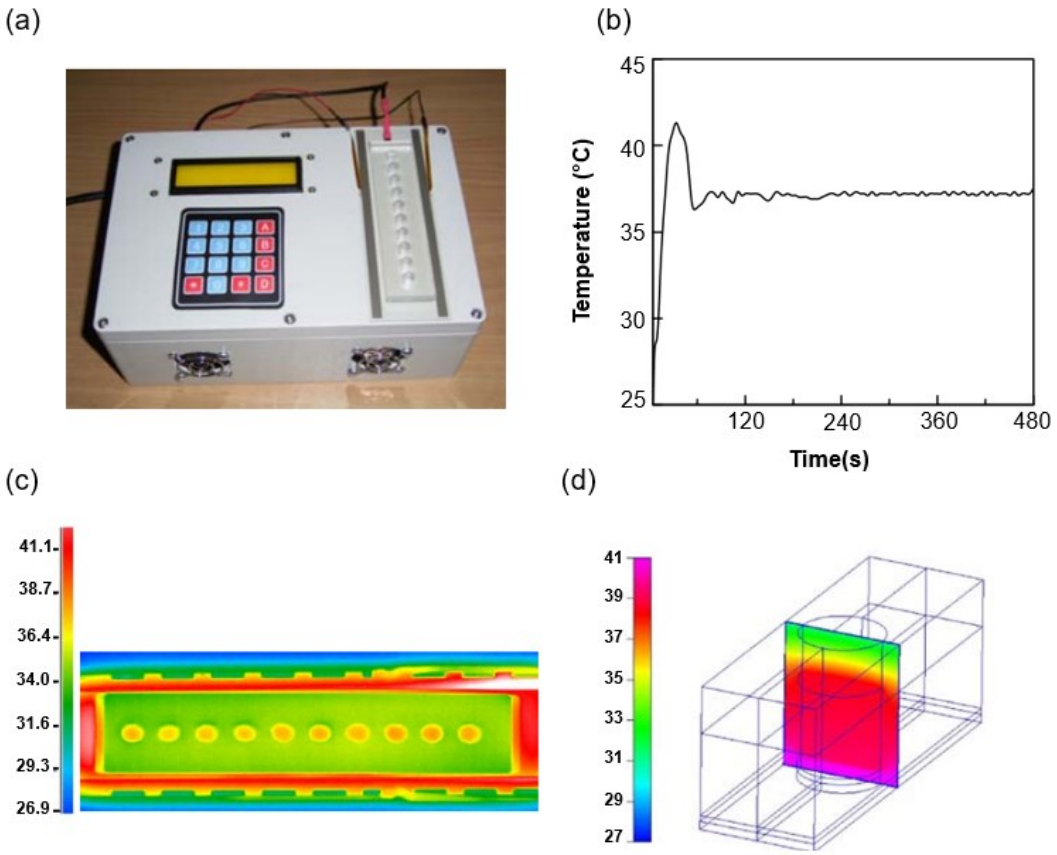

Figure 2- 16 Temperature control (a) A photograph of the handheld microcontroller (17.1 cm × 11.6 cm × 6.5 cm) with an ITO microheater chip connected and a perfusion block, (b) temperature profile over time (The set temperature was 37°C and the temperature deviation was evaluated to be within 0.2°C, (c) 2-dimensional IR images of top surface of ITO microheater chip and chambers, (d) numerical simulation based temperature evaluation inside the PDMS microbioreactor chamber (figure adapted from [130])

The thermal control mechanism is based on a feedback control loop. In their study, a thermocouple was used to monitor the local temperature over the sample

where the thermal field needs to be closely regulated. Then, the generated temperature profile was inputted to the microcontroller module to constantly adjust the output electric current and maintain the temperature. The accuracy of temperature control was experimentally measured as shown in Figure 2-16 (b), indicating high degree of temperature control with slight deviation of ±0.2°C following the heat-up phase. The heat-up phase was reasonable short (~60 s) to reach the target temperature of 37°C from initial room temperature of ~26°C. Temperature distribution uniformity over the culture samples was evaluated by numerical simulation and experimental evaluation. Experimental evaluation was carried out by IR imaging after filling each micro-bioreactor chamber with cell culture medium. IR imaging demonstrated that a uniform thermal field can be obtained at the top surface of each micro-bioreactor chamber with slight variation of ±0.2°C as shown in Figure 2-16 (c). Despite the uniformity of temperature distribution at the top surfaces, simulation results revealed that uniform temperature distribution could not be achieved vertically (bottom to top variation) inside each chamber. Figure 2-16 (d) indicates a non-uniform vertical temperature distribution in one chamber with variations higher than 5°C. Another drawback of this microheater system is temperature overshooting (~4°C higher than the target temperature) during the heat-up phase. This may be a major disadvantage since large variations at hyperthermic temperatures can significantly affect the cellular/molecular response even within short periods.

Petronis *et al.*[132] also presented a cell culture chip integrated with indium-tin-oxide heater to provide steady and spatially uniform thermal conditions using a PID feedback control system. The software adjusted the voltage (2.2–2.9 V) applied to the heater based on the temperature readings to maintain the temperature of the cell culture. The cell culture chip was composed of five poly (methyl methacrylate) sheets,

cell culture chamber (7.6 × 13.0 mm^2) with inlet and outlet media perfusion, and a thermistor connected to the computer and the external power source for temperature control. In their study, the microheater was tested for thermal control stability and they reported an accurate control of temperature with slight variation (±0.26°C). Similar to Lin *et al.*[130], the simulation based analysis was performed to evaluate the temperature distribution uniformity throughout the cell culture chamber. Results of 2-D temperature distribution modeling indicate heterogeneity up to 3°C along the cell culture chamber during a steady state heating of 37°C.

Recently, Nieto *et al.*[134] reported fabrication of a glass based microheater (5 × 5 mm^2) that was comparable to conventional cell incubators for cell culture in terms of temperature rise and decay characteristics and localized heating. Thermal characterization of the microheater was measured by an IR Camera that was placed over the microheater to record the local temperature when the microheater was subjected to different applied voltages Figure 2-17 (a).

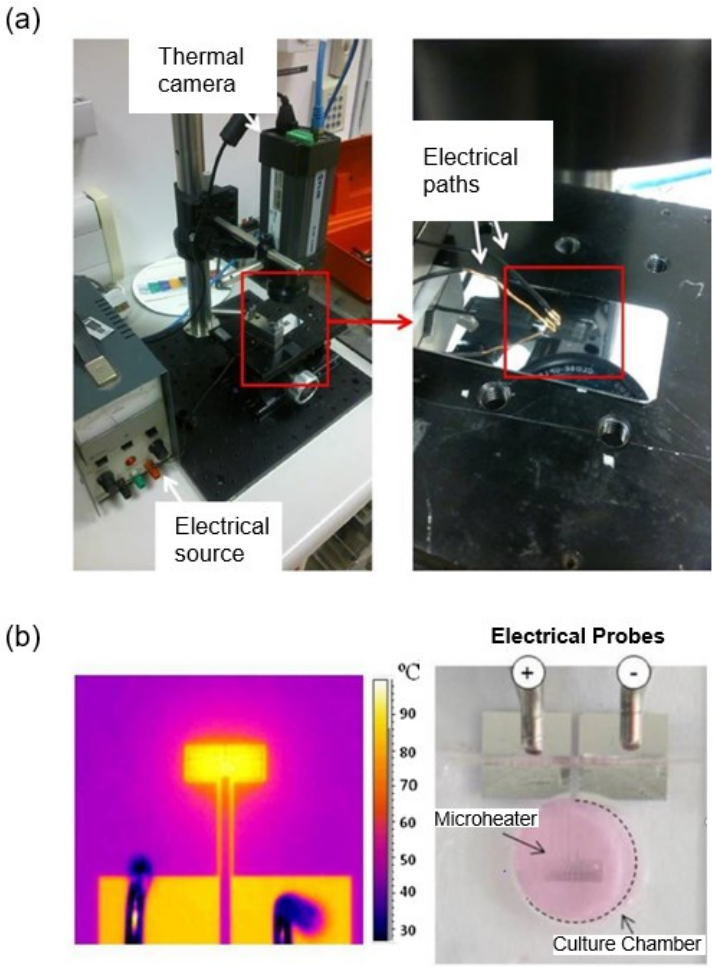

Figure 2- 17 Experimental setup for IR camera setup used for analyzing the heating capabilities of the microheaters and an IR image of the microheater including (a) detailed view of microheater and electrical connectors, (b) IR image of the microheater obtained by the thermal camera during heating as well as top view of culture chamber used for performing cell culture. The bright spot on the ablation area of the microheater shows the peak temperature of 100°C (figure adapted from [134])

There was no measurement regarding the temperature ramp rate or the accuracy of temperature control inside the cell culture chamber. The main weakness of their experimental measurements was that only the response characteristics of the microheater chip was measured and not the cell culture chamber. Temperature distribution throughout both the cell culture chamber and the microheater was

captured by an IR camera which can be visualized in Figure 2-17 (b). Regions near the microheater chip demonstrate higher temperatures compared to regions further away from the microheater chip, indicating a non-uniform temperature distribution (~10°C variation) inside the whole cell culture chamber. One reason for this heterogeneity could be due to the large size (2 mm in depth and 8 mm in diameter with the total volume of 900 μL) of cell culture chamber compared to regular 96-well plates that are supplied with less volume (~200 μL per well) of cell culture media.

2.3.7 Microfluidic systems

A number of heating techniques have been reported using microfluidic devices. While they have not been widely used in hyperthermia research, they offer experimental flexibility to culture cells within a controlled environment[136], [137]. Approaches to accurately control the temperature within microfluidic systems have been already proposed. De Mello *et al.*[138] showed controlled ohmic heating in a running channel. However, precise control of Joule heating for large variations of temperatures remains difficult regarding the conductivity of ionic liquid. Moreover, this method did not lead to temperature uniformity due to boundary effects.

Burke *et al.*[139] used a millifluidic device to quantify the content of released liposomes following mild hyperthermia. Their system consisted of a quartz capillary tube which was anchored on top of the Peltier heating elements while was attached to a syringe pump as demonstrated in Figure 2-18 (a). In their study, the output power was adjusted to the Peltier elements to control the temperature. This was done through a feedback loop based on thermocouple temperature readings. Feedback thermocouples were placed in the water reservoir and inside the tube 8mm from the outflow.

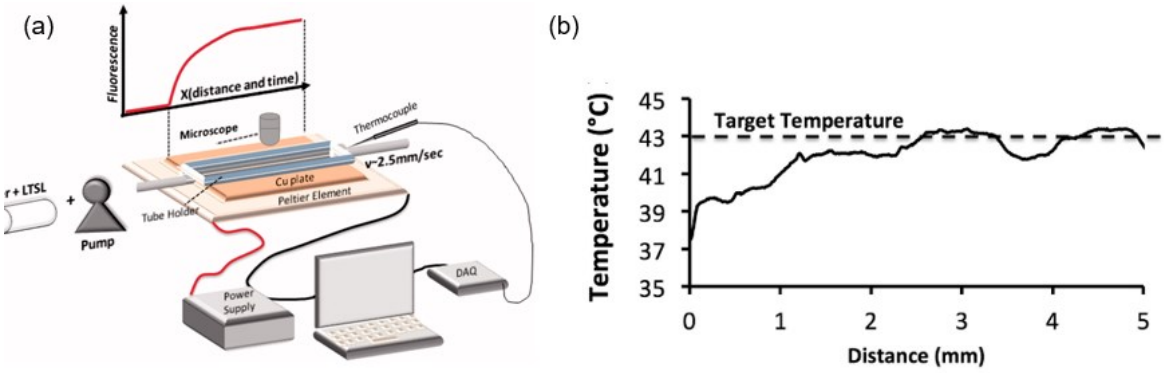

Figure 2- 18 (a) Schematic of experimental setup for millifluidic release assay. The tube was heated to the desired hyperthermic temperature through a temperature-controlled Peltier element, (b) fluid entering the capillary tube reached the desired temperature within 3 mm, corresponding to 0.3 s. The Peltier temperature is measured by a thermocouple and a control algorithm regulates the output power to control the temperature (figure reproduced from ([139]))

The developed millifluidic system enabled quantification of content release of liposomes affected by mild hyperthermia at very high temporal resolution of less than 1 s. Figure 2-18 (b) shows the measured temperature of the fluid entering the capillary tube that reached the desired hyperthermic temperature of 43°C within 3 mm, corresponding to 0.3 s at a flow velocity of 10 mm/s. As demonstrated, temperature control was performed with an accuracy of ~1°C during hyperthermia exposure. To investigate the temperature uniformity, point measurements were made throughout the surface of the heating element. Heating uniformity at the surface of peltier element was within 2°C. Thus, to improve this, use of a thin copper layer was reported that was

secured on top of the element. This resulted in improved heating uniformity from 2°C to 0.5°C.

Cantoni *et al.*[140] also reported use of a flexible microfluidic device with temperature control ability for biomedical applications. In their study, eppendorf tubes (0.5–5 mL) can be inserted into the carrier according to experimental needs (Figure 2-19 (a)). The carrier consisted of an integrated perfusion system to recirculate the culture media by using piezo pumps while a thermocouple was placed against the heater to provide temperature control feedback. Stable temperature control at 37°C with ~0.2°C accuracy was obtained by placing a thin heating layer under the chip.

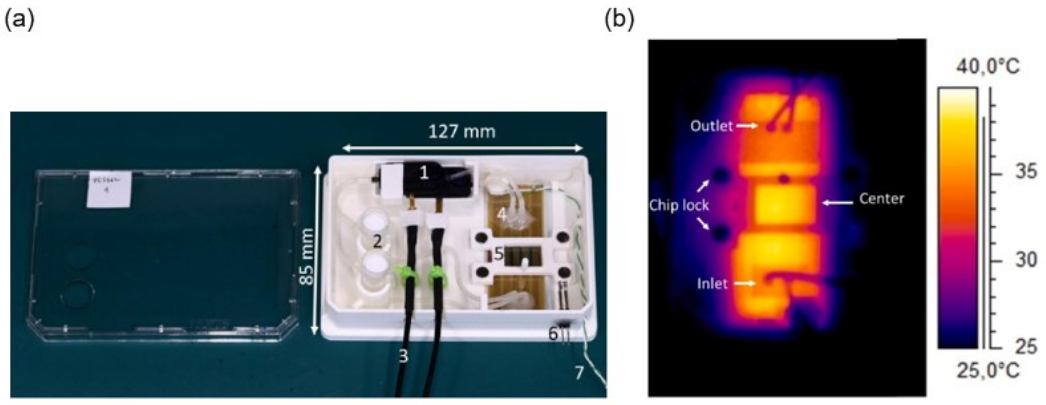

Figure 2- 19 (a) Microfluidic chip on the carrier consisting of piezo pumps, cell media reservoirs and the pump connectors and the thermocouple. Each pump is connected to an eppendorf tube placed vertically inside the carrier which acts as a cell media reservoir, (b) the temperature distribution measured by IR camera after the recovery of the cell media turnover inside the microfluidic chip (figure reproduced from ([140]))

Temperature uniformity along the channel was investigated by using an IR camera (Figure 2-19 (b)). A temperature gradient of ~0.5°C was detected at the inlet and the center of the chip for 30 s when a flow of 50 µl/min was applied. Similar to

Burke *et al.*[139], one of the limitation of this study was inability to measure the sample temperature distribution. Although the temperature uniformity was monitored at the surface of the heating element, there was no report of actual cell culture sample uniformity during heating phase.

Microfluidics enables the precise application of experimental conditions to study the behavior of cells. The advantages of microfluidic cell culture over the macro-scale methods include fast ramping rate (i.e. less than 1 s), reduced risk of contamination, design flexibility and most importantly, ability to provide cell's natural microenvironment. Although microfluidic devises can provide great flexibility with respect to experimental design, transferring cells from a macroscopic culture environment of flasks, dishes and well-plates to microfluidic cell culture requires revision of culture protocols, and thus increased complexity of the system. Furthermore, variation of velocity across the tube diameter may increase systemic error as described by Burke *et al.*[139]. Another error source in these systems could arise from photobleaching phenomenon which significantly limits the heat exposures duration of cell culture samples[139], [141].

2.4 Summary

2.4.1 Comparative analysis

In vitro studies with high degree of control of thermal profiles within cells in culture have been essential for understanding the relationship between bioeffects and applied thermal doses. To perform an accurate analysis, cell culture samples would ideally be subjected to uniform heating, raised from, and returned to, baseline rapidly following addition/removal of the thermal source, for a known heating duration under ideal isothermal condition. The present article has surveyed a variety of heating

modalities that have been used for *in vitro* studies investigating bioeffects of heating. These techniques offer different advantages or drawbacks in terms of integration and control over heating parameters such as ramp rate, accuracy, uniformity and ease of use that are summarized in Table 2-1.

Table 2- 1 *In vitro* heating techniques along with the corresponding specifications

Cell carrier	Sample size	Heating modality	Toutput (°C)	Input	Ramping (s)	Accuracy (°C)	Uniformity(°C)	Complexity	$T_{initial}$ (°C)	T sensors (#)
Petri-dish-10cm[103]	10 mL	Incubator (not preheated)	41.5	42°C	2400	0.1–0.5	0.25	+	37	1
96 WP[81]	100 µL	Incubator (preheated)	47.2	48°C	1320	0.2–0.8	2	+	37	5
96 WP[81]	100 µL	Incubator (preheated)	47.2	48°C	3000	0.2–0.8	2	+	37	5
96 WP sealed[84]	200 µL	Water bath (immersed)	46.6	46.8°C	152	0.2	NA	++	22	2
96 WP sealed[84]	200 µL	Water bath (floating)	52.8	55.8°C	251	3	NA	++	22	2
0.5mL PCR tube[84]	200 µL	Water bath (floating)	46.3	46.9°C	52	0.6	NA	++	22	2
96 WP-wrapped[81]	100 µL	Water bath (immersed)	48.6	48.6°C	1200	0.2	0.2	++	26	5
T25 Flask[110]	70 mL	Water bath (hot media injection)	49.5, 49.8	50°C	12, 60	0.2–0.5	NA	+++	37	2
96 WP[72]	100–200 µL	Water bath (hot PBS injection)	45–60	45–60°C	Instant	1.4	NA	+++	37	1
6 WP[113]	3 mL	Microwave	50	10–20 W	420–180	2	4	+++	25	4
48 WP[115]	500 µL	Microwave	50–60	15 W	30–50	NA	NA	+++	37	1
Beaker[142]	30 mL	Microwave	40–60	1–25 W	17–36	1	NA	+++	25	Self
Petri-dish-35mm[114]	2.5 mL	Microwave	39.5	6.8 W	30	0.1–2.5	NA	++++	27	1+Self
Petri-dish-30mm[92]	1.2 mL	Laser	40–60	3–16 W	10	NA	2–15	+++++	37	21
Petri-dish-35mm[143]	1 mL	Laser	30	0.2 W	240	NA	2–6	+++++	22	1
48 WP[144]	150 µL	Laser	60	3.8 W/cm²	300	2	NA	++++++	37	1
Centrifugal tube[91]	75 µL	Laser	37–70	2 W	30–200	2	NA	+++	24	1
Collagen gel[97]	129 × 86 mm²	Ultrasound	45	1100 W/cm²	300	NA	5	+++++	23	1
Agarose phantom[99]	20 × 75 mm²	Ultrasound	45	4.4 MPa	6	NA	3–5	+++++	37	1
wells[98]	0.3 × 0.3 × 0.3 mm³	Ultrasound	37	10 V	900	0.02	0.3	+++++	23	2
96 WP[127]	420 µL	Ultrasound	45	213 W/cm²	120	2.29	NA	+++++	34	1
Agarose phantom[145]	25 × 25 × 20 mm³	Ultrasound	30	1.54 MHz	70	1.1	4	+++++	22	3
Culture dish-60mm[146]	30 mL	Microheater	37	5 W	240	2–3	NA	+++	32	1
Culture chamber[128]	1 mL	Microheater	37	2 W	1200	0.2–1.5	0.4–2.9	+++	24	Self
Culture chamber[147]	50 µL	Microheater	65	0.22 W	1800	5	10	+++	24	2
Culture chamber[132]	7.6 mm × 13 mm	Microheater	37	2.5 V	No heating	0.26	3	+++	37	Self
Glass slide[148]	20 µL	Microheater	50	1 V	4	0.5	10	+++	24	1
Chamber[139]	2–3 mL	Millifluidic device	43	3000 AU	0.3	1	0.5	++++	37	1
Eppendorf tube[140]	0.5–5 mL	Microfluidic device	37	0.65 W	210	0.2	0.5	+++++	36.5	1

2.4.1.1 Heating accuracy

While most heating modalities have been suitable for delivering the heat in a temperature-controlled manner, the control over thermal parameters varies considerably. Use of water baths lead to stable heating with relatively small variations (±0.3°C) over the heating period while other heating modalities using electromagnetic waves such as microwave and lasers irradiations are associated with larger variations (0.8–4°C) in terms of temperature stability. This is a drawback of using microwaves, lasers and also traditional cell culture incubators since even slight temperature variations (±0.5°C) during long treatments periods can significantly affect cellular response[125], [149], causing inaccurate *in vitro* thermal analysis.

2.4.1.2 Ramping rate

The heating rate in conventional water baths and CO_2 incubators is very slow, requiring a long heat-up period (80–2400 s) to reach the desired hyperthermic temperatures (42–50°C), hence it will be difficult to obtain a detailed thermal history (i.e., temperature × time) at cellular levels using these traditional techniques. On the other hand, more integrated heating modalities including microwave, laser, focused ultrasound (FUS), and microfluidic systems can achieve fast temperature ramp rates ranging from 0.1 to 10°C/s, indicating their major advantage over traditional heating techniques. The slow temperature ramp rate in water bath heating modalities can be significantly improved by incorporating a number of modifications in the system design as follows:

1- Use of hot media exchange technique during the transition phase and prior to immersion in water bath results in an ideally quick heat-up period (~5s) to reach

the target temperature as described by Rylander *et al.* [110] and Herea *et al.*[83]. Unfortunately, this heating approach necessitates the use of large sample volumes (~70 mL) while use of smaller sample volumes such as 96-well plates will not be practical. This is because each of the wells in a 96-well plate usually contain small volumes (100–200 μL) of cell culture sample, thus in well temperature may drop quickly within few seconds following injection and prior to immersion in preheated water bath. Heating larger sample volumes tend to show less uniformity and/or accuracy during heating phase, so the proposed approach may have its own drawbacks despite its major advantage. On the other hand, use of very small volumes (in the scale of microliters) leads to instant temperature drop and inaccuracy of temperature control during heating[72].

2- Another technique that can be used to compensate for the slow temperature ramp rate during water bath heating is using multiple water baths in the treatment design: One water bath set to a significantly higher temperature (e.g., 80°C) than the target hyperthermic temperature (42–50°C), to be used during the transition phase, and one water bath set to target hyperthermic temperature to be used during steady-heating phase. This heating technique, however may introduce a complexity to the heating platform since switching the culture samples from first water bath to the second one must be performed in exact timing to avoid further temperature rise of the samples above the target hyperthermic temperature[150].

2.4.1.3 Heating uniformity

Another characteristic that has been emphasized by several authors is uniformity of temperature distribution during hyperthermia exposures[92], [99], [151]–[153]. Using

96-well plate formats is ideal for subjecting cells to uniform heating due to the small sample volume (100–200 μL) in each well. Water baths and cell culture CO_2 incubators can be easily integrated with 96-well plates, resulting in ideal uniform heating inside each well. Unfortunately, most newly developed *in vitro* heating modalities including microwave, FUS, laser, microheaters, and microfluidic devices involve the use of large sample volumes (e.g., T75 culture flasks, 6 well-plates, 30 mm petri dishes, beakers or agar gels) due to technical limitations of the design. This can lead to higher variations (2–5°C) in temperature distribution during heating. Therefore, level of complexity is not necessarily a determining factor in selecting ideal *in vitro* heating modalities.

2.4.1.4 Biological effects considerations

An ideal *in vitro* heating modality should not affect the cellular/molecular activity if used under normothermic (36.5–37.5°C) conditions. This is to ensure that the resulted change in cellular/molecular behavior can be solely attributed to the heat effects; otherwise inaccurate thermal analysis may be made. Recently, Asano *et al.*[114] reported decreased cell viability following subjecting cultured cells to normothermic conditioned microwave irradiation (37°C for 1 h), indicating that microwave irradiation may not be an ideal *in vitro* heating modality for studying the thermal dose dependency of cell viability. Similarly, use of conventional water baths may affect cell viability even at normothermic temperatures[81], but this is possibly due to biological contamination, hence careful handling and sufficient sealing need to be performed during the hyperthermia exposure of cell culture samples. There was no change in viability of the cultured cells that were exposed to very low doses of laser irradiation[92]; however, other physiological changes were reported such as overexpression of heat shock proteins[154], [155], this may result

in inaccurate analysis between hyperthermia induced cell viability and protein expression kinetics when using laser irradiation as the heating modality. Moreover, there have been reports of artifacts and induced cell death arising from chemical interaction between cell culture samples and polydimethylsiloxane (PDMS) formulations which is most commonly used in microfluidic cell culture devices[136], [156].

Many studies have been conducted to address the differences in biological effects induced by various *in vitro* hyperthermia approaches that can contribute to hyperthermia treatment in clinical practice. For instance, microwave hyperthermia can induce caspase-3 dependent apoptosis while reducing the levels of mitochondrial membrane potential in lung cancer cells[112] as well as squamous carcinoma cells[115]. The results revealed that accumulation of reactive oxygen species was observed in the microwave treated cells, leading to DNA damage and increased apoptosis compared to the cells that were treated with water bath approach. In ultrasound-based hyperthermia studies, other mechanisms such as cavitation can take part beside thermal effects in tissue damaging process[157], therefore, researchers have also focused on enhancing the lethality of anticancer agents with ultrasound exposures. There is also evidence showing that the response of cancer cells to ultrasound are more severe than normal cells, indicating that cancer cells show more sensitivity to ultrasound treatment than normal cells[158]. In the context of thermotherapies adjuvant to traditional cancer treatments, NIR laser irradiation has shown to enhance the efficiency of radiotherapy in melanoma cancer cells by inducing radiosensitivity[159]. Moreover, it has been shown that NIR laser irradiation can stimulate immunogenic cell death by activating adaptive immune response against dead-cell-associated antigens. This process induces rapid release of specific biomarkers

responsible for immunogenic cell death such as HSP70, HSP90 and HMGB1 from cancer cells[160].

3. *In vitro* measurement and mathematical modeling of thermally induced injury in pancreatic cancer cells[2]

3.1 Introduction

Pancreatic cancer is the fourth leading cause of cancer related death in the United States, and accounts for 8% of cancer deaths, with a low five-year survival rate of approximately 10% [4], [161]. Surgical resection remains the most effective treatment strategy; however, only approximately 20% of patients are surgical candidates at the time of diagnosis [2,3]. For patients with unresectable pancreatic cancer, use of chemotherapy alone or in conjunction with surgery remains the gold standard, although long-term survival rates are poor and the regimen comes with risks for major complications in patients with advanced disease [4,5]. Thermal ablation [30], and other non-ionizing energy-based local interventions such as irreversible electroporation, are under investigation as potential adjuvant or stand-alone treatment options for patients with unresectable pancreatic adenocarcinoma [166]. In addition to ablative effects, heating in the mild hyperthermia range (39–43°C) may offer a means for thermally triggered drug

[2] This chapter has been published as: F. Chamani, M. Pyle, T. Shrestha, J. Sebek, S. Bossmann, M. Basel, R. Sheth and P. Prakash, "In Vitro Measurement and Mathematical Modeling of Thermally-Induced Injury in Pancreatic Cancer Cells", Cancers., Vol. 15, Issue. 3, 2023. (https://doi.org/10.3390/cancers15030655) by MDPI. www.MDPI.com

delivery [167]–[169] or serve as an adjuvant to ionizing radiation and/or chemotherapy [170]–[173].

The bioeffects induced by heating are a function of the time-temperature profile during heating, and may vary across cell types. Mathematical models relating changes in cell viability, stress protein expression, and other biomarkers, to the time-temperature history during heating have been reported [54]. Cell/tissue-specific parameters for these models can be determined from experiments on cells *in vitro* [174]–[176]. One of the most widely used models is the Arrhenius thermal injury model [175], which describes cell death following heating as a first-order exponential relationship between temperature and duration of heating, and has been applied to assess thermal damage in various cell types, including liver cancer cells [56], prostate tumor cells [57], and breast cancer cells [58]. The thermal isoeffective dose model, which relates an arbitrary transient temperature profile to equivalent minutes of heating at a reference temperature, typically taken to be 43°C, is derived from the Arrhenius model [59]. Despite its wide usage, the standard Arrhenius model fails to represent thermally induced injury or cell death at mild hyperthermic temperatures (39–43 °C) for several cell types, showing significant over-prediction of the initial 'shoulder' region as explained by Pearce [175]. Augmenting the Arrhenius model with a time delay term has been proposed to account for the delayed cell death at low temperatures [177]. Other models for thermal injury have been proposed, including a two-state statistical thermodynamic model by Feng *et al.* [176] and a three-compartment reaction-based model by O'Neill *et al.* [178]. While thermal injury parameters for a range of cell types have been reported, there are few published data reporting on viability of pancreatic cancer cells following heating. Identification of

thermal injury parameters is important to inform design of thermal therapy devices and systems, select treatment doses, and to inform interpretation of experimental and clinical studies involving heat as a therapeutic modality.

The objective of the present study was to determine the kinetics of thermal injury to pancreatic cancer cells *in vitro* following thermal exposure to temperatures up to 50°C and use these data to evaluate predictive models for thermal injury. Given the central role of experimental murine models in pancreatic cancer research, we conducted studies on two murine pancreatic cancer cell lines (KPC and Pan02), as well as a normal murine fibroblast cell line (STO). The KPC murine model (KRAS/TP53 point mutation)[179] is an established genetically-engineered and clinically relevant model of pancreatic ductal adenocarcinoma that represents many histopathological features observed in human disease. The murine pancreatic adenocarcinoma cell line Pan02 [180], [181] syngeneic to C57BL/6 is an established grade III model widely used for pre-clinical evaluation of single and combination therapies. Given the significance of the stroma in pancreatic tumors, we also evaluated the kinetics of thermal injury on STO cells. For each of these cell lines, monolayer cell cultures were heated in water baths to temperatures in the range 42.5–50°C for 3–60 min, and cell viability following heating was assessed up to 24 h following hyperthermia and compared to 37°C control. The kinetics of thermal injury were estimated from the measured viability data. Finally, we comparatively assessed three mathematical models for predicting thermally-induced changes in cell viability based on the measured *in vitro* data.

3.2 Materials and Methods

3.2.1 Cell culture

KPC and STO cells were cultured with DMEM's medium (Gibco™ 11995065, Fisher Scientific) with 10% fetal bovine serum (Corning™ 35015CV, Fisher Scientific) and 1% penicillin-streptomycin (Gibco™ 15140148). Pan02 cells were cultured with RPMI 1640 Medium (Gibco™ 11875093, Fisher Scientific) supplemented with sodium pyruvate and 10% fetal bovine serum. Cultures were maintained in a 37°C, 5% CO_2 incubator in 75 cm^2 phenolic culture flasks. In preparation for hyperthermia treatment, cells were seeded in n = 6 wells of 96-well culture plates at a density of ~30,000 cells/cm^2 at a volume of 200 µL medium/well and maintained in a 37°C, 5% CO_2 incubator for 24 h to allow cells to reach log phase prior to hyperthermia.

3.2.2 *In vitro* hyperthermia to monolayer cell culture

To expose cells in culture to hyperthermia, sealed 96-well plates containing cells were immersed in temperature-controlled water baths (shown to be an effective method for accurate and uniform heating of cell culture samples)[182]. To assess temperatures during hyperthermia, transient temperature profiles were recorded using five T-type thermocouples embedded within distinct wells of a dummy plate that contained no cells while filled with 200 µL of water/well. The dummy well plate was immersed in water baths simultaneously with the cell-containing plate, thus providing a reasonable assessment of the temperatures within the cell-containing wells. Figure 3-1 illustrates the dummy plate design, including five thermocouples positioned and sealed within four corner wells and one central well.

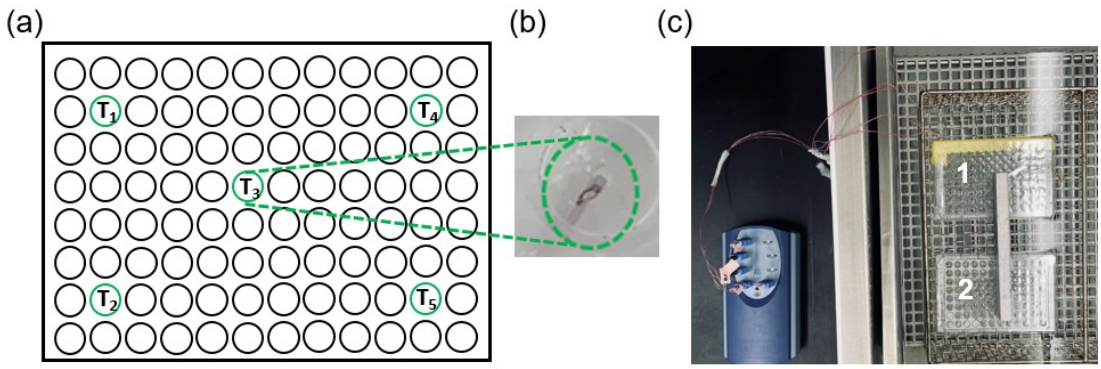

Figure 3- 1 (a) Dummy plate design with five thermocouples for monitoring temperature during hyperthermia sealed within four corner wells and one central well. (b) Photograph of a thermocouple sealed within a well. (c) Cell-containing and dummy plates immersed within the water bath during hyperthermia

Since the time to reach the setpoint temperature can be rather slow, we employed a two-step approach. First, both the cell-containing and dummy well plates were immersed in a water bath set at an elevated temperature of ~80°C. When the temperature recorded by thermocouples in the dummy plate reached within 0.2°C of the target temperature (i.e. 42.5, 44, 46, or 50°C), plates were immediately transferred to another pre-heated water bath that was set to the desired target hyperthermic temperature for a predetermined duration in the range of 3–60 min. A USB thermocouple data acquisition module (TC-08 OMEGA) was used to record the temperature data from the thermocouples embedded within the dummy plate. Following hyperthermia treatment, sealing films were removed and the 96-well culture plates were returned to a 37°C incubator for subsequent 6 h and 24 h recovery of thermal injury. For each cell line, an additional plate containing cells was also immersed in a 37°C water bath for the experimental durations considered in this study, providing a no-hyperthermia control.

3.2.3 Cell viability evaluation

After an incubation period of 6 h and 24 h post-heating (shown to be effective evaluation periods for measuring cell viability [177]), cell culture supernatant was discarded from each 96-well culture plate and viability was determined using the 3-(4,5-dimethylthiazol-2-yl)-2,5-diphenyl-2H-tetrazolium bromide (MTT) colorimetric assay [183] which is based on the reduction of a yellow tetrazolium salt to purple formazan crystals by metabolically active cells. The measured optical density for each time-temperature combination was normalized to the optical density measured for no-heat control plates immersed in a 37°C water-bath for the same time duration. The normalized values thus represent the average concentration of viable cells across n=6 wells following hyperthermia exposure for each experimental group.

3.2.4 Thermal injury analysis

3.2.4.1 Arrhenius model of thermal injury

The Arrhenius cell injury method models cell death as a first order chemical reaction where the source materials (viable cells) are transformed to the product (non-viable cells). After identification of the rate parameters for the reaction, the Arrhenius model allows prediction of cell injury for arbitrary time-temperature profiles. Equations (1) and (2) describe the Arrhenius model:

$$\Omega\,(t) = \ln\left(\frac{C_0}{C(t)}\right) \qquad (1)$$

$$\Omega\,(t) = A\int_0^t e^{\frac{-E_a}{RT(\tau)}}\,d\tau,\; P = 100\,(1 - e^{-\Omega}) \qquad (2)$$

where C_o is the initial concentration of live cells prior to thermal exposure, $C(t)$ is the concentration of live cells after t seconds of heating, $\Omega(t)$ is a positive number representing extent of thermal damage at time t, A is the frequency factor (s^{-1}), E_a is the activation energy (J/mole), R is the universal gas constant (8.31 $J \cdot K^{-1} \cdot mol^{-1}$), and T is temperature [K]. The value of $\Omega(t)$ can be cast as a probability, P, of thermally induced injury.

$$S = e^{-kt} \tag{3}$$

$$\ln(k) = \ln(A) - \frac{E_a}{RT} \tag{4}$$

The parameters of the model, A and E_a, are cell line specific, and can be determined from experiments where cells are exposed to isothermal heating. As the first step, the rate of decay in cell viability *(k)* can be determined from viability measurements following heating as a function of time at multiple temperatures[54], by fitting *Equation (3)* to the experimentally measured cell survival, *S*. Then, using *Equation (4)*, the relationship between the natural logarithm of the constant *(k)* and the reciprocal of temperature (*1/T*) is plotted to find A and E_a from the slope and y-intercept of the fit, respectively.

3.2.4.2 Arrhenius injury model with time delay

As described by Feng *et al.* [176] and Pearce *et al.* [177], some cell lines initially exhibit a significant shoulder region where cell viability remains high until a threshold lethal thermal dose is attained. The conventional Arrhenius model may not accurately represent changes in cell viability for these cells. To address this limitation of the standard Arrhenius thermal injury model, an improved Arrhenius model was presented by Pearce

et al. [177], by adding a temperature-dependent time delay (t_d) using the slope (m) and intercept (b) to compensate for the measured viability data within the shoulder region:

$$t_d = b - m\,T \tag{5}$$

$$\Omega\,(t) = \begin{cases} 0, & t < t_d \\ A\int_0^t e^{\frac{-E_a}{R\,T(\tau)d\tau}}, & t \geq t_d \end{cases} \tag{6}$$

Where t represents total heat exposure duration, t_d denotes the time delay in seconds, T is the temperature in Kelvin, and m and b represent relevant coefficients obtained by slope and intercept of the equation, respectively. The ordinary Arrhenius injury process is initiated when $t > t_d$ and is calculated from that point forward.

3.2.4.3 Two-state injury model

Feng *et al.* [176] presented a two-state cell damage model under hyperthermia conditions which was reported to be in good agreement with experimental data. In their study, a general two-state model was proposed to characterize the entire cell population with two distinct and measurable subpopulations of cells, in which each cell is in one of the two substates, of either viable (live) or damaged (dead). The resulting cell viability can be expressed as follows:

$$C(\tau, \mathrm{T}) = \frac{e^{\left(\frac{-\Phi(\tau,\mathrm{T})}{\mathrm{KT}}\right)}}{1 + e^{\left(\frac{-\Phi(\tau,\mathrm{T})}{\mathrm{KT}}\right)}} \tag{7}$$

$$\ln\left(\frac{C(\tau,\mathrm{T})}{1 - C(\tau,\mathrm{T})}\right) = \left(\frac{\gamma}{\mathrm{T}}\right) - \beta - \alpha\tau \tag{8}$$

$$C(\tau, T) = \frac{e^{\left(\frac{\gamma}{T}\right)-\beta-\alpha\tau}}{1 + e^{\left(\frac{\gamma}{T}\right)-\beta-\alpha\tau}} \quad (9)$$

$\Phi(\tau, T)$ was defined as a function that is linear in exposure time τ when the temperature T is fixed and K is constant. In their study, *in vitro* cell viability data from hyperthermia experiments on human PC3 prostate cancer cells and normal RWPE-1 cells was compared against the two-state damage model and used to determine the parameters in the function $\Phi(\tau, T)$. This model requires three experimentally derived fit coefficients (α, β and γ) that were estimated using a standard bilinear least-squares regression algorithm. Finally, the fractional cell survival at any time point can be calculated using Equation *(9)*.

3.2.4.5 Determination of cell injury thermal dose (CEM_{43})

The Sapareto-Dewey thermal isoeffective dose model is a means to compare thermal damage accumulated after heating with an arbitrary time-temperature profile against t_{43}, the equivalent time needed to achieve the same level of damage when heated to 43°C (CEM 43) [184], [185]. t_{43} can be calculated with *Equation (10)*.

$$t_{43} = \sum_{i=1}^{n} t_i \, R_{CEM}^{(43-T_i)} \quad (10)$$

Where t_{43} is the cumulative number equivalent time (min) at 43°C, T_i is the temperature at the i-th time interval t_i, and R_{CEM} is 0.5 when T_i > 43°C and R_{CEM} is 0.25 when $T_i \leq$ 43°C. In *Equation (10)*, R_{CEM} represents the rate at which time taken to achieve a thermal damage isoeffect drops for each unit rise in temperature.

3.2.5 Model assessment

The accuracy of our developed injury predictive models was assessed on murine KPC pancreatic cancer cell lines that were exposed to non-isothermal heating to temperature in the range 47–51°C. A coupled electromagnetic–bioheat transfer computational model simulating microwave thermal ablation (MWA, 50 W, 10 min with a 14 G water-cooled applicator), as described in our prior studies[186], was used to identify time-temperature profiles at the periphery of the ablation zone. Detailed information regarding the heat transfer model, parameters and the numerical method is explained in the supplementary file.

Finally, in vitro hyperthermia experiments were performed to expose KPC cells to temperature profiles similar to those at the periphery of the ablation zone. The measured cell viability was compared against model predictions.

3.3 Results

3.3.1 Temperature profile in dummy well plates

Figure 3-2 shows the measured temperature profile inside five wells of the dummy 96-well plate during a 46°C hyperthermia exposure. Also illustrated are parameters used to quantitatively assess the heating profiles, including: ramp time, duration of the steady-state phase, target error, homogeneity of heating, and duration of the cool-down phase. Table 3-1 lists the mean values and ranges for each of these parameters across heating experiments for target setpoint temperatures of 42.5, 44, 46, and 50°C for all three cell lines considered in this study. Accuracy represents the error between the target temperature and mean recorded temperature based on five sealed thermocouples during constant heating phase, ramp time represents the time required to reach the target

temperature from physiological temperature (37°C), and cooling phase showing the time it takes to drop to physiological temperature from target temperature following hyperthermia exposure.

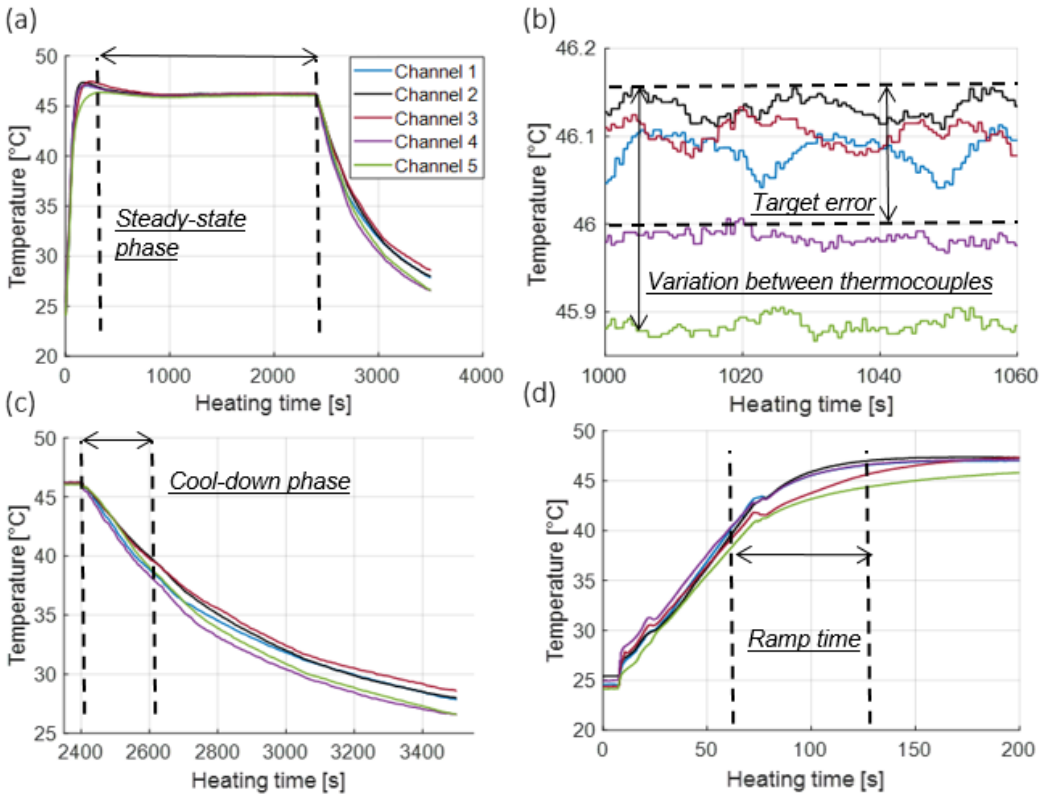

Figure 3- 2 (a) Illustration of temperature recorded by thermocouples in the dummy plate during a 46°C, 40 min hyperthermia exposure (b) illustration of temperatures over 1 min of the steady-state phase (c) illustration of temperatures during the cool-down phase, and (d) illustration of temperatures during the heat-up phase

Table 3- 1 Assessment of transient temperature profiles during *in vitro* heating

Target temperature [°C]	Mean error [°C] [min–max]	Mean variation between thermocouples [°C] [min–max]	Mean ramp time [s] [min–max]	Mean cool-down phase [s] [min–max]
42.5	0.2 [0.1–0.3]	0.2 [0.05–0.35]	85 [65–130]	130 [95–165]
44	0.25 [0.1–0.45]	0.35 [0.05–0.55]	75 [55–110]	320 [300–340]
46	0.25 [0.15–0.35]	0.15 [0.1–0.3]	75 [50–150]	267 [230–300]
50	0.18 [0.1–0.3]	0.2 [0.15–0.45]	80 [65–125]	320 [290–380]

3.3.2 Cell viability measurement

Figure 3-3 shows the measured cell viability assessed using the MTT assay for all three cell lines at 6 h and 24 h post hyperthermia.

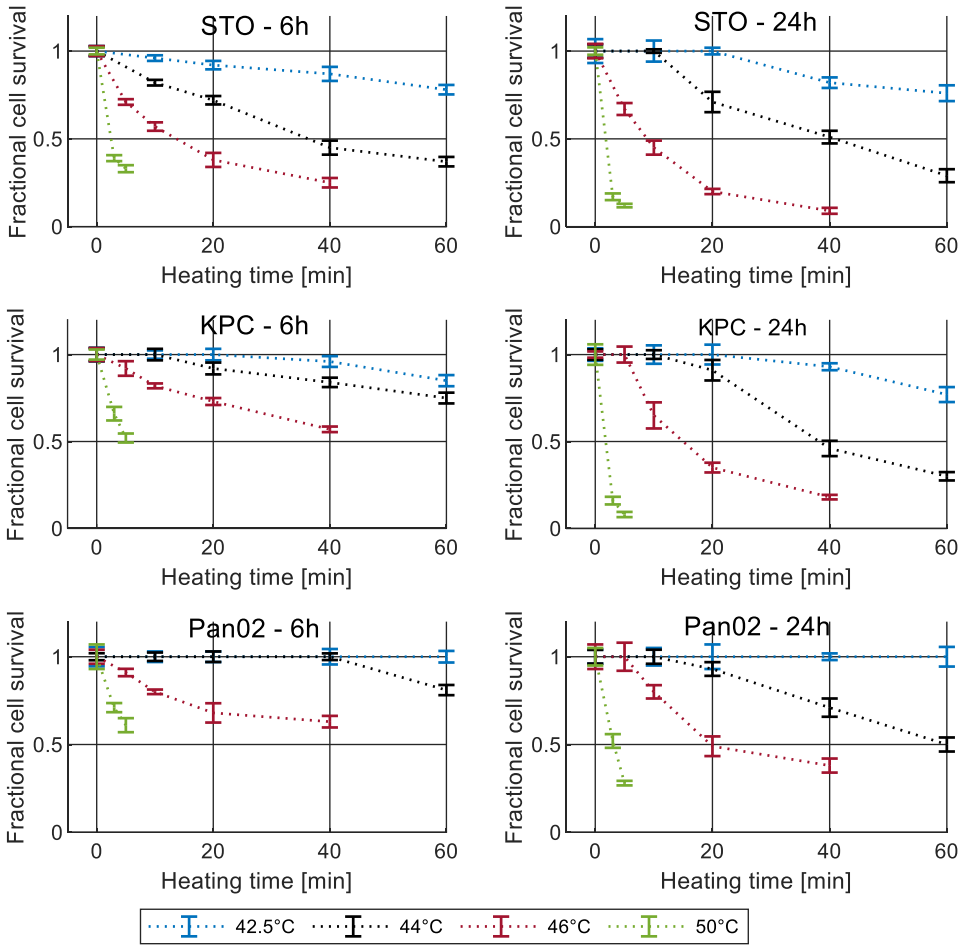

Figure 3- 3 Measured cell viability for all three cell lines normalized to 37°C control for different recovery times. Error bars represent one standard deviation

3.3.4 Arrhenius thermal injury models

Figure 3-4 (a) illustrates the relationship between ln (k) and 1/T for data measured at 24 h post-heating. The thermal damage kinetic coefficients A and E_a are determined from the intercept and slope, respectively, of the best-fit line to the data.

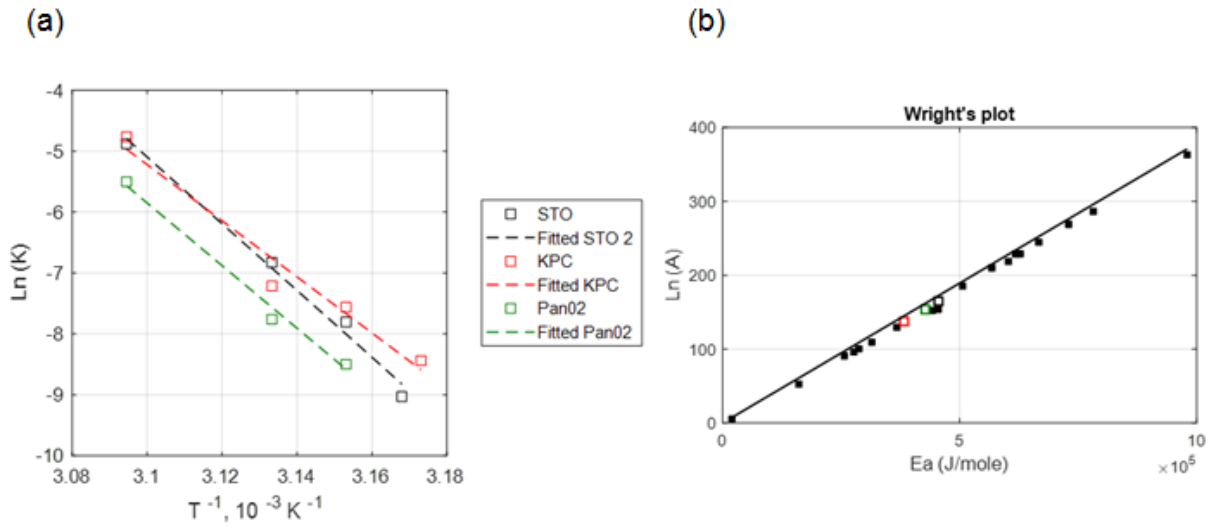

Figure 3- 4 (a) Correlation between the kinetic coefficients, ln (A) and Ea (KPC + Pano2 + STO), (b) comparison between the Wright's plot (relationship between Arrhenius coefficients based on the literature) shown in solid black square markers and obtained Arrhenius coefficients for three different cell lines in our study. Hollow black, red and green square markers indicate the obtained Arrhenius coefficients for STO, KPC and Pano2 cells, respectively at 24 h post treatment in our study

Table 3-2 lists the thermal damage kinetic parameters of E_a, A, and time delay parameters (m, b) that were calculated from the measured viability data 24 h post hyperthermia for each of the three cell types.

Table 3- 2 Obtained Arrhenius coefficients for all three cell lines

Cell type	E_a (J/mole)	A (s^{-1})	b	m
STO	455,630	$e^{164.79}$	127,460	400
KPC	383,112	$e^{137.63}$	254,920	800
Pan02	427,712	$e^{153.63}$	127,460	400

The coefficient of determination (R^2) for calculated kinetic parameters was in the range of 95–99%, indicating the suitability of the Arrhenius injury models for predicting the extent of heat induced cell injury. The measured and calculated damage were compared as shown in Figure 3-5 (a) and Figure 3-5 (b) for the simple Arrhenius model and the Arrhenius model with time delay, respectively. The Root Mean Square Error (RMSE) for the simple Arrhenius model and the Arrhenius thermal damage model with time delay were 12.24% and 8.48%, respectively.

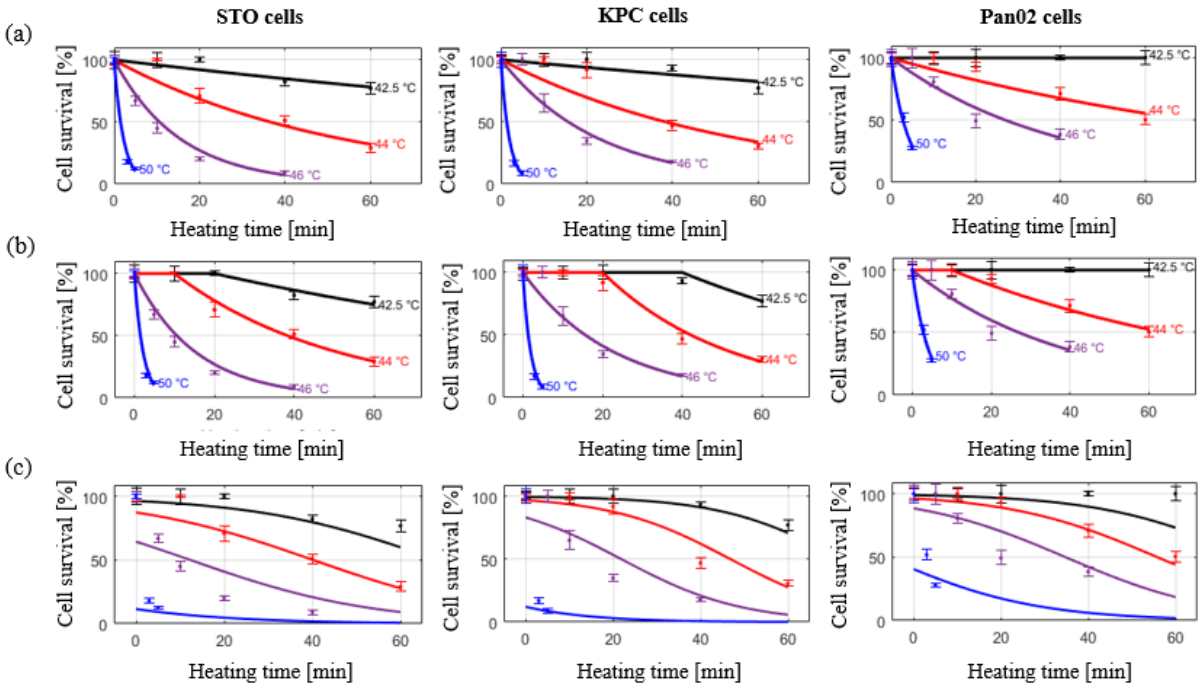

Figure 3- 5 Cell viability assessed at 24 h post in vitro hyperthermia exposure in KPC, Pan02, and STO cell lines. Markers indicate measured data points. (a) Solid lines represent the simple Arrhenius model; (b), solid lines represent the improved Arrhenius model with time delay; (c) solid lines represent the predictive two- state model

3.3.5 Two-state model of thermal injury

The measured and calculated damage were compared as described in Figure 3-5 (c). Cell viability data across all considered thermal doses in all three cell lines was investigated. RMSE for 6 h and 24 h recovery was 31.66% and 51.22%, respectively.

3.3.6 CEM_{43} calculation

Table 3-3 lists the R_{CEM} values measured in the present study and compares against R_{CEM} values for other cell types reported in the literature.

Table 3- 3 Calculated RCEM values for pancreatic cancer cells compared to other cell lines

Cell types in our study	R (T > 43 °C)	Cell type from the literature	R (T > 43°C)
STO (Mice fibroblasts)	0.607	Prostate tumor cells [57]	0.474 –50.624
KPC (Mice pancreatic tumor)	0.588	Baby hamster kidney cells [187]	0.550
Pan02 (Mice pancreatic tumor)	0.596	Porcine kidney cells [188]	0.596

Figure 3-6 (b) illustrates the mean value of recorded temperature based on five sealed thermocouples in the 96-well dummy plate as well as clinically relevant simulated temperature time history.

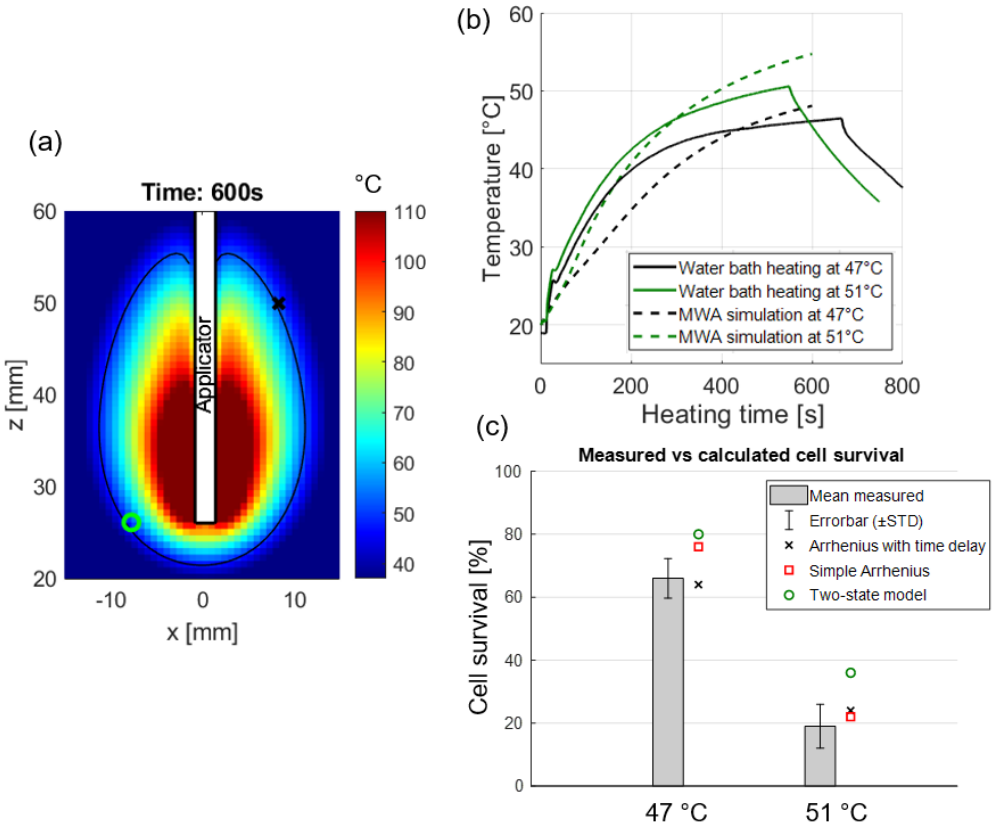

Figure 3- 6 (a) Simulated temperature map in a perfused pancreas tissue following 10 min of MWA, the white contour indicates the regions where 50°C was achieved while the green circle and red x illustrate two positions along the periphery of the ablation zone where time-temperature history over 10 min was analyzed; (b) temperature plots calculated from the bio-heat transfer model (shown in dashed lines) during 10 min of MWA as well as experimentally measured temperatures in water bath settings (solid lines); (c) comparison between measured and calculated cell survival

Figure 3-6 (c) shows the comparison between measured and calculated percentage of cell survival following hyperthermia exposures that were obtained by MTT assay and our developed predictive models, respectively.

3.4 Discussion

Knowledge of thermal sensitivity of representative target cells is informative for the design and optimization of thermal therapy protocols (i.e., temperature and heating time). Prior studies have investigated the kinetics of thermal injury of hepatocellular carcinoma, prostate cancer and renal carcinoma cells at temperatures from 37–63°C using different heating modalities [57], [72], [189], [190]. However, there have been few reports of the kinetics of thermal injury to pancreatic cancer cells.

Overall, we have shown that exposure to heat stress decreased cell viability in pancreatic cancer cells (i.e., KPC and Pan02), in agreement with other *in vitro* and *in vivo* studies examining hyperthermia's effectiveness as a potential therapeutic modality for treating pancreatic cancer [191]–[197]. As expected, the rate of decline in cell viability was more rapid as the applied temperature increased. KPC cells exhibited slightly greater resistance to thermal stress than the STO cells, indicated by their higher cell viabilities following heat treatment while Pan02 cells showed the most resistance to heat treatment. We quantified the cell viability at 6 h and 24 h post heat exposure to visualize the progression of heat-induced cell death over time. For all three cell lines, the viability continued to decrease dramatically at 24 h post exposure for high temperature exposures (i.e., T = 50°C, t > 5 min, T = 46°C, t > 20 min) compared to the viability at 6 h post exposure. Baumann and colleagues [198] also exposed pancreatic cancer cells (PANC-1 and BxPC-3) to 45-50°C for 5 min and measured the viability in different time points up to 7 days post exposure. The results were similar to ours, showing that near-complete cell death can occur following exposure to high temperatures (e.g., 50°C) where complete cell death was not observed immediately post treatment, but instead took longer to fully manifest *in*

vitro. Ludwig *et al.* [196] also assessed the effect of hyperthermia on BxPC-3 human pancreatic cancer cells and showed that exposure to hyperthermia treatment at 41°C and 43°C for 1 h have almost no impact on cell viability which was also reflected in our measured *in vitro* results.

Lage *et al.* [199] investigated the thermal sensitivity of human gastric (EPG85-257) and pancreatic carcinoma (EPP85-181) cell lines using water bath hyperthermia and calculated the Arrhenius injury model parameters. However, in their study, hyperthermia temperature was limited to 45°C. In the present study, the optimized values for activation energy (E_a) and frequency factor (A) in murine pancreatic cancer cells (i.e., KPC and Pan02) were calculated under near-isothermal heating conditions. The obtained kinetic coefficients were aligned with the Wright's line plot of the Arrhenius coefficients from Pearce [200]. The range of coefficient of determination in this study ($0.95 < R^2 < 0.98$, see Figure 3-4) for temperatures between 42.5–50°C is similar to the values derived from other hyperthermia studies ($0.95 < R^2$ for T > 40 °C) [54], [110], indicating the suitability of the Arrhenius model for predicting thermally-induced injury in pancreatic cancer cell lines *in vitro*.

Similar to O'Neill [178] and Feng [176] we observed initial shoulder region where cell viability was not affected at low temperatures with short durations, hence an improved Arrhenius model was used to provide a better fit since the traditional Arrhenius parameters (activation energy and frequency factor) calculated from low temperature, long duration exposures may not accurately predict cell death resulting from high temperature, low duration exposures [54], [72]. Calculated RMSE values for all three cell lines were considerably improved when switching to the improved Arrhenius model from

the traditional Arrhenius model. The thermal dose was also calculated using R_{CEM} that was derived from our temperature dependent cell survival data. The calculated R_{CEM} values for KPC and Pan02 cells were 0.588 and 0.596, respectively. This was in agreement with the results presented by Mouratidis *et al.* [151] where the R_{CEM} value for human colon cancer cell lines were calculated to be in the range of 0.5–0.53 at temperatures above 43°C.

We also assessed the suitability of the two-state injury model by Feng et al. [176] for predicting changes in viability following heating of pancreatic cancer cells. The results presented by Feng reasonably accurately demonstrates the shoulder region of cell viability curves in their study on PC3 cell lines. However, in our study a rather poor fit between the two-state model and our collected in vitro data was observed, as illustrated in Figure 3-5. This might be due to limited number of temperatures considered in this study, as the model relies on additional measured data at longer heating times where the viability tends to drop dramatically. Moreover, Feng et al. point out that the Arrhenius fit might actually provide a better estimation of cell viability at the higher temperatures where the shoulder region is not relevant. As previously described by Pearce [175], inclusion of more thermodynamic states may improve the accuracy of the two-state model.

Our study was limited to monolayer cell cultures, which may not accurately represent tumor cell response to heating *in vivo*. Previous *in vivo* studies have demonstrated a lower thermal threshold for destruction of tumors when compared to cell culture *in vitro* under thermal exposure profiles [57], [201], [202]. The thermal damage model coefficients reported in this manuscript may be used to guide the selection of time-temperature profiles that can be anticipated to yield a specified level of thermal damage in pancreatic

tumors, although caution should be taken when applying results to the clinical scenario given the use of murine cell lines in the present study. Notably, this study highlighted variable susceptibility of different cell lines to hyperthermic exposure. Pancreatic tumors exhibit relatively high inter-tumor and intra-tumor heterogeneity[203]; understanding of the differential thermal susceptibility of various cell populations to thermal exposure can inform prediction of the range of thermal damage levels anticipated for a given time-temperature profile delivered in the clinical scenario. Further, in the clinical setting, thermal profiles are likely to vary across the targeted tumor due to the constraints of practical heating technology. Given time-temperature profiles observed during heating that can be measured with MRI or other thermometry techniques, quantitative analysis of thermal damage profiles can be performed using the reported thermal damage coefficients. Such analyses, coupled with post-treatment imaging of the targeted tumors, can provide means to assess and interpret treatment response[204].

3.5 Conclusion

We measured the extent of thermal injury in murine pancreatic cancer cell lines after exposures to temperatures between 42.5–50°C as informed by *in vitro* studies, and derived thermal injury kinetic model parameters. Our results suggest that the improved Arrhenius model incorporating the time delay [177] to address the shoulder region is most suitable for use in mild hyperthermia therapies up to 60 min of heating. Finally, the accuracy of our developed injury predictive models were experimentally validated when cells were subjected to time-temperature profiles similar to those anticipated at the periphery of an ablation zone.

4. Modeling of temperature dependent release of Hsp70, Hsp90 and HMGB1 from pancreatic cancer cells

4.1 Introduction

Thermal therapies, including stand-alone thermal ablation and mild hyperthermia adjuvant to radiation/chemotherapy, are in varying stages of clinical use for treatment of tumors in diverse anatomic sites, and have been proposed as part of multi-modality treatment regimens for pancreatic cancer. Thermal therapies are known to induce expression of damage associated molecular patterns (DAMPs) at temperatures in the range 41– 43°C (i.e. in regions not heated to ablative temperatures)[42]. DAMPs such as heat shock protein (Hsp) family, high mobility group box 1 (HMGB1), and S100 proteins are increased following heat stress in the tumor region and are considered to have a pathogenic role in inflammatory diseases. Heat-induced expression of DAMPs may assist in refolding and repair of denatured proteins and aid in synthesis of new proteins in response to injury in cancer cells[205], [206]. Although Hsp family perform critical homeostasis function in normal cells, upregulation of Hsp in tumor cells due to the thermal stress may lead to poor treatment outcomes by enhancing tumor cell viability and imparting cellular resistance to chemotherapy and radiation treatments which may be employed in conjunction with hyperthermia [207], [208]. Gibbons *et al.*[209] hypothesized that increased expression of Hsp family may represent an important

survival factor in prostate cancer cell lines, and showed that heating cells results in the increased expression of Hsp family that is associated with resistance to radiation-induced apoptosis. For thermal ablation treatments, where heat is used as a stand-alone modality, tissue regions on the periphery of the ablation zone are within the hyperthermia range.

Extracellular and membrane-bound DAMPs are recognized as playing a role in tumor-immune system interactions [210]. There is growing evidence that hyperthermia stimulates the release of DAMPs, leading to immunomodulatory effects of on the tumor microenvironment (TME) such as reoxygenation and increased tumor perfusion, and increased pro-inflammatory cytokines[42], [211], [212]. Zawawi *et al.*[53] investigated the effects of thermal treatment on tumor regression in breast tumors and demonstrated that heating at 43°C may reduce tumor progression while significantly increasing the median survival of tumor-bearing mice. In their study, immunohistochemical analysis revealed a significant reduction in cells proliferation of heated tumors accompanied with abundance of Hsp70.

The objective of the studies presented in this chapter was to determine the relationship of hyperthermia exposures up to 50°C with extracellular release of HSP70, HSP90, and HMGB1 from pancreatic cancer cells with application to develop computational models of the effects of heat treatment on tumor-immune system interactions. *In vitro* heating experiments were performed on two murine pancreatic cancer cell lines (KPC and Pan02), and protein release measurements were assessed by ELISA. Pan02 cells are derived from C57BL/6 mice given orthotopic 3-methyl-cholanthrene and contain a loss of function mutation in the SMAD4 gene which is functionally similar to mutations in ~30% of human

pancreatic cancers[213], [214]. The KPC mouse is involved with a point mutation in the KRAS gene (KRASG12D) and is a well-established and clinically relevant model of pancreatic ductal adenocarcinoma (PDA) that shows many key features observed in human PDA. The measured data were incorporated with computational models of bioheat transfer.

4.2 Materials and methods

4.2.1 Cell culture

KPC cells were cultured with DMEM's medium (Gibco™ 11995065, Fisher Scientific, Hampton, NH, USA) with 10% fetal bovine serum (Corning™ 35015CV, Fisher Scientific) and 1% penicillin-streptomycin (Gibco™ 15140148). Pan02 cells were cultured with RPMI 1640 Medium (Gibco™ 11875093, Fisher Scientific) supplemented with sodium pyruvate and 10% fetal bovine serum. Cultures were maintained in a 37 °C, 5% CO_2 incubator in 75 cm^2 phenolic culture flasks. In preparation for hyperthermia treatment, cells were seeded in T300 culture plates at a density of ~20,000 cells/cm^2 at a volume of 30 mL medium/flask and maintained in a 37 °C, 5% CO_2 incubator for 24 h to allow cells to reach log phase prior to hyperthermia.

4.2.2 *In vitro* hyperthermia to monolayer cell culture flasks

To expose cancer cells to hyperthermia, the caps of the T300 culture flasks were sealed with parafilm and then immersed in temperature-controlled water baths. To assess temperatures during hyperthermia, transient temperature profiles were recorded using three T-type thermocouples embedded within different locations of a dummy flask that contained no cells while filled with 30 ml of water/flask. The dummy flask was immersed in water baths simultaneously with the cell-containing flask, thus providing a reasonable

assessment of the temperatures within the cell-containing flasks. Figure 4-1 illustrates the dummy flask design, including three thermocouples positioned and sealed within three locations.

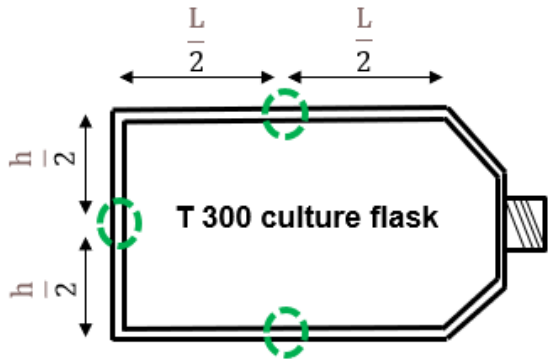

Figure 4- 1 Dummy flask design sealed with three thermocouples at the bottom of the flask for monitoring temperature distribution during hyperthermia exposures

Since the time to reach the setpoint temperature can be rather slow, we employed a two-step approach. First, both the cell-containing and dummy well plates were immersed in a water bath set at an elevated temperature of ~80°C. When the temperature recorded by thermocouples in the dummy flask reached within 0.5°C of the target temperature (i.e., 42.5, 44, 46, or 50°C), flasks were immediately transferred to another pre-heated water bath that was set to the desired target hyperthermic temperature for a predetermined duration in the range of 3–60 min. A USB thermocouple data acquisition module (TC-08 OMEGA) was used to record the temperature data from the thermocouples embedded within the dummy flask. Following hyperthermia treatment, parafilm was removed and the T300 culture flasks were returned to a 37 °C incubator for subsequent 24 h recovery of thermal injury. For each cell line, an additional flask

containing cells was also immersed in a 37°C water bath for the experimental durations considered in this study, providing a no-heat control.

4.2.3 Heat-induced protein release evaluation

After an incubation period of 24 h post-heating (shown to be effective evaluation periods for measuring protein expression[215]), the cell culture supernatant was collected from each culture flask and was centrifuged for 20 min at 1000 g at 5°C to remove the cell debris. The samples then were concentrated using 10k molecular-weight cut-offs centrifuge tubes. Finally, the concentrated samples were normalized using the whole protein assay (BCA). Similar to[216] enzyme-linked immunosorbent assay (ELISA) was performed to measure the concentration of Hsp70, Hsp90 and HMGB1 in concentrated supernatant samples. ELISA test is very sensitive and is used to detect and quantify substances, including antibodies, antigens, proteins, and hormones[217]. The detection of these products is done by antigen-antibody bindings to produce a measurable result. The measured optical density for each time-temperature combination was normalized to the optical density measured for no-heat controls immersed in a 37 °C water bath for the same time duration. The normalized values thus represent the average concentration of proteins across 3 flasks following hyperthermia exposure for each experimental group.

4.2.4 Determination of heat-induced thermal dose (CEM_{43})

The Sapareto–Dewey thermal isoeffective dose model is a means to compare thermal damage accumulated after heating with an arbitrary time-temperature profile against t_{43}, the equivalent time needed to achieve the same level of damage when heated to 43°C (CEM 43)[59], [125]. t_{43} can be calculated with Equation (1).

$$t_{43} = \sum_{i=1}^{n} t_i R_{CEM}^{(43-T_i)} \qquad (1)$$

where t_{43} is the cumulative number equivalent time (min) at 43 °C, T_i is the temperature at the i-th time interval t_i, and R_{CEM} is 0.5 when $T_i > 43$°C and R_{CEM} is 0.25 when $T_i \leq 43$°C. In Equation (10), R_{CEM} represents the rate at which time taken to achieve a thermal damage isoeffect drops for each unit rise in temperature.

4.2.5 Mathematical modeling of of heat-induced protein release

A thermal dose (CEM43) dependent model was developed to compute the extent of DAMPs release following hyperthermia exposures. This model represents a mixture of two Gaussian functions as illustrated in *equation (2)*.

$$Hsp(CEM43) = (\alpha 1 \times e^{-4\ln(2)\times\frac{(CEM43-\beta 1)^2}{(\gamma 1)^2}}) + (\alpha 2 \times e^{-4\ln(2)\times\frac{(CEM43-\beta 2)^2}{(\gamma 2)^2}}) \qquad (2)$$

Where the ($\alpha 1$, $\beta 1$, γ1) and ($\alpha 2$, $\beta 2$, γ2) are the optimized coefficients for the first and second Gaussian function, respectively by fitting the model to the experimentally measured *in vitro* data. This Gaussian function is expressed in terms of the full width at half maximum (FWHM) represented by γ, indicating that α is the height of the peak, and β is the center of the blob.

4.2.6 Integration of bioheat transfer in computational modeling

A bioheat transfer model was implemented to simulate temperature profiles within pancreatic tissue during microwave ablation with a 2.45 GHz water-cooled interstitial antenna using a coupled 3D electromagnetic-bioheat transfer model, as previously described[218]. The spatial profile of DAMPs release as a function of thermal dose was integrated with the bioheat transfer model. The time-harmonic electromagnetic wave equation *(Equations 3-4)* was solved to determine the spatial electromagnetic profile in tissue, and the associated electromagnetic power absorbed in tissue is given by Equation 4. The Pennes' bioheat transfer equation *(Equation (5))* was used to model spatial distribution of temperature at each time step.

$$\nabla^2\mathbf{E} + {\beta_0}^2(\varepsilon_r - \frac{j\sigma}{\omega\varepsilon_0})\mathbf{E} = 0 \qquad (3)$$

$$Q_{mw} = \frac{1}{2}\sigma \mid \mathbf{E} \mid^2 \qquad (4)$$

$$\rho c\frac{\partial T}{\partial t} = \nabla . k\nabla T + Q_{mw} - m_b c_b(T - T_b) \qquad (5)$$

Where ρc represents volumetric heat capacity [J/m3/K], k is thermal conductivity [W/m/K], T is the temperature in Kelvin, Q_{mw} is the time-averaged MW power absorbed in tissue [W/m3], σ [S/m] is electrical conductivity, c_b is blood specific heat capacity [J/kg/K], T_b is the temperature of inflowing arterial blood [K], β_0 is the wavenumber in free space [1/m], ε_r is the relative permittivity, ε_0 is the permittivity of free space [F/m], and ω is the angular frequency [rad/s]. Following each time step of the transient solver, tissue properties were updated based on the current temperature, and the electric field and associated power loss density were re-computed, before solving the bioheat transfer equation for the next time step. The simulation proceeded in such an iterative manner for

the 10 min of simulated MW ablation. Table 4-1 summarizes the nominal values of tissue physical properties (at 37°C) used in our study. The temperature dependent thermal properties of pancreatic tissue have been reported in the literature, and these temperature dependencies were incorporated within our simulations. To our knowledge, the temperature dependent dielectric properties of pancreatic tissue across the ablative temperature range have not been reported; in this study, we applied a similar temperature dependency to pancreatic tissue dielectric properties as has been reported for other tissue types such as liver and lung[219], [220]. The model was implemented with COMSOL Multiphysics v6.0.

Table 4- 1 Pancreas tissue biophysical properties employed in simulations

Tissue property	Nominal value at 37 °C	Reference for temperature dependency
Relative permittivity ε_r	57.2 [221]	Adapted from [219], [220]
Electrical conductivity σ	1.97 S/m [221]	Adapted from [219], [220]
Volumetric heat capacity ρc	3.73×10^6 J/m^3/K [222]	[222]
Thermal conductivity k	0.53 W/m/K [222]	[222]
Perfusion rate m_b	767 ml/min/kg [223]	Reduced to 0 above 60 °C to simulate microvascular stasis [224]

The initial temperature in all tissue domains was set to 37°C. We used a first order scattering boundary condition at simulation boundaries and thermal insulation boundary condition around the periphery of the tissue domain. The metallic parts of MW applicator are highly conductive and thus perfect electric conductor boundary condition was applied to those surfaces. Additionally, a convective heat-flux boundary condition shown in

Equation 6 was applied to the exterior surface of MW applicator shaft to account for the cooling effects of circulating water through the MW applicator.

$$q_0 = h(T_{ext} - T) \qquad (6)$$

Where heat transfer coefficient (h) and external temperature were selected to be 200 [W/ m^3/K] and 20 °C, respectively.

A non-uniform mesh with tetrahedral elements was employed in our study, with mesh density highest around the input port of MW applicator while being allowed to grow coarser around the applicator shaft. The maximal tetrahedral element edge length was 0.2 mm, 0.5 mm and 1–2 mm at MW input port, around the applicator shaft, and around tissue boundaries, respectively.

4.3 Results

4.3.1 Temperature profiles during *in vitro* heating experiments

Figure 4-2 shows the measured temperature profile inside the dummy T300 flask during hyperthermia exposures. Parameters used to quantitatively assess the heating profiles are also illustrated, including: ramp time, duration of the steady-state phase, target error, homogeneity of heating, and duration of the cool-down phase.

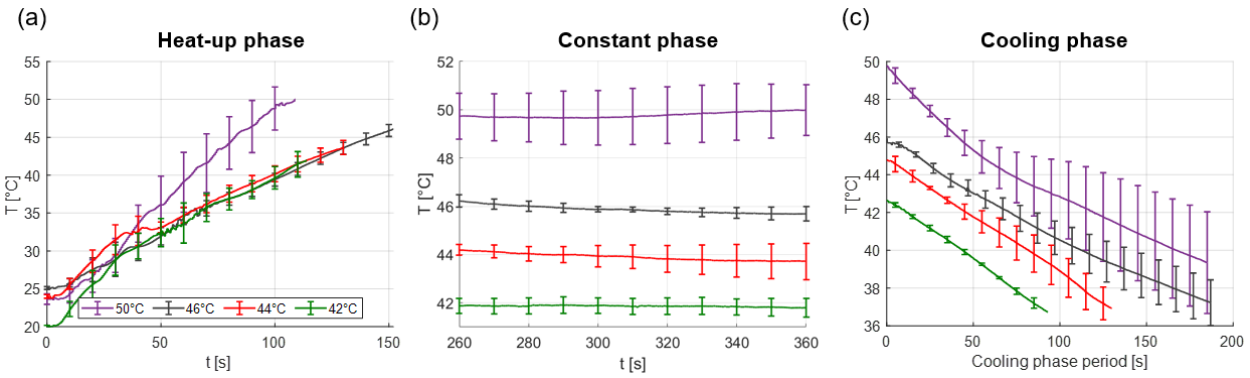

Figure 4- 2 Illustration of recorded temperature (mean ± STD) by thermocouples in the dummy flask during heat exposures to 42°C, 44°C, 46 °C and 50°C, (a) illustration of temperatures during the heat-up phase (b) illustration of temperatures over 100 seconds of the steady-state phase and (c) illustration of temperatures during the cool-down phase

Table 4-2 lists the mean values and ranges for each of these parameters across heating experiments for target setpoint temperatures of 42, 44, 46, and 50°C for all three cell lines considered in this study. Accuracy represents the error between the target temperature and mean recorded temperature based on five sealed thermocouples during the constant heating phase, ramp time represents the time required to reach the target temperature from physiological temperature (37°C), and the cooling phase represents the time it takes to drop to physiological temperature from target temperature following hyperthermia exposure. These data demonstrate the suitability of the experimental setup for assessment of DAMPs release following exposures to temperatures up to 50°C.

Table 4- 2 Assessment of transient temperature profiles during in vitro heating

Target temperature [℃]	Mean error [℃] [min–max]	Mean variation between thermocouples [℃] [min–max]	Mean ramp time [s] [min–max]	Mean cool-down phase [s] [min–max]
42	0.2 [0.1–0.3]	0.2 [0.05–0.35]	85 [65–130]	130 [95–165]
44	0.25 [0.1–0.45]	0.35 [0.05–0.55]	75 [55–110]	320 [300–340]
46	0.25 [0.15–0.35]	0.15 [0.1–0.3]	75 [50–150]	267 [230–300]
50	0.18 [0.1–0.3]	0.2 [0.15–0.45]	80 [65–125]	320 [290–380]

4.3.2 Measurement of heat-induced DAMPs release

Figure 4-3 and figure 4-4 show the measured protein release from the supernatant samples obtained from ELISA for two murine cancer cell 24 h post hyperthermia.

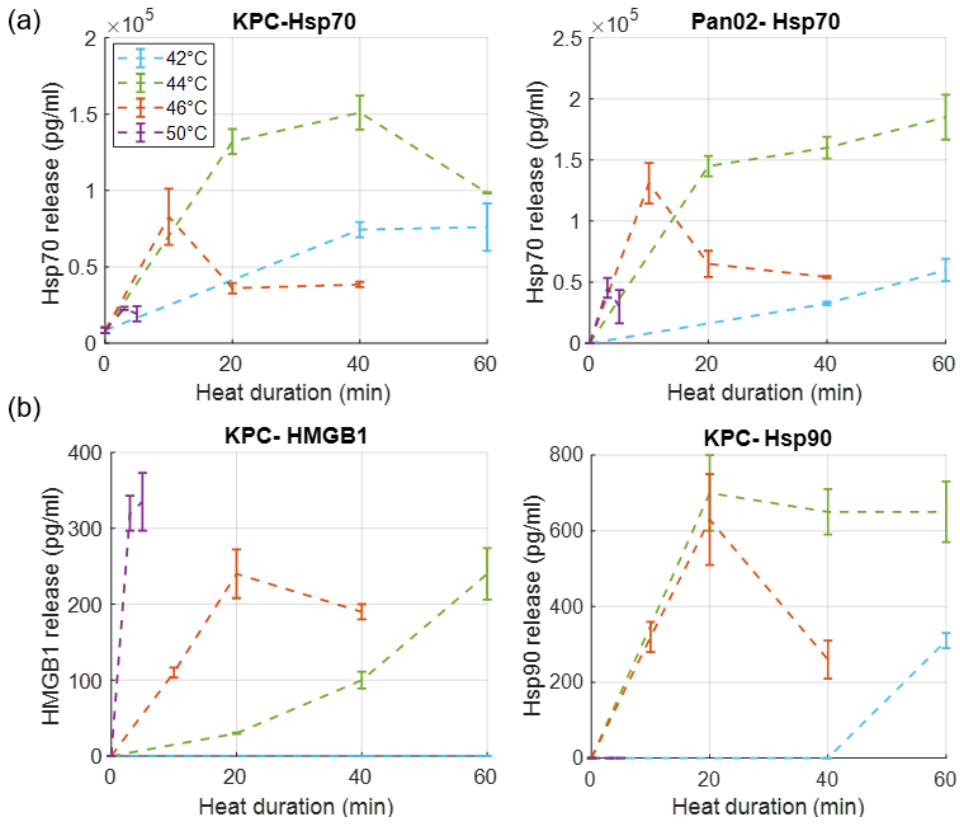

Figure 4- 3 (a) Heat induced extracellular release of Hsp70 within concentrated supernatant samples as a function of heating time and temperature determined with ELISA and evaluated at 24 h post heat exposure for KPC and Pan02 cells. The values were normalized based on the total protein assay. (b) heat induced extracellular release of Hsp90 and HMGB1 within concentrated KPC supernatant samples

As illustrated in figure 4-3, greater than 15-fold increase in HSP70 levels was induced in both KPC and Pan02 cells compared to non-heated controls, with maximum release of 140-200 ng/ml occurring at 44°C, 40-60 min while diminishing substantially at higher temperature exposures of 46°C and 50°C in both cell types. Maximum extracellular release of HSP90 and HMGB1 from KPC cells was observed at 44°C, 20 min for HSP90 (700 pg/ml) and at 50°C, 5 min for HMGB1 (350 pg/ml). There was no

detectable release of HSP90 and HMGB1 from Pan02 cells at all temperatures considered in this study, suggesting Pan02 cells greater robustness to thermal stress compared to KPC cells.

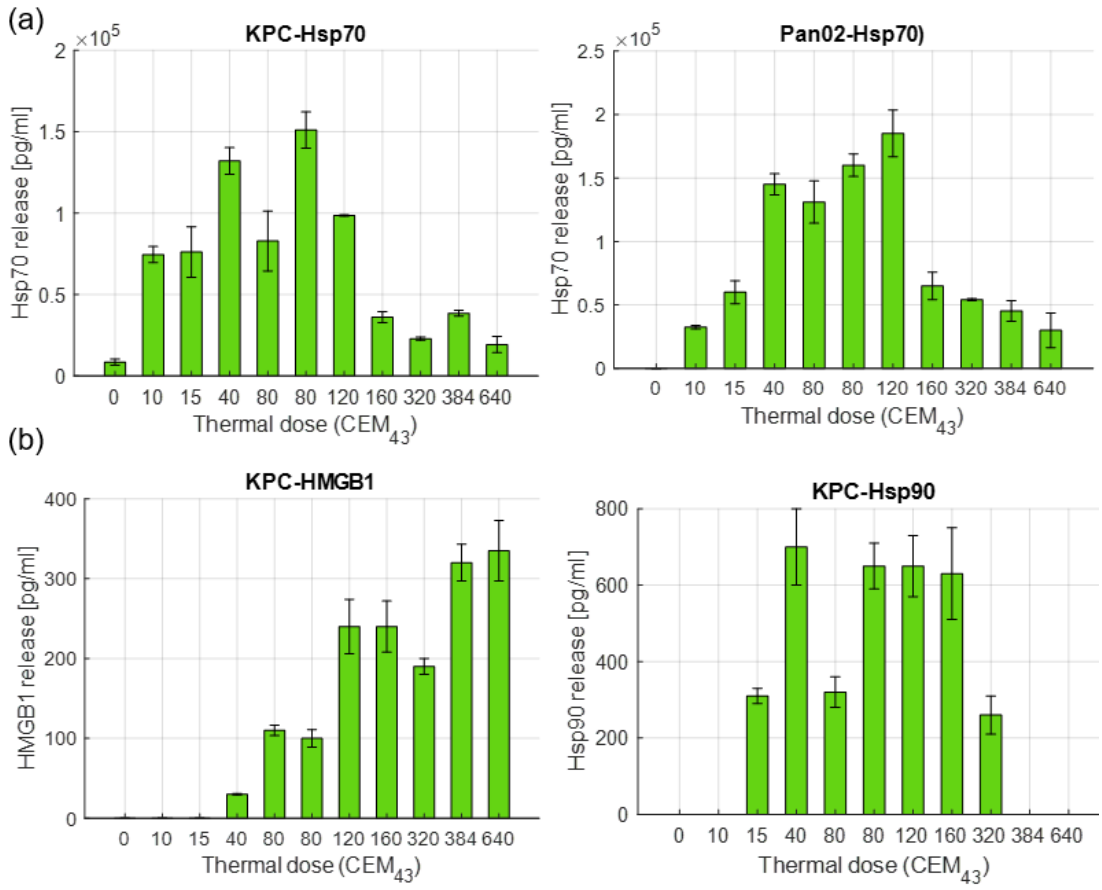

Figure 4- 4 (a) Heat induced extracellular release of Hsp70 within concentrated supernatant samples as a function of thermal dosage (CEM 43) determined with ELISA and evaluated at 24 h post heat exposure for KPC and Pan02 cells. The values were normalized based on the total protein assay. (b) heat induced extracellular release of Hsp90 and HMGB1 within concentrated KPC supernatant samples

Figure 4-5 represents the relationship between the DAMPs release from KPC cells and the cell viability following hyperthermia treatments.

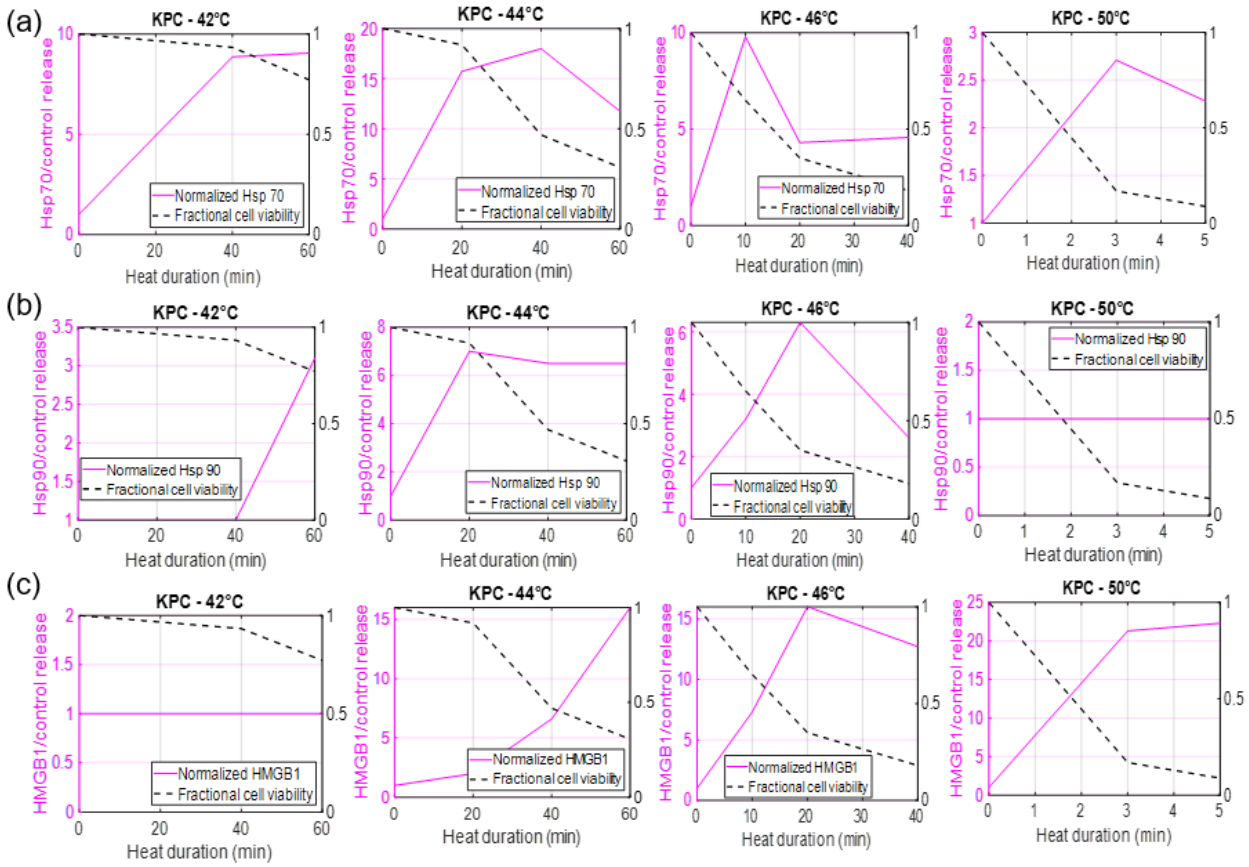

Figure 4- 5 (a) Comparison of measured cell viability with (a) Hsp70 in KPC cells (b) Hsp90 and HMGB1 in KPC cells and (c) HMGB1 in KPC cells as a function of temperature and heating duration

4.3.3 Mathematical modeling of heat-induced DAMPs release

Figure 4-6 represents the comparison between the experimental measurements and the mixture of Gaussians fit as a function of thermal dose.

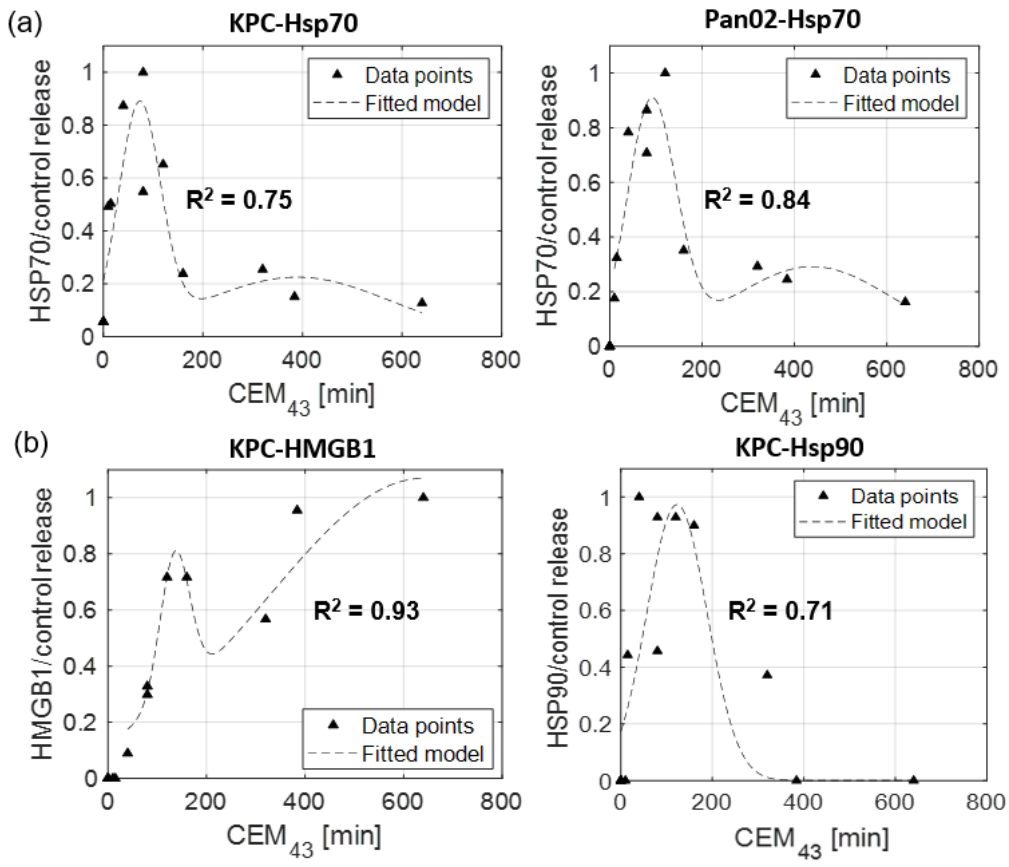

Figure 4- 6 Comparison between measured and model-predicted (a) Hsp70 release from KPC and Pan02 cells and (b) Hsp90 and HMGB1 release from KPC cells

Table 4-3 lists the optimized model parameters that were calculated from the measured DAMPs release data 24 h post hyperthermia for KPC and Pan02 cells.

Table 4- 3 Optimized coefficients for predictive DAMPs release model

Cell line/protein	$\alpha 1$	$\beta 1$	$\gamma 1$	$\alpha 2$	$\beta 2$	$\gamma 2$
KPC/Hsp70	*0.83*	*72.67*	*98.71*	*0.22*	*388.63*	*440*
KPC/Hsp90	*0.98*	*129.81*	*162.77*	*0*	*0*	*0*
KPC/HMGB1	*0.51*	*135.9*	*70.84*	*1.06*	*640*	*739.58*
Pan02/Hsp70	*0.86*	*90.58*	*123.99*	*0.29*	*438.71*	*413.26*

4.3.4 Simulation results for heat-induced DAMPs release

Figures 4-7 and 4-8 illustrate the simulated DAMPs release following 5-10 min of MW ablation between 10 W and 40 W in pancreatic tumors.

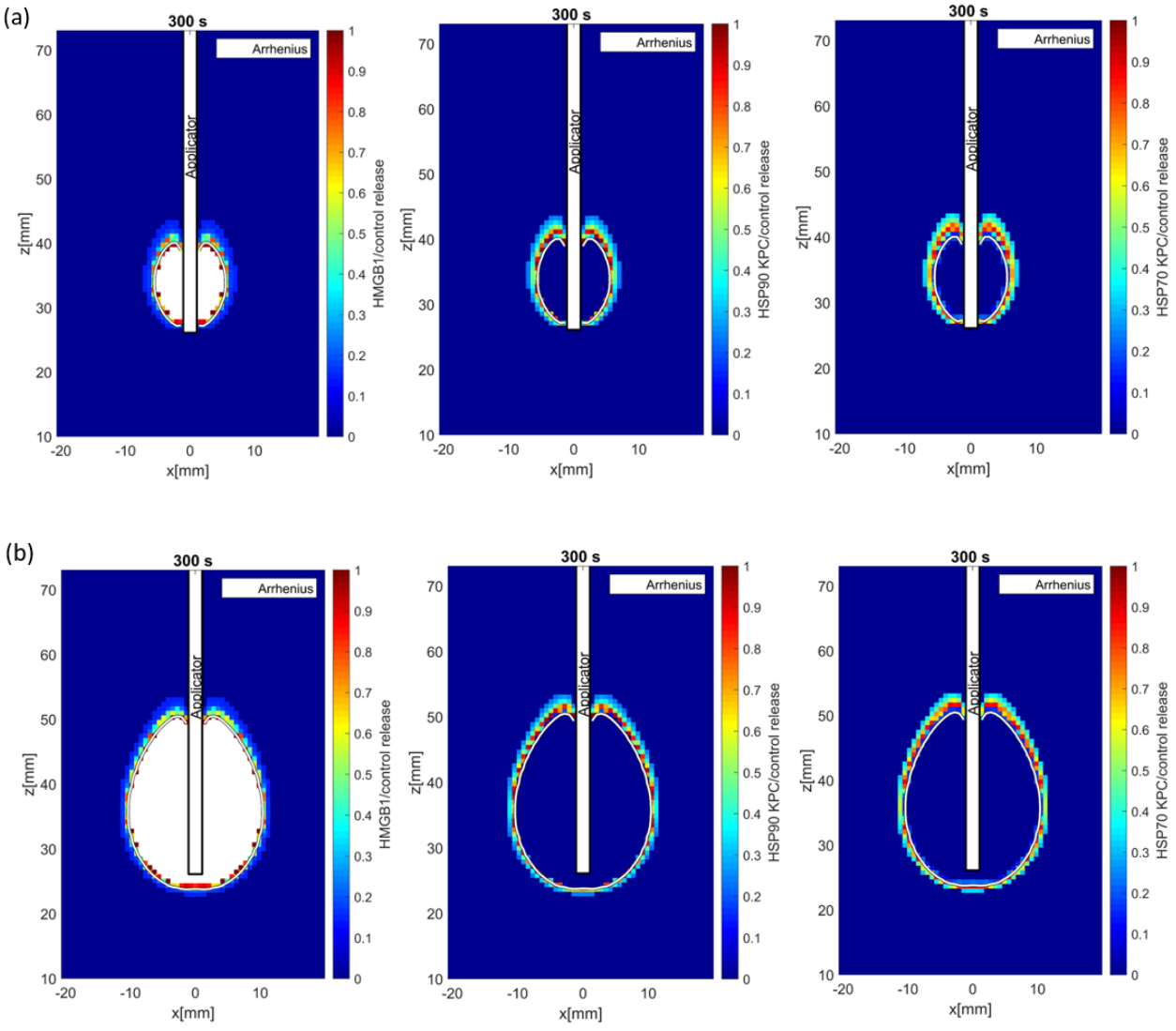

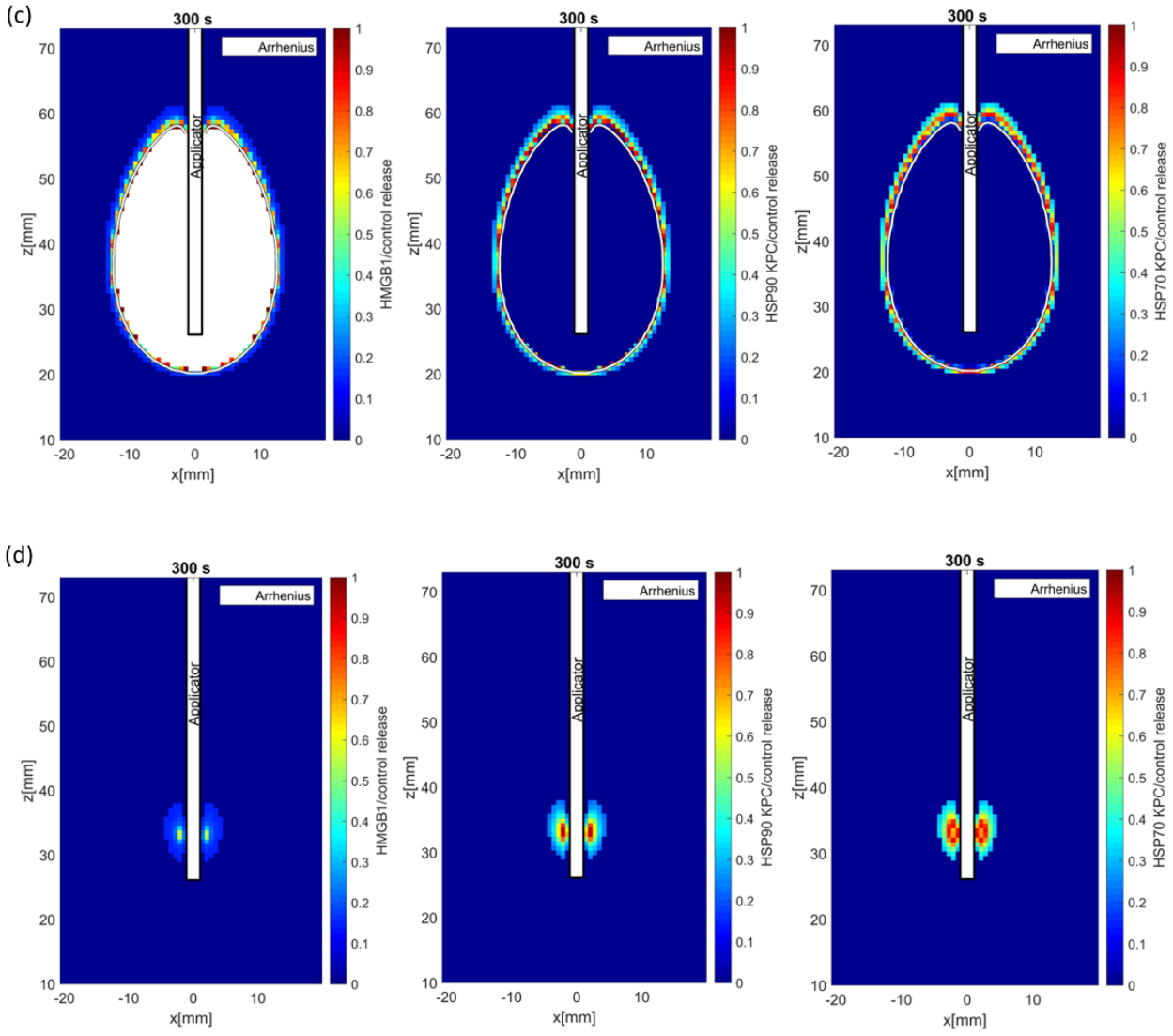

Figure 4- 7 Simulation results for DAMPs release where white contour indicates the extent of Arrhenius based thermal injury and the white pixels indicate uncertainty of the simulated data due to lack of experimental in vitro data: (a) simulation result for DAMPs distribution following 10 W applied power during microwave thermal ablation for 5 min, (b) simulation result for DAMPs distribution following 20 W applied power during microwave thermal ablation for 5 min (c) simulation result for DAMPs distribution following 40 W applied power during microwave thermal ablation for 5 min (d) simulation result for DAMPs distribution following 20 W

applied power while limiting the maximum tissue temperature to 50°C during microwave thermal ablation for 5 min

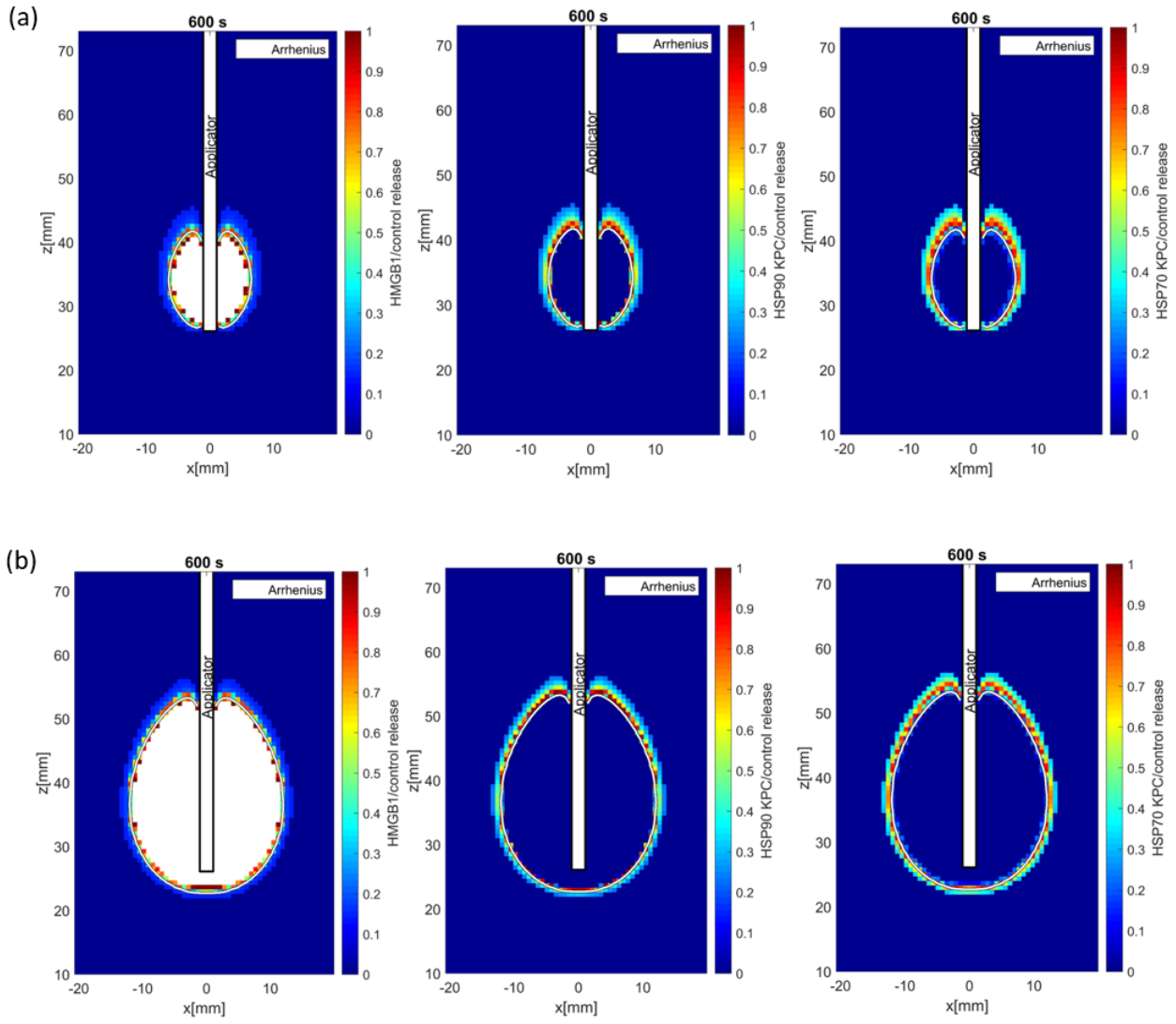

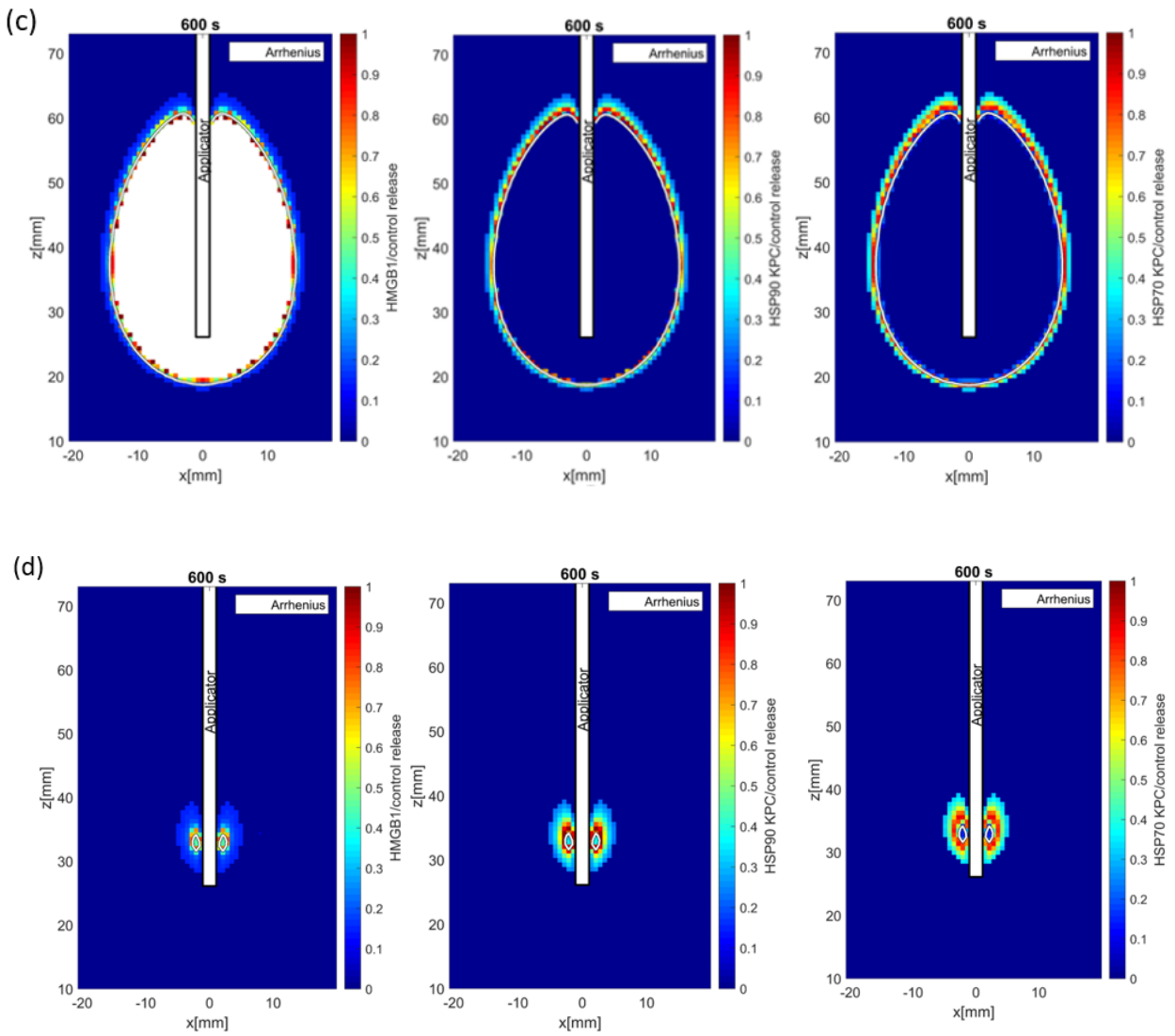

Figure 4- 8 Simulation results for DAMPs release where white contour indicates the extent of Arrhenius based thermal injury and the white pixels indicate uncertainty of the simulated data due to lack of experimental in vitro data: (a) simulation result for DAMPs distribution following 10 W applied power during microwave thermal ablation for 10 min, (b) simulation result for DAMPs distribution following 20 W applied power during microwave thermal ablation for 10 min (c) simulation result for DAMPs distribution following 40 W applied power during microwave thermal ablation for 10 min (d) simulation result for DAMPs distribution following 20 W

applied power while limiting the maximum tissue temperature to 50°C during microwave thermal ablation for 10 min

4.4 Discussion

Knowledge of heat bioeffects is informative for the design and optimization of thermal therapy protocols (i.e., temperature and heating time). Prior studies have investigated the heat-induced expression of DAMPs in prostate cancer cells[174], kidney cancer cells[225], mesenchymal stem cells[226] and breast cancer cells[227] using different heating modalities, however, there are few reports on studies investigating the heat-induced release of DAMPs such as Hsp family and HMGB1 proteins from pancreatic cancer cells.

In the present study, significant Hsp70 release (greater than 15 folds) was induced following heat stress, whereas Hsp90 and HMGB1 elevations were minimal. The most dramatic increase in DAMPs release was associated with Hsp70, indicating that it may play a significant role in modulating tumor-immune system interactions following heat stress in pancreatic cancer cells as previously reported by Giri *et al.*[228]. As expected, the rate of increase in Hsp70, Hsp90 and HMGB1 release from pancreatic cancer cells was more rapid as the applied temperature increased. Pan02 cells exhibited slightly greater resistance to thermal stress than the KPC cells, indicated by not only their higher cell viabilities but also lower release of DAMPs following heat stress. The release of heat-induced Hsp family from pancreatic cancer cells showed a thermal dose (CEM43) dependent Gaussian trend, increasing in mid thermal doses while significantly diminishing to the basal levels when higher thermal dose is achieved. This was in agreement with the results presented by Rylander *et al.*[174], where the Hsp70 expression

levels from PC3 prostate cancer cells increased at temperatures in the range 44-46°C for 10 min while diminishing at longer heating durations. Forika *et al.*[229] also reported on upregulation of Hsp70 from pancreatic cancer cells (Panc1) at 42°C for 60 min which is in agreement with the results presented in our study.

Knowledge of the relationship between temperature distribution during thermal treatment of tumors in clinical settings and spatial Hsp distribution *in vivo* may be valuable for predicting regions of treatment success or failure. The use of computational models for predicting the extent of the ablation zone for planning ablation procedures has been extensively studied. This work illustrates how current modeling platforms can be extended to include the dynamics of DAMPs release following treatments, and thus contribute to planning of ablation treatments performed together with immunotherapy. [230]–[232]. As illustrated in figure 4-7, Hsp70 and Hsp90 release distribution was primarily observed at the boundary of thermal ablation. The microwave heating applicator was surrounded by two distinct zones including the central and periphery zone. The central zone was associated with coagulative necrosis where high thermal doses were achieved, while the periphery zone at the boundary of thermal ablation was associated with sub-lethal reversible thermal injury and showed increased levels of Hsp release, potentially resulting in interaction with antigen presenting cells, attracting immune cells and stimulating the anti-tumor immune response. This was in agreement with the results presented by Li *et al.*[233], where a radiofrequency ablation (RFA) device was used for thermal ablation of the lung cancer. Zhou *et al.*[234] also confirmed this hypothesis in their study, where significant upregulation of Hsp70 and $CD^{+}8$ T cells was observed in residual liver tumor regions following incomplete radiofrequency tumor ablation.

The mechanism as to how the DAMPs are released (e.g., through extracellular vesicles (EVs) or binding to receptors) from stressed/dying cells and how these molecules are engaged in activating the anti-tumor immune response was not investigated in the present study, constituting an area of interest for future further in-depth investigation. Another subject of widespread investigation is how thermal therapies can induce a systemic tumor-specific response in patients with pancreatic cancer, potentially enhancing tumor susceptibility to immunotherapeutic agents by blocking the immunosuppressive signals deep in the tumor, and enhancing tumor blood perfusion for immune cells infiltration which leads to reduced risk of cancer metastasis, increased drug accumulation and improved anti-tumor immune response in patients with pancreatic cancer.

4.5 Conclusion

We have measured the release of thermally induced HSP70, HSP90, and HMGB1 from murine pancreatic cancer cells after exposure to temperatures in the range 42–50°C as informed by *in vitro* studies and derived heat-induced DAMPs release model parameters. The model coefficients reported in this study may enable development of predictive models for protein release as a function of thermal stress to design more effective hyperthermia treatments. These models may inform future studies investigating how thermal therapy influences cancer immunotherapy approaches.

5. A microwave patch antenna for hyperthermia treatment of cell culture models

5.1 Introduction

Thermal therapy is a type of medical treatment where the target tumor tissue is exposed to temperatures above the body temperature for therapeutic benefits. Several clinical studies have highlighted the benefits of thermal ablation in patients with pancreatic cancer by heating tumors to cytotoxic temperatures of 50°C or higher for 4 minutes or longer[23]–[26]. Over the last decade, minimally invasive thermal therapy either as a stand-alone ablative or as an adjuvant to chemoradiotherapy has received substantial attention for the treatment of many local malignancies[21]. Aside from ablative cytotoxic effects in thermal ablation (T>50°C) modalities, it has been shown that mild hyperthermia exposure (39–42°C) for >30 min, induces many biological effects such as tumor reoxygenation[31], [32], anti-tumor immunity[33]–[35], improved drug delivery[36], [37], sensitization of cancer cells to DNA damaging agents[38], [39], and activating promoters for gene therapy[40], [41].

Thermal therapy can be induced to the target regions through a wide range of energy modalities such as non-invasive high-intensity ultrasound (HIFU[17], image guided minimally invasive percutaneous or endoscopically delivered microwave (MW) electromagnetic heating[18], [235], lasers[19], and radiofrequency (RF) currents[20],

[236], [237]. According to the clinical data, preoperative hyperthermia combined with radiation and/or chemotherapy with surgery may benefit patients with locally advanced cancer by decreasing local recurrence and improving the survival rate within patients.

Bioeffects of heating including changes in cell viability, stress protein expression, and other biomarkers have been defined as a complex function of heat intensity and duration of heating (i.e., time - temperature history) which may vary across all tissue types. Overgaard et al. showed that the time–temperature relationship follows a variable pattern, indicating that each 0.5°C drop in the temperature below 43°C and each 1°C reduction above 43°C will double the treatment time required to obtain an equivalent therapeutic effect[126]. Cell/tissue-specific parameters for these models can be determined from experiments on cells *in vitro* [54]. Hence, *in vitro* studies are needed to study the bioeffects of heat on cellular levels and to develop tools that allow us to simulate clinical trials with sufficient details to study treatment outcomes in different conditions. By using these predictive models, clinicians can test and predict treatment failures in simulations rather than in patients, resulting in improved treatment design and reduced risks and side effects.

While *in vitro* experiments on monolayers are informative, 3D cell cultures (e.g., spheroid, organoids) provide an experimental platform accommodating multiple cell types in an environment that may be more representative of tumors *in vivo*. Furthermore, while the water-bath based *in vitro* platform applied for monolayers is well suited to achieving near-uniform temperature profiles, *in vivo* delivery of hyperthermia often yields a gradient of temperatures that is not achieved through water-bath based heating.

Several MW patch antennas have been reported for use in biological tissues including a microstrip C patch antenna[238], a microstrip contact flexible antenna[239], a rectangular patch antenna[240] and annular ring patch antenna[241]. However, there have been very few studies focusing on developing hyperthermia microstrip platform for *in vitro* use.

The objective of the present study was to develop an *in vitro* platform for exposing cells in 3D culture (co-culture of multiple cell populations) to MW hyperthermia. The MW patch antenna includes a printed patch antenna and associated thermal management elements and is optimized for resonance at 2.45 GHz. Numerical simulations for antenna design optimization are carried out using electromagnetic (EM) simulation software. The developed MW hyperthermia platform was used to study changes in gene expression profile of a 3D culture of PDAC cancer cells (Pan02) and fibroblasts. This non-contact microwave heating approach may help enable additional studies for exploring the bioeffects of heat on cancer cells.

5.2 Materials and Methods

5.2.1 Antenna and fixture design

Figure 5-1 shows the sketch of MW patch antenna with coaxial feeding designed in present study as well as the fixture design for placement of the MW applicator for *in vitro* use. Coaxial feeding is one of the most common techniques used for feeding the MW patch antennas. As illustrated in figure 5-1, the inner conductor of the coaxial connector extends through the dielectric and is connected to the radiating metal patch, while the outer conductor is connected to the ground plane.

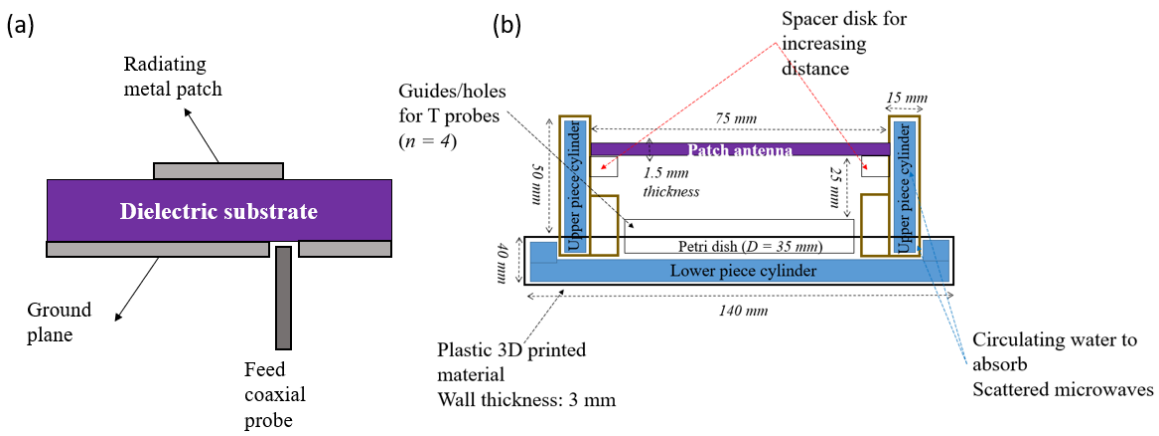

Figure 5- 1 Sketch design of (a) MW patch antenna sketch with coaxial feeding, (b) designed fixture for use of the patch antenna in a 35 mm petri dish

The antenna was designed on 1.5 mm thick substrate with 75 mm of length which includes a radiating metal patch, ground metal plane, dielectric substrate, and a coaxial feed line. The coaxial feeding cable consists of outer and inner conductors soldered to the ground plane and the radiating metal patch, respectively. The functioning and performance of microstrip antenna is dependent on the geometry of the patch, feeding position, substrate properties and feeding techniques[242]. Rectangular shape patch is the most popular type of patch used in microstrip antennas which was used in our study. The dielectric substrate should ideally offer low dielectric constant, low loss coefficient and sufficient thickness for better radiation efficiency and bandwidth. However, there is a trade-off between these properties since although dielectric substrates with lower loss provide better performance in radiation, they also result in larger devices in size with narrower bandwidths[243], [244].

The patch geometrical parameters including dimensions of the rectangular patch (L and W) as well as the thickness of the substrate (h) were obtained and evaluated based on the relative permittivity of the manufacturer's substrate (Table 5-1).

Table 5- 1 Optimized design parameters

Parameters	Value
$2.2 < \varepsilon_r < 12$	4.5
$\boldsymbol{\lambda} = \frac{C}{f \times \sqrt{\varepsilon r}}$	6 cm
$L = \frac{\lambda}{2}$	3 cm
$0.003\,\boldsymbol{\lambda}$ < Dielectric thickness < $0.05\,\boldsymbol{\lambda}$	1.5 mm

Where the ε_r represents the relative permittivity (i.e., dielectric constant) of the substrate obtained from the manufacturer's website, C is the speed of light (3×10^8 m/s), f is the resonance frequency (2.45 GHz) and L is the length of the patch, resulting in a $3\ cm \times 3\ cm$ dimensions.

The position of the feed can also be altered to control the input impedance which will affect the overall performance of the antenna. The optimized feed position was determined using parametric sweeps in the numerical simulations to meet the design objective of resonance at 2.45 GHz with best impedance matching as illustrated in figure 5-2.

5.2.2 Electromagnetic simulations

Electromagnetic (EM) simulations were carried out which solves time-harmonic wave equation for the electric field. Heat transfer module was also used in the simulation to calculate for time-dependent temperature distribution throughout the culture media inside the petri dish during MW heating. The dielectric properties used in the numerical simulations are tabulated in Table 5-2. The boundaries of the computational domain were assigned as perfectly matched layers to absorb the scattered radiated EM fields in frequency-domain. Swept frequency simulations were carried out for finding the optimal coaxial feeding position on the radiating metal patch at 2.45 GHz.

Table 5- 2 Dielectric properties at 2.45 GHz

Materials	Relative permittivity	Electrical conductivity (S/m)
Fr 14 (antenna substrate)	4.3	0.0117
Copper (metal patch and ground plane)	1	60000000
Water (medium)	78	1.31
Air (gap between antenna and media)	1	0
Teflon (feed insulation layer)	2.1	0

Figure 5-2 shows the developed geometry of the model along with the top view of the MW patch antenna for finding the optimal feeding position.

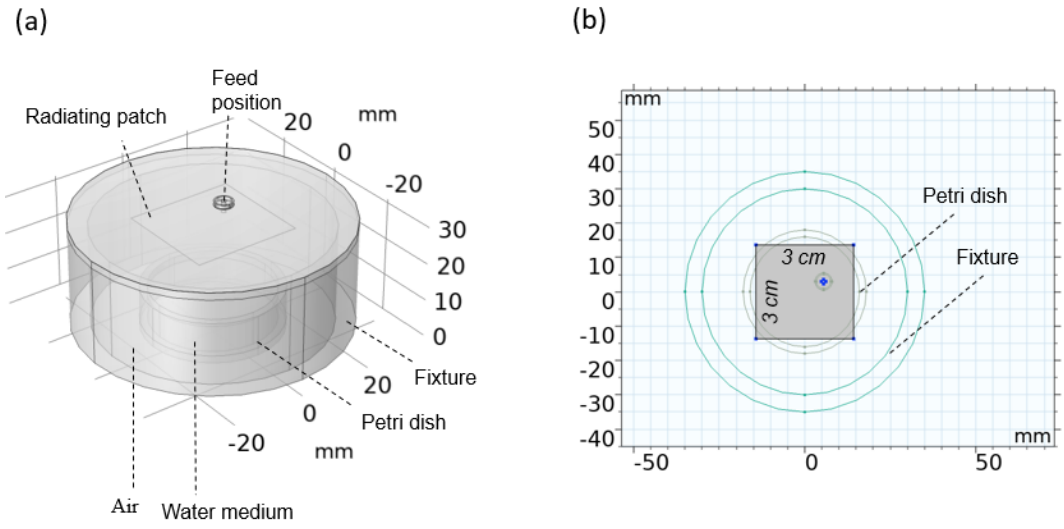

Figure 5- 2 (a) Developed model geometry including the radiating metal patch, feeding port, the fixture and petri dish containing water (b) top view of the MW patch antenna placed on the designed fixture for heating the petri dish

5.2.3 Antenna and fixture fabrication

Figure 5-3 illustrates the 3D printed fixture along with the fabricated antenna suitable for heating the cell culture contents in the 35 mm petri dish. A dummy dish was introduced to the system which contains water to monitor the temperature during MW hyperthermia exposure (see figure 5-3). To avoid measurement errors due to interference in electromagnetic environment, fiber optic temperature sensors were used instead of thermocouples in this study.

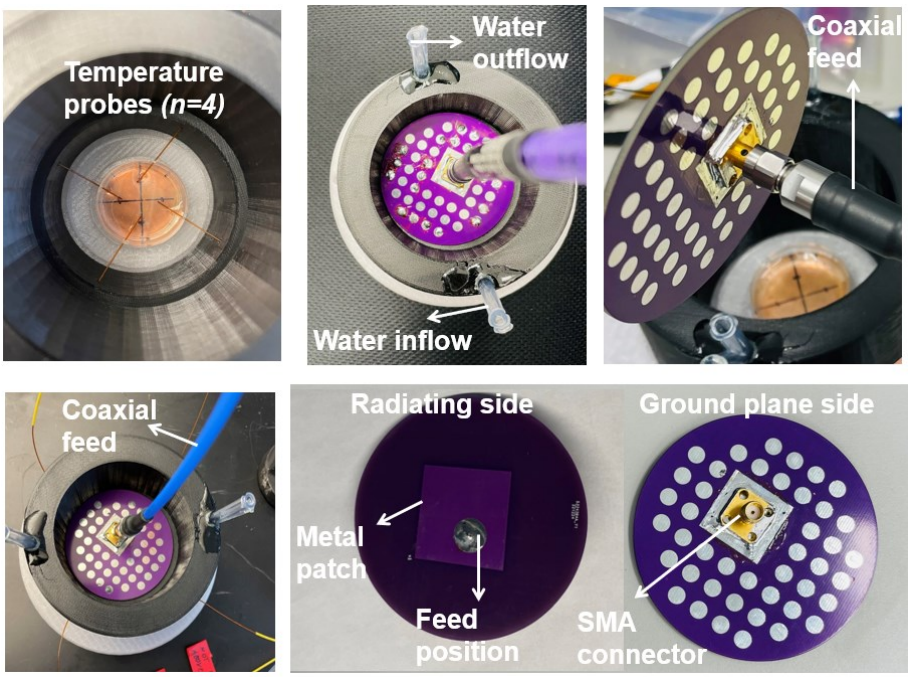

Figure 5- 3 Experimental photograph of the patch antenna long with the fixture and the placed temperature sensors (n=4) to monitor the temperature in the dummy petri dish filled with 5 ml volume of water during MW hyperthermia exposure

To assess temperatures during MW hyperthermia, transient temperature profiles were recorded using four fiber optic temperature sensors radially placed within the dummy petri dish that was filled with 5 mL of water. The fixture was equipped with inflow and outflow ports to be filled with water and to absorb scattered electromagnetic radiation.

5.2.4 3D cell culture hyperthermia platform

Since the designed MW hyperthermia system requires to remove the petri dish lid for more efficient heating, the heat experiments were performed on 3D culture dishes inside the biosafety cabinet, avoiding contamination from the air. Figure 5-4 illustrates the experimental setup for heating 3D cell culture dishes inside a biosafety cabinet.

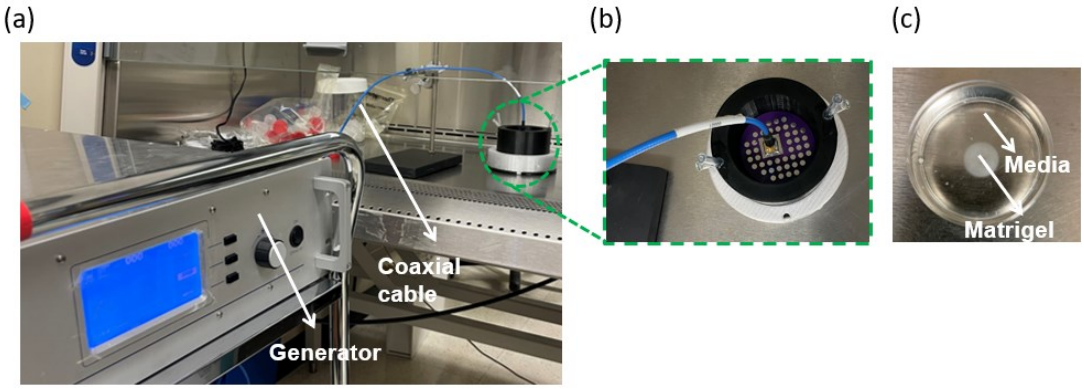

Figure 5- 4 (a) Experimental setup of MW hyperthermia treatment in vitro including the generator, coaxial cable and MW antenna (b) top view of the MW antenna placed in the designed fixture (c) 3D cultured sample containing Pan02 and STO cells inside the 35 mm petri dish

5.3 Results and discussion

5.3.1 Simulation results

5.3.1.1 S parameters and electric field

Figure 5-5 shows simulated electric field intensity near developed patch antenna and heating losses profile in medium inside the petri dish.

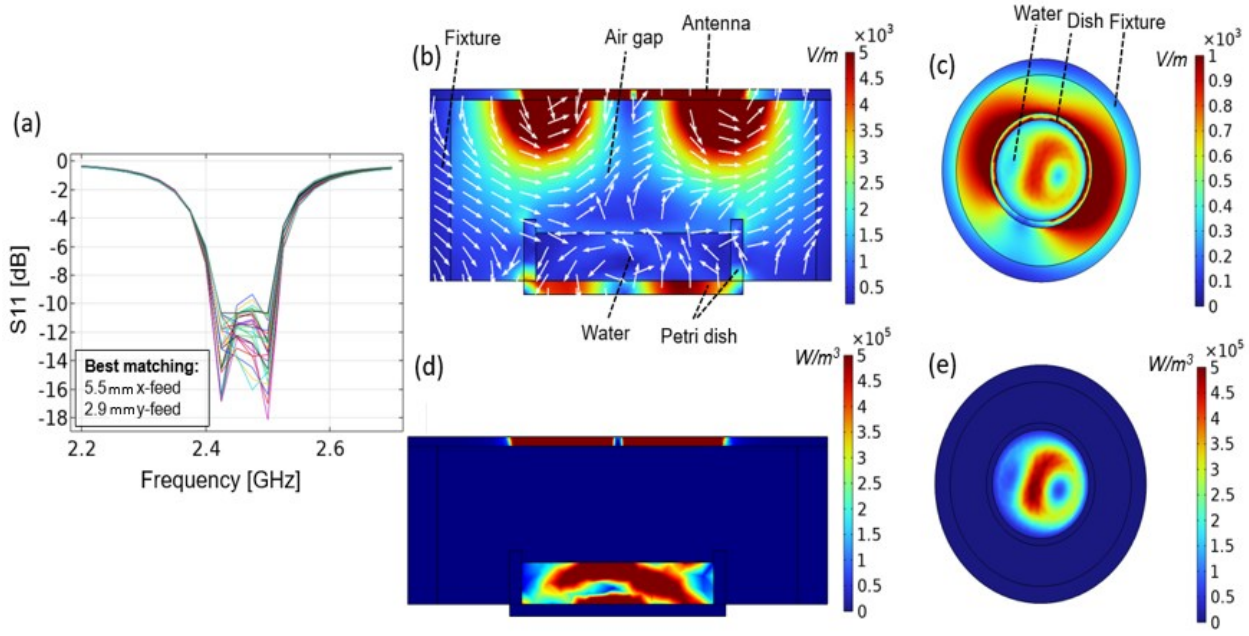

Figure 5- 5 Simulated electrical results of designed patch antenna (a) S11 calculation for different feeding positions located on the metal patch (b) and (c) respectively represent the sagittal and axial plane of the electric field norm with white arrows indicating the orientation of electric field vector, while (d) and (e) respectively represent the sagittal and axial plane of the power loss density when 20 W power is applied at the feeding port of the antenna

Figure 5-5 (a) shows simulated reflection coefficients (s11) profiles of developed patch antenna as a function of various positions of coaxial feeding point, ranging from 5.1 mm to 5.9 mm offset from center of radiating patch in x-axis and 2.7 mm to 3.5 mm in y-axis. Overall, the central frequency of -10 dB bandwidth of the antenna is located at 2.45GHz. By off-setting feeding point of antenna in both x and y axis, the bandwidth of antenna was enhanced by introducing 2 resonant peeks with slightly different resonant

frequencies with their average value being the target frequency of 2.45 GHz. Such enhancement is necessary to ensure that manufactured antenna will retain the acceptable matching (<8 dB) at 2.45 GHz even with dimensions which could change within manufacturer tolerance range. Figures 5-5 (b-c) show the distribution of electric field within the fixture in space between patch antenna and petri-dish filled with medium. It is illustrated that due to the high relative permittivity of medium with respect to surrounding materials, only a portion of electric field propagates inside media. However, in figure 5-5 (d-e) it is visible that the electric field in media still results in appreciable heating (W/m3), raising the temperature to ablative temperature range. As shown in figure 5-5 (d) and (e), the MW electromagnetic radiation at 2.45 GHz frequency can efficiently generate heat by rapid changes in the electric field within lossy media (water).

5.3.1.2 Temperature map simulation

Figure 5-6 shows the simulated temperature distribution uniformity throughout the heated media (water) inside the petri dish when 20 W power was applied at the antenna's port for 10 min.

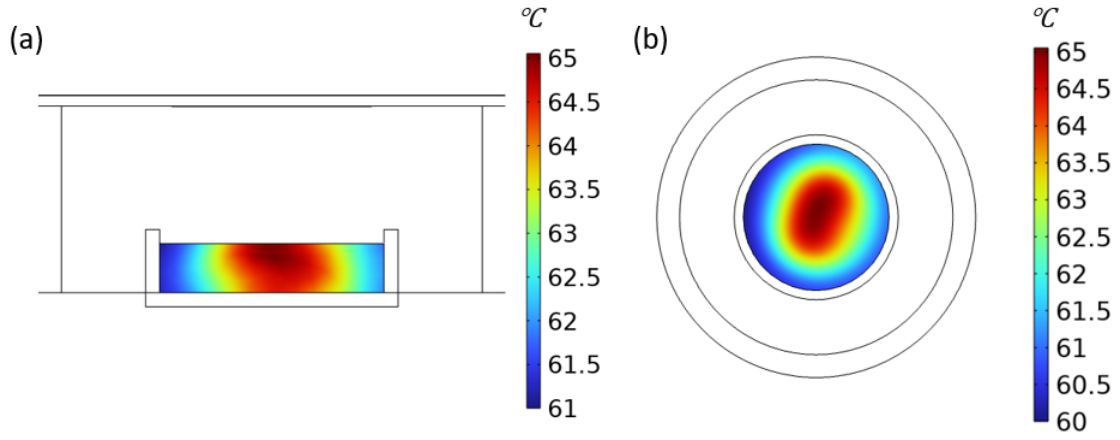

Figure 5- 6 Numerical simulation-based temperature evaluation (a) vertically and (b) 2D plane of top surface of the media (Water) following 10 min of heating at 20 W applied power at the antenna's feeding port

Simulation results demonstrated that a uniform thermal field can be obtained vertically (bottom to top variation) with slight variation of ±0.4°C as shown in figure 5-6 (a). Despite the uniformity of temperature distribution vertically, simulation results revealed that non-uniform temperature distribution (~5°C) was achieved at the top surface inside the petri dish (figure 5-6 (b)).

5.3.2 Experimental results

5.3.2.1 S parameters

Figure 5-7 illustrates the experimentally measured return loss (S11) of two fabricated antennas in our study.

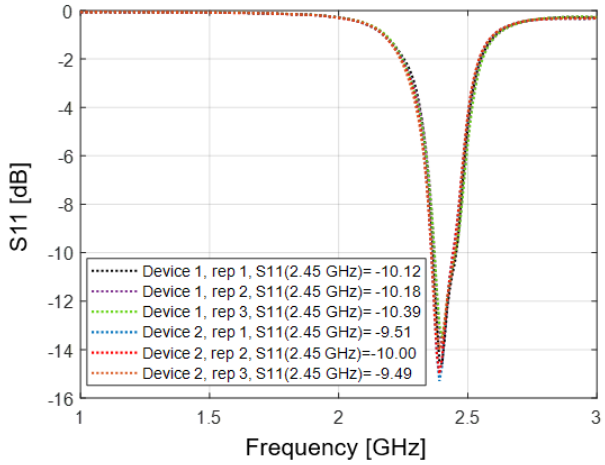

Figure 5- 7 Measured S11 parameters for two fabricated antennas with three repetitions (n=3) per antenna

As illustrated in figure 5-7, the S_{11} at the operating frequency of 2.45 GHz was measured to be -15 dB across all measurements, meaning that around 97% of the received power goes through the antenna while only 3% of the power will be reflected. This measurement agrees with a previous study where a compact C-type MW patch antenna was designed for heating the tissues at 434 MHz frequency. In their study, the measured S_{11} was reported to be approximately -15 dB[245]. Furthermore, the consistency of the fabricated antennas with regards to their electrical performance was confirmed in the present study.

5.3.2.2 Temperature measurement

Figure 5-8 shows the obtained temperature profiles obtained during MW hyperthermia exposures for different power and time combinations.

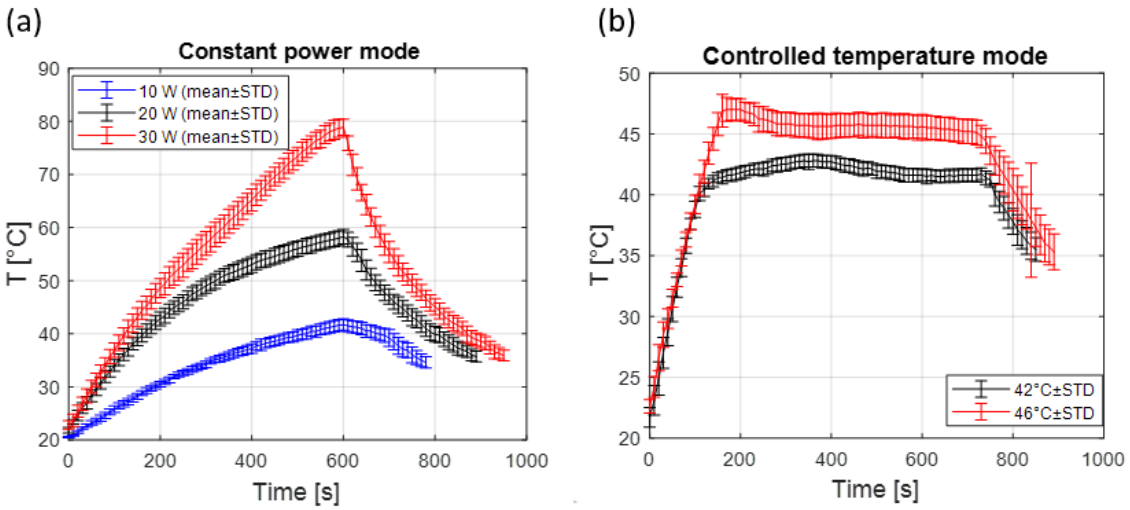

Figure 5- 8 Transient temperature profile of (a) constant MW power heating mode (b) controlled temperature MW heating mode measured by five temperature sensors during the ramping, 10 min of steady-state and cooling phase

Temperature inside the media samples can be controlled by adjusting the intensity (radiating power) and duration (exposure time) of MW radiation. Similar to Asano *et al.*[114], the power was adjusted at varied output levels to maintain the sample temperature inside the petri dish. Ramp time represents the time required to reach the target temperature from physiological temperature (37°C), and the cooling phase represents the time it takes to drop to physiological temperature from target temperature following hyperthermia exposure.

To heat the 3D culture samples inside the petri dish, the initial generated power was selected to be 40 W for 2 min and 2.5 min for reaching to 42°C and 46°C controlled heating, respectively. This was followed by 20 min of temperature-controlled MW heating by reducing the power level from 40 W to 3 W and 5 W for 42°C and 46°C, respectively. Finally, the power was set to zero until the temperature dropped to 37°C (cooling phase). The ramping as well as cooling phase in present study were significantly shorter than the

raping and cooling phase that were obtained from the *in vitro* MW hyperthermia device presented by kiourti *et al.*[111]. This indicates a major advantage of the developed MW hyperthermia system in present study since longer durations at hyperthermic temperature range during raping or cooling phase may significantly affect the cellular/molecular response.

5.4 Conclusion

A 2.45 GHz MW patch antenna is developed that is suitable for hyperthermia treatment of monolayer/3D cell culture inside the petri dish. Simulation results indicate that the designed patch antenna can provide heating with ~5°C temperature uniformity throughout the 5 mL volume of culture media. Experimental results showed that that the 2.45 GHz patch antenna is simple and easy to use for heating the cell culture samples to desired hyperthermic temperature with a fast-ramping time of ~1 min while maintaining the target temperature in the steady-state phase during the hyperthermia exposure.

References

[1] "Pancreatic Cancer." https://www.cancer.org/cancer/pancreatic-cancer.html (accessed Mar. 07, 2023).

[2] N. Khalaf, H. B. El-Serag, H. R. Abrams, and A. P. Thrift, "Burden of Pancreatic Cancer: From Epidemiology to Practice," *Clin Gastroenterol Hepatol*, vol. 19, no. 5, pp. 876–884, May 2021, doi: 10.1016/j.cgh.2020.02.054.

[3] S. Menini, C. Iacobini, M. Vitale, C. Pesce, and G. Pugliese, "Diabetes and Pancreatic Cancer—A Dangerous Liaison Relying on Carbonyl Stress," *Cancers (Basel)*, vol. 13, no. 2, p. 313, Jan. 2021, doi: 10.3390/cancers13020313.

[4] J. D. Mizrahi, R. Surana, J. W. Valle, and R. T. Shroff, "Pancreatic cancer," *Lancet*, vol. 395, no. 10242, pp. 2008–2020, Jun. 2020, doi: 10.1016/S0140-6736(20)30974-0.

[5] "Pancreatic Cancer Surgery," Oct. 13, 2021. https://www.hopkinsmedicine.org/health/conditions-and-diseases/pancreatic-cancer/pancreatic-cancer-surgery (accessed Mar. 21, 2023).

[6] K. D. Lillemoe, S. Kaushal, J. L. Cameron, T. A. Sohn, H. A. Pitt, and C. J. Yeo, "Distal Pancreatectomy: Indications and Outcomes in 235 Patients," *Annals of Surgery*, vol. 229, no. 5, p. 693, May 1999, doi: 10.1097/00000658-199905000-00012.

[7] C.-K. Ho, J. Kleeff, H. Friess, and M. W. Büchler, "Complications of pancreatic surgery," *HPB (Oxford)*, vol. 7, no. 2, pp. 99–108, 2005, doi: 10.1080/13651820510028936.

[8] A. L. Blackford, M. I. Canto, A. P. Klein, R. H. Hruban, and M. Goggins, "Recent Trends in the Incidence and Survival of Stage 1A Pancreatic Cancer: A Surveillance, Epidemiology, and End Results Analysis," *J Natl Cancer Inst*, vol. 112, no. 11, pp. 1162–1169, Nov. 2020, doi: 10.1093/jnci/djaa004.

[9] D. Ansari, A. Gustafsson, and R. Andersson, "Update on the management of pancreatic cancer: Surgery is not enough," *World J Gastroenterol*, vol. 21, no. 11, pp. 3157–3165, Mar. 2015, doi: 10.3748/wjg.v21.i11.3157.

[10] L. Huang *et al.*, "Resection of pancreatic cancer in Europe and USA: an international large-scale study highlighting large variations," *Gut*, vol. 68, no. 1, pp. 130–139, Jan. 2019, doi: 10.1136/gutjnl-2017-314828.

[11] W. Park, A. Chawla, and E. M. O'Reilly, "Pancreatic Cancer: A Review," *JAMA*, vol. 326, no. 9, pp. 851–862, Sep. 2021, doi: 10.1001/jama.2021.13027.

[12] B. Chauffert *et al.*, "Phase III trial comparing intensive induction chemoradiotherapy (60 Gy, infusional 5-FU and intermittent cisplatin) followed by maintenance gemcitabine with gemcitabine alone for locally advanced unresectable pancreatic cancer. Definitive results of the 2000–01 FFCD/SFRO study," *Annals of Oncology*, vol. 19, no. 9, pp. 1592–1599, Sep. 2008, doi: 10.1093/annonc/mdn281.

[13] P. J. Loehrer *et al.*, "Gemcitabine Alone Versus Gemcitabine Plus Radiotherapy in Patients With Locally Advanced Pancreatic Cancer: An Eastern Cooperative Oncology Group Trial," *J Clin Oncol*, vol. 29, no. 31, pp. 4105–4112, Nov. 2011, doi: 10.1200/JCO.2011.34.8904.

[14] D. J. Klaassen, J. M. MacIntyre, G. E. Catton, P. F. Engstrom, and C. G. Moertel, "Treatment of locally unresectable cancer of the stomach and pancreas: a randomized comparison of 5-fluorouracil alone with radiation plus concurrent and maintenance 5-fluorouracil--an Eastern Cooperative Oncology Group study.," *JCO*, vol. 3, no. 3, pp. 373–378, Mar. 1985, doi: 10.1200/JCO.1985.3.3.373.

[15] J. Tao *et al.*, "Targeting hypoxic tumor microenvironment in pancreatic cancer," *Journal of Hematology & Oncology*, vol. 14, no. 1, p. 14, Jan. 2021, doi: 10.1186/s13045-020-01030-w.

[16] S. Yang, Q. Liu, and Q. Liao, "Tumor-Associated Macrophages in Pancreatic Ductal Adenocarcinoma: Origin, Polarization, Function, and Reprogramming," *Front Cell Dev Biol*, vol. 8, p. 607209, Jan. 2021, doi: 10.3389/fcell.2020.607209.

[17] Y.-F. Zhou, “High intensity focused ultrasound in clinical tumor ablation,” *World J Clin Oncol*, vol. 2, no. 1, pp. 8–27, Jan. 2011, doi: 10.5306/wjco.v2.i1.8.
[18] G. Carrafiello *et al.*, “Microwave tumors ablation: Principles, clinical applications and review of preliminary experiences,” *International Journal of Surgery*, vol. 6, pp. S65–S69, Jan. 2008, doi: 10.1016/j.ijsu.2008.12.028.
[19] R. J. Stafford, D. Fuentes, A. A. Elliott, J. S. Weinberg, and K. Ahrar, “Laser-induced thermal therapy for tumor ablation,” *Crit Rev Biomed Eng*, vol. 38, no. 1, pp. 79–100, 2010, doi: 10.1615/critrevbiomedeng.v38.i1.70.
[20] “Radiofrequency ablation for cancer - Mayo Clinic.” https://www.mayoclinic.org/tests-procedures/radiofrequency-ablation/about/pac-20385270 (accessed Mar. 21, 2023).
[21] D. T. Debela *et al.*, “New approaches and procedures for cancer treatment: Current perspectives,” *SAGE Open Med*, vol. 9, p. 20503121211034370, Aug. 2021, doi: 10.1177/20503121211034366.
[22] D. Korenaga *et al.*, “Preoperative hyperthermia combined with chemotherapy and radiotherapy for patients with rectal carcinoma may prevent early local pelvic recurrence,” *Int J Colorect Dis*, vol. 7, no. 4, pp. 206–209, Dec. 1992, doi: 10.1007/BF00341222.
[23] W. Farmer, G. Hannon, S. Ghosh, and A. Prina-Mello, “Thermal ablation in pancreatic cancer: A scoping review of clinical studies,” *Front Oncol*, vol. 12, p. 1066990, Nov. 2022, doi: 10.3389/fonc.2022.1066990.
[24] P. R. Stauffer and S. N. Goldberg, “Introduction: thermal ablation therapy,” *Int J Hyperthermia*, vol. 20, no. 7, pp. 671–677, Nov. 2004, doi: 10.1080/02656730400007220.
[25] E. N. Petre and C. Sofocleous, “Thermal Ablation in the Management of Colorectal Cancer Patients with Oligometastatic Liver Disease,” *Visc Med*, vol. 33, no. 1, pp. 62–68, Mar. 2017, doi: 10.1159/000454697.
[26] A. Marien, I. Gill, O. Ukimura, N. Betrouni, and A. Villers, “Target ablation--image-guided therapy in prostate cancer,” *Urol Oncol*, vol. 32, no. 6, pp. 912–923, Aug. 2014, doi: 10.1016/j.urolonc.2013.10.014.
[27] G. Carrafiello *et al.*, “Microwave ablation of pancreatic head cancer: safety and efficacy,” *J Vasc Interv Radiol*, vol. 24, no. 10, pp. 1513–1520, Oct. 2013, doi: 10.1016/j.jvir.2013.07.005.
[28] A. Giardino *et al.*, “Triple approach strategy for patients with locally advanced pancreatic carcinoma,” *HPB (Oxford)*, vol. 15, no. 8, pp. 623–627, Aug. 2013, doi: 10.1111/hpb.12027.
[29] P. Figueroa-Barojas *et al.*, “Safety and efficacy of radiofrequency ablation in the management of unresectable bile duct and pancreatic cancer: a novel palliation technique,” *J Oncol*, vol. 2013, p. 910897, 2013, doi: 10.1155/2013/910897.
[30] T. J. Vogl *et al.*, “Microwave ablation of pancreatic tumors,” *Minim Invasive Ther Allied Technol*, vol. 27, no. 1, pp. 33–40, Feb. 2018, doi: 10.1080/13645706.2017.1420664.
[31] C. W. Song, A. Shakil, J. L. Osborn, and K. Iwata, “Tumour oxygenation is increased by hyperthermia at mild temperatures. 1996,” *Int J Hyperthermia*, vol. 25, no. 2, pp. 91–95, Mar. 2009, doi: 10.1080/02656730902744171.
[32] Z. Vujaskovic *et al.*, “Temperature-dependent changes in physiologic parameters of spontaneous canine soft tissue sarcomas after combined radiotherapy and hyperthermia treatment,” *International Journal of Radiation Oncology, Biology, Physics*, vol. 46, no. 1, pp. 179–185, Jan. 2000, doi: 10.1016/S0360-3016(99)00362-4.
[33] B. Frey *et al.*, “Old and new facts about hyperthermia-induced modulations of the immune system,” *Int J Hyperthermia*, vol. 28, no. 6, pp. 528–542, 2012, doi: 10.3109/02656736.2012.677933.
[34] H.-G. Zhang, K. Mehta, P. Cohen, and C. Guha, “Hyperthermia on immune regulation: a temperature’s story,” *Cancer Lett*, vol. 271, no. 2, pp. 191–204, Nov. 2008, doi: 10.1016/j.canlet.2008.05.026.

[35] S. R. Gameiro *et al.*, “Combination therapy with local radiofrequency ablation and systemic vaccine enhances antitumor immunity and mediates local and distal tumor regression,” *PLoS One*, vol. 8, no. 7, p. e70417, 2013, doi: 10.1371/journal.pone.0070417.
[36] J. A. Tashjian, M. W. Dewhirst, D. Needham, and B. L. Viglianti, “Rationale for and measurement of liposomal drug delivery with hyperthermia using non-invasive imaging techniques,” *Int J Hyperthermia*, vol. 24, no. 1, pp. 79–90, Feb. 2008, doi: 10.1080/02656730701840147.
[37] L. Li *et al.*, “Improved intratumoral nanoparticle extravasation and penetration by mild hyperthermia,” *J Control Release*, vol. 167, no. 2, pp. 130–137, Apr. 2013, doi: 10.1016/j.jconrel.2013.01.026.
[38] A. L. Oei, L. E. M. Vriend, J. Crezee, N. A. P. Franken, and P. M. Krawczyk, “Effects of hyperthermia on DNA repair pathways: one treatment to inhibit them all,” *Radiat Oncol*, vol. 10, no. 1, p. 165, Dec. 2015, doi: 10.1186/s13014-015-0462-0.
[39] E. P. Armour, Z. H. Wang, P. M. Corry, and A. Martinez, “Sensitization of rat 9L gliosarcoma cells to low dose rate irradiation by long duration 41 degrees C hyperthermia,” *Cancer Res*, vol. 51, no. 12, pp. 3088–3095, Jun. 1991.
[40] N. Nomikou and A. P. McHale, “Microbubble-enhanced ultrasound-mediated gene transfer--towards the development of targeted gene therapy for cancer,” *Int J Hyperthermia*, vol. 28, no. 4, pp. 300–310, 2012, doi: 10.3109/02656736.2012.659235.
[41] C. Y. Li and M. W. Dewhirst, “Hyperthermia-regulated immunogene therapy,” *Int J Hyperthermia*, vol. 18, no. 6, pp. 586–596, Dec. 2002, doi: 10.1080/0265673021000017082.
[42] Z. Li, J. Deng, J. Sun, and Y. Ma, “Hyperthermia Targeting the Tumor Microenvironment Facilitates Immune Checkpoint Inhibitors,” *Frontiers in Immunology*, vol. 11, p. 2823, 2020, doi: 10.3389/fimmu.2020.595207.
[43] J. J. Skitzki, E. A. Repasky, and S. S. Evans, “Hyperthermia as an immunotherapy strategy for cancer,” *Curr Opin Investig Drugs*, vol. 10, no. 6, pp. 550–558, Jun. 2009.
[44] L. Galluzzi *et al.*, “Consensus guidelines for the definition, detection and interpretation of immunogenic cell death,” *J Immunother Cancer*, vol. 8, no. 1, p. e000337, Mar. 2020, doi: 10.1136/jitc-2019-000337.
[45] M. V. Sitkovsky, “T regulatory cells: hypoxia-adenosinergic suppression and re-direction of the immune response,” *Trends Immunol*, vol. 30, no. 3, pp. 102–108, Mar. 2009, doi: 10.1016/j.it.2008.12.002.
[46] M. Sitkovsky and D. Lukashev, “Regulation of immune cells by local-tissue oxygen tension: HIF1 alpha and adenosine receptors,” *Nat Rev Immunol*, vol. 5, no. 9, pp. 712–721, Sep. 2005, doi: 10.1038/nri1685.
[47] R. D. Issels *et al.*, “Neo-adjuvant chemotherapy alone or with regional hyperthermia for localised high-risk soft-tissue sarcoma: a randomised phase 3 multicentre study,” *The Lancet Oncology*, vol. 11, no. 6, pp. 561–570, Jun. 2010, doi: 10.1016/S1470-2045(10)70071-1.
[48] E. L. Jones *et al.*, “Thermochemoradiotherapy improves oxygenation in locally advanced breast cancer,” *Clin Cancer Res*, vol. 10, no. 13, pp. 4287–4293, Jul. 2004, doi: 10.1158/1078-0432.CCR-04-0133.
[49] L. Li *et al.*, “Mild hyperthermia triggered doxorubicin release from optimized stealth thermosensitive liposomes improves intratumoral drug delivery and efficacy,” *J Control Release*, vol. 168, no. 2, pp. 142–150, Jun. 2013, doi: 10.1016/j.jconrel.2013.03.011.
[50] P. Schildkopf *et al.*, “Application of hyperthermia in addition to ionizing irradiation fosters necrotic cell death and HMGB1 release of colorectal tumor cells,” *Biochemical and Biophysical Research Communications*, vol. 391, no. 1, pp. 1014–1020, Jan. 2010, doi: 10.1016/j.bbrc.2009.12.008.

[51] S. A. Dromi *et al.*, “Radiofrequency Ablation Induces Antigen-presenting Cell Infiltration and Amplification of Weak Tumor-induced Immunity,” *Radiology*, vol. 251, no. 1, pp. 58–66, Apr. 2009, doi: 10.1148/radiol.2511072175.
[52] L.-S. Teng, K.-T. Jin, N. Han, and J. Cao, “Radiofrequency ablation, heat shock protein 70 and potential anti-tumor immunity in hepatic and pancreatic cancers: a minireview,” *Hepatobiliary Pancreat Dis Int*, vol. 9, no. 4, pp. 361–365, Aug. 2010.
[53] W. F. A. Wan Mohd Zawawi, M. H. Hibma, M. I. Salim, and K. Jemon, “Hyperthermia by near infrared radiation induced immune cells activation and infiltration in breast tumor,” *Sci Rep*, vol. 11, no. 1, Art. no. 1, May 2021, doi: 10.1038/s41598-021-89740-0.
[54] X. He, S. Bhowmick, and J. Bischof, “Thermal therapy in urologic systems: a comparison of arrhenius and thermal isoeffective dose models in predicting hyperthermic injury.,” *Journal of biomechanical engineering*, 2009, doi: 10.1115/1.3128671.
[55] W. C. Dewey, “Arrhenius relationships from the molecule and cell to the clinic,” *Int J Hyperthermia*, vol. 25, no. 1, pp. 3–20, Feb. 2009, doi: 10.1080/02656730902747919.
[56] R. N. Aravalli *et al.*, “Spectroscopic and calorimetric evaluation of chemically induced protein denaturation in HuH-7 liver cancer cells and impact on cell survival,” *Technol Cancer Res Treat*, vol. 11, no. 5, pp. 467–473, Oct. 2012, doi: 10.7785/tcrt.2012.500271.
[57] X. He, W. F. Wolkers, J. H. Crowe, D. J. Swanlund, and J. C. Bischof, “In situ thermal denaturation of proteins in dunning AT-1 prostate cancer cells: implication for hyperthermic cell injury,” *Ann Biomed Eng*, vol. 32, no. 10, pp. 1384–1398, Oct. 2004, doi: 10.1114/b:abme.0000042226.97347.de.
[58] M. Paruch, “Mathematical Modeling of Breast Tumor Destruction Using Fast Heating during Radiofrequency Ablation,” *Materials (Basel)*, vol. 13, no. 1, p. E136, Dec. 2019, doi: 10.3390/ma13010136.
[59] S. A. Sapareto and W. C. Dewey, “Thermal dose determination in cancer therapy,” *International Journal of Radiation Oncology*Biology*Physics*, vol. 10, no. 6, pp. 787–800, Apr. 1984, doi: 10.1016/0360-3016(84)90379-1.
[60] F. Chamani *et al.*, “In Vitro Measurement and Mathematical Modeling of Thermally-Induced Injury in Pancreatic Cancer Cells,” *Cancers*, vol. 15, no. 3, Art. no. 3, Jan. 2023, doi: 10.3390/cancers15030655.
[61] J. A. Tashjian, M. W. Dewhirst, D. Needham, and B. L. Viglianti, “Rationale for and measurement of liposomal drug delivery with hyperthermia using non-invasive imaging techniques,” *Int J Hyperthermia*, vol. 24, no. 1, pp. 79–90, Feb. 2008, doi: 10.1080/02656730701840147.
[62] L. Li *et al.*, “Improved intratumoral nanoparticle extravasation and penetration by mild hyperthermia,” *J Control Release*, vol. 167, no. 2, pp. 130–137, Apr. 2013, doi: 10.1016/j.jconrel.2013.01.026.
[63] C. Y. Li and M. W. Dewhirst, “Hyperthermia-regulated immunogene therapy,” *Int J Hyperthermia*, vol. 18, no. 6, pp. 586–596, Dec. 2002, doi: 10.1080/0265673021000017082.
[64] N. Nomikou and A. P. McHale, “Microbubble-enhanced ultrasound-mediated gene transfer--towards the development of targeted gene therapy for cancer,” *Int J Hyperthermia*, vol. 28, no. 4, pp. 300–310, 2012, doi: 10.3109/02656736.2012.659235.
[65] B. Frey *et al.*, “Old and new facts about hyperthermia-induced modulations of the immune system,” *Int J Hyperthermia*, vol. 28, no. 6, pp. 528–542, 2012, doi: 10.3109/02656736.2012.677933.
[66] P. Schildkopf *et al.*, “Biological rationales and clinical applications of temperature controlled hyperthermia--implications for multimodal cancer treatments,” *Curr. Med. Chem.*, vol. 17, no. 27, pp. 3045–3057, 2010.
[67] H.-G. Zhang, K. Mehta, P. Cohen, and C. Guha, “Hyperthermia on immune regulation: a temperature’s story,” *Cancer Lett.*, vol. 271, no. 2, pp. 191–204, Nov. 2008, doi: 10.1016/j.canlet.2008.05.026.

[68] E. L. Jones *et al.*, "International Phase III Trial of Chemoradiotherapy ± Hyperthermia for Locally Advanced Cervix Cancer: Interim Update on Toxicities," *International Journal of Radiation Oncology*Biology*Physics Proceedings of the American Society for Therapeutic Radiology and Oncology 49th Annual Meeting, 49th Annual Meeting of the American Society for Therapeutic Radiology and Oncology*, vol. 69, no. 3, Supplement 1, pp. S392–S393, Nov. 2007.
[69] P. K. Sneed *et al.*, "Survival benefit of hyperthermia in a prospective randomized trial of brachytherapy boost +/- hyperthermia for glioblastoma multiforme," *Int J Radiat Oncol Biol Phys*, vol. 40, no. 2, pp. 287–95, Jan. 1998.
[70] R. D. Issels *et al.*, "Neo-adjuvant chemotherapy alone or with regional hyperthermia for localised high-risk soft-tissue sarcoma: a randomised phase 3 multicentre study," *Lancet Oncol.*, vol. 11, no. 6, pp. 561–570, Jun. 2010, doi: 10.1016/S1470-2045(10)70071-1.
[71] L. M. Knab, R. Salem, and D. M. Mahvi, "Minimally invasive therapies for hepatic malignancy," *Curr Probl Surg*, vol. 50, no. 4, pp. 146–179, Apr. 2013, doi: 10.1067/j.cpsurg.2013.01.001.
[72] G. Reddy, M. R. Dreher, C. Rossmann, B. J. Wood, and D. Haemmerich, "Cytotoxicity of hepatocellular carcinoma cells to hyperthermic and ablative temperature exposures: In vitro studies and mathematical modelling," *International Journal of Hyperthermia*, vol. 29, no. 4, pp. 318–323, Jun. 2013, doi: 10.3109/02656736.2013.792125.
[73] S. L. Jacques, C. Newman, and X. Y. He, "Thermal coagulation of tissues. Liver studies indicate a distribution of rate parameters, not a single rate parameter, describes the coagulation process: Winter Annual Meeting of the American Society of Mechanical Engineers," *Advances in Biological Heat and Mass Transfer*, pp. 71–73, 1991.
[74] C. Brace, "Thermal Tumor Ablation in Clinical Use," *IEEE Pulse*, vol. 2, no. 5, pp. 28–38, Sep. 2011, doi: 10.1109/MPUL.2011.942603.
[75] A. Gasselhuber, M. R. Dreher, F. Rattay, B. J. Wood, and D. Haemmerich, "Comparison of conventional chemotherapy, stealth liposomes and temperature-sensitive liposomes in a mathematical model," *PLoS ONE*, vol. 7, no. 10, p. e47453, 2012, doi: 10.1371/journal.pone.0047453.
[76] S. R. Gameiro *et al.*, "Combination therapy with local radiofrequency ablation and systemic vaccine enhances antitumor immunity and mediates local and distal tumor regression," *PLoS ONE*, vol. 8, no. 7, p. e70417, 2013, doi: 10.1371/journal.pone.0070417.
[77] S. P. Haen, P. L. Pereira, H. R. Salih, H.-G. Rammensee, and C. Gouttefangeas, "More than just tumor destruction: immunomodulation by thermal ablation of cancer," *Clin. Dev. Immunol.*, vol. 2011, p. 160250, 2011, doi: 10.1155/2011/160250.
[78] M. W. Dewhirst, Z. Vujaskovic, E. Jones, and D. Thrall, "Re-setting the biologic rationale for thermal therapy," *Int J Hyperthermia*, vol. 21, no. 8, pp. 779–90, Dec. 2005.
[79] B. Hildebrandt *et al.*, "The cellular and molecular basis of hyperthermia," *Crit Rev Oncol Hematol*, vol. 43, no. 1, pp. 33–56, Jul. 2002.
[80] Y. Rong and P. Mack, "Apoptosis induced by hyperthermia in Dunn osteosarcoma cell line in vitro," *International Journal of Hyperthermia*, vol. 16, no. 1, pp. 19–27, Jan. 2000, doi: 10.1080/026567300285394.
[81] Y. G. Shellman *et al.*, "Fast response temperature measurement and highly reproducible heating methods for 96-well plates," *BioTechniques*, vol. 36, no. 6, pp. 968–976, Jun. 2004, doi: 10.2144/04366ST01.
[82] A. Debes, R. Willers, U. Göbel, and R. Wessalowski, "Role of heat treatment in childhood cancers: Distinct resistance profiles of solid tumor cell lines towards combined thermochemotherapy," *Pediatric Blood & Cancer*, vol. 45, no. 5, pp. 663–669, 2005, doi: https://doi.org/10.1002/pbc.20266.

[83] D.-D. Herea, C. Danceanu, E. Radu, L. Labusca, N. Lupu, and H. Chiriac, “Comparative effects of magnetic and water-based hyperthermia treatments on human osteosarcoma cells,” *IJN*, vol. 13, pp. 5743–5751, Sep. 2018, doi: 10.2147/IJN.S174853.
[84] A. J. Massey, “A high content, high throughput cellular thermal stability assay for measuring drug-target engagement in living cells,” *PLOS ONE*, vol. 13, no. 4, p. e0195050, Apr. 2018, doi: 10.1371/journal.pone.0195050.
[85] S. M. Amini, S. Kharrazi, and M. R. Jaafari, “Radio frequency hyperthermia of cancerous cells with gold nanoclusters: an in vitro investigation,” *Gold Bull*, vol. 50, no. 1, pp. 43–50, Mar. 2017, doi: 10.1007/s13404-016-0192-6.
[86] M. J. Ware *et al.*, “Optimizing non-invasive radiofrequency hyperthermia treatment for improving drug delivery in 4T1 mouse breast cancer model,” *Sci Rep*, vol. 7, no. 1, Art. no. 1, Mar. 2017, doi: 10.1038/srep43961.
[87] D. Yang, M. C. Converse, D. M. Mahvi, and J. G. Webster, “Measurement and Analysis of Tissue Temperature During Microwave Liver Ablation,” *IEEE Trans. Biomed. Eng.*, vol. 54, no. 1, pp. 150–155, Jan. 2007, doi: 10.1109/TBME.2006.884647.
[88] P. Philips, C. R. Scoggins, J. K. Rostas, K. M. McMasters, and R. C. Martin, “Safety and advantages of combined resection and microwave ablation in patients with bilobar hepatic malignancies,” *International Journal of Hyperthermia*, vol. 33, no. 1, pp. 43–50, Jan. 2017, doi: 10.1080/02656736.2016.1211751.
[89] S. H. Choi, J. W. Kim, J. H. Kim, and K. W. Kim, “Efficacy and Safety of Microwave Ablation for Malignant Renal Tumors: An Updated Systematic Review and Meta-Analysis of the Literature Since 2012,” *Korean J Radiol*, vol. 19, no. 5, pp. 938–949, Oct. 2018, doi: 10.3348/kjr.2018.19.5.938.
[90] Z. Yu, J. Geng, M. Zhang, Y. Zhou, Q. Fan, and J. Chen, “Treatment of osteosarcoma with microwave thermal ablation to induce immunogenic cell death,” *Oncotarget*, vol. 5, no. 15, pp. 6526–6539, Aug. 2014.
[91] C. A. Manderson, H. McLiesh, R. Curvello, R. F. Tabor, J. Manolios, and G. Garnier, “Photothermal incubation of red blood cells by laser for rapid pre-transfusion blood group typing,” *Sci Rep*, vol. 9, no. 1, p. 11221, Dec. 2019, doi: 10.1038/s41598-019-47646-y.
[92] Y. Miura *et al.*, “Continuous-wave Thulium Laser for Heating Cultured Cells to Investigate Cellular Thermal Effects,” *Journal of Visualized Experiments*, p. 9, 2017.
[93] C. Mu *et al.*, “Chemotherapy Sensitizes Therapy-Resistant Cells to Mild Hyperthermia by Suppressing Heat Shock Protein 27 Expression in Triple-Negative Breast Cancer,” *Clin Cancer Res*, vol. 24, no. 19, pp. 4900–4912, Oct. 2018, doi: 10.1158/1078-0432.CCR-17-3872.
[94] C. Shirata *et al.*, “Near-infrared photothermal/photodynamic therapy with indocyanine green induces apoptosis of hepatocellular carcinoma cells through oxidative stress,” *Sci Rep*, vol. 7, no. 1, p. 13958, Dec. 2017, doi: 10.1038/s41598-017-14401-0.
[95] M. S. Bani *et al.*, “Casein-Coated Iron Oxide Nanoparticles for in vitro Hyperthermia for Cancer Therapy,” *SPIN*, vol. 09, no. 02, p. 1940003, Jun. 2019, doi: 10.1142/S2010324719400034.
[96] A. Ito *et al.*, “Tumor regression by combined immunotherapy and hyperthermia using magnetic nanoparticles in an experimental subcutaneous murine melanoma,” *Cancer Science*, vol. 94, no. 3, pp. 308–313, 2003, doi: 10.1111/j.1349-7006.2003.tb01438.x.
[97] S. C. Brüningk, I. Rivens, P. Mouratidis, and G. ter Haar, “Focused Ultrasound-Mediated Hyperthermia in Vitro: An Experimental Arrangement for Treating Cells under Tissue-Mimicking Conditions,” *Ultrasound in Medicine and Biology*, vol. 45, no. 12, pp. 3290–3297, Dec. 2019, doi: 10.1016/j.ultrasmedbio.2019.06.410.
[98] B. Vanherberghen *et al.*, “Ultrasound-controlled cell aggregation in a multi-well chip,” *Lab on a Chip*, vol. 10, no. 20, pp. 2727–2732, 2010, doi: 10.1039/C004707D.

[99] E. Mylonopoulou, M. Bazán-Peregrino, C. D. Arvanitis, and C. C. Coussios, “A non-exothermic cell-embedding tissue-mimicking material for studies of ultrasound-induced hyperthermia and drug release,” *International Journal of Hyperthermia*, vol. 29, no. 2, pp. 133–144, Mar. 2013, doi: 10.3109/02656736.2012.762553.
[100] H. Bridle, M. Millingen, and A. Jesorka, “On-chip fabrication to add temperature control to a microfluidic solution exchange system,” *Lab Chip*, vol. 8, no. 3, pp. 480–483, Feb. 2008, doi: 10.1039/B718368B.
[101] C. Picard *et al.*, “A micro-incubator for cell and tissue imaging,” *Biotechniques*, vol. 48, no. 2, pp. 135–138, Feb. 2010, doi: 10.2144/000113245.
[102] P. X. E. Mouratidis, I. Rivens, and G. ter Haar, “A study of thermal dose-induced autophagy, apoptosis and necroptosis in colon cancer cells,” *International Journal of Hyperthermia*, vol. 31, no. 5, pp. 476–488, Jul. 2015, doi: 10.3109/02656736.2015.1029995.
[103] K. J. Nytko, P. Thumser-Henner, M. S. Weyland, S. Scheidegger, and C. R. Bley, “Cell line-specific efficacy of thermoradiotherapy in human and canine cancer cells in vitro,” *PLOS ONE*, vol. 14, no. 5, p. e0216744, May 2019, doi: 10.1371/journal.pone.0216744.
[104] T. Mantso *et al.*, “Hyperthermia induces therapeutic effectiveness and potentiates adjuvant therapy with non-targeted and targeted drugs in an in vitro model of human malignant melanoma,” *Sci Rep*, vol. 8, no. 1, p. 10724, Dec. 2018, doi: 10.1038/s41598-018-29018-0.
[105] A. Markezana *et al.*, “Moderate hyperthermic heating encountered during thermal ablation increases tumor cell activity,” *International Journal of Hyperthermia*, vol. 37, no. 1, pp. 119–129, Jan. 2020, doi: 10.1080/02656736.2020.1714084.
[106] H. Lee *et al.*, “Response of Breast Cancer Cells and Cancer Stem Cells to Metformin and Hyperthermia Alone or Combined,” *PLoS One*, vol. 9, no. 2, p. e87979, Feb. 2014, doi: 10.1371/journal.pone.0087979.
[107] W. Jiang, L. Bian, N. Wang, and Y. He, “Proteomic analysis of protein expression profiles during hyperthermia-induced apoptosis in Tca8113 cells,” *Oncology Letters*, vol. 6, no. 1, pp. 135–143, Jul. 2013, doi: 10.3892/ol.2013.1354.
[108] B. D. Beck and J. R. Dynlacht, “Heat-Induced Aggregation of XRCC5 (Ku80) in Nontolerant and Thermotolerant Cells,” *rare*, vol. 156, no. 6, pp. 767–774, Dec. 2001, doi: 10.1667/0033-7587(2001)156[0767:HIAOXK]2.0.CO;2.
[109] K.-L. Yang *et al.*, “In vitro comparison of conventional hyperthermia and modulated electro-hyperthermia,” *Oncotarget*, vol. 7, no. 51, pp. 84082–84092, Aug. 2016, doi: 10.18632/oncotarget.11444.
[110] M. N. Rylander, K. R. Diller, S. Wang, and S. J. Aggarwal, “Correlation of HSP70 Expression and Cell Viability Following Thermal Stimulation of Bovine Aortic Endothelial Cells,” *Journal of Biomechanical Engineering*, vol. 127, no. 5, pp. 751–757, May 2005, doi: 10.1115/1.1993661.
[111] A. Kiourti, M. Sun, X. He, and J. L. Volakis, “Microwave Cavity with Controllable Temperature for In Vitro Hyperthermia Investigations,” *Journal of electromagnetic engineering and science*, vol. 14, no. 3, pp. 267–272, Sep. 2014, doi: 10.5515/JKIEES.2014.14.3.267.
[112] Y.-Y. Zhao *et al.*, “Microwave hyperthermia promotes caspase-3-dependent apoptosis and induces G2/M checkpoint arrest via the ATM pathway in non-small cell lung cancer cells,” *Int J Oncol*, vol. 53, no. 2, pp. 539–550, Jun. 2018, doi: 10.3892/ijo.2018.4439.
[113] P. Manop, P. Keangin, N. Nasongkla, and K. Eawsakul, “In Vitro Experiments of Microwave Ablation in Liver Cancer Cells (Effects of Microwave Power and Heating Time),” in *2020 IEEE 7th International Conference on Industrial Engineering and Applications (ICIEA)*, Apr. 2020, pp. 805–813. doi: 10.1109/ICIEA49774.2020.9102010.

[114] M. Asano *et al.*, “Effects of Normothermic Conditioned Microwave Irradiation on Cultured Cells Using an Irradiation System with Semiconductor Oscillator and Thermo-regulatory Applicator,” *Sci Rep*, vol. 7, no. 1, p. 41244, Mar. 2017, doi: 10.1038/srep41244.
[115] L. Chen *et al.*, “Mild microwave ablation combined with HSP90 and TGF-β1 inhibitors enhances the therapeutic effect on osteosarcoma,” *Molecular Medicine Reports*, vol. 22, no. 2, pp. 906–914, Aug. 2020, doi: 10.3892/mmr.2020.11173.
[116] J. A. Schwartz *et al.*, “Feasibility study of particle-assisted laser ablation of brain tumors in orthotopic canine model,” *Cancer Res*, vol. 69, no. 4, pp. 1659–1667, Feb. 2009, doi: 10.1158/0008-5472.CAN-08-2535.
[117] E. Schena, P. Saccomandi, and Y. Fong, “Laser Ablation for Cancer: Past, Present and Future,” *Journal of Functional Biomaterials*, vol. 8, no. 2, Art. no. 2, Jun. 2017, doi: 10.3390/jfb8020019.
[118] K. Inagaki, T. Shuo, K. Katakura, N. Ebihara, A. Murakami, and K. Ohkoshi, “Sublethal Photothermal Stimulation with a Micropulse Laser Induces Heat Shock Protein Expression in ARPE-19 Cells,” *J Ophthalmol*, vol. 2015, p. 729792, 2015, doi: 10.1155/2015/729792.
[119] F. Tang, Y. Zhang, J. Zhang, J. Guo, and R. Liu, “Assessment of the efficacy of laser hyperthermia and nanoparticle-enhanced therapies by heat shock protein analysis,” *AIP Advances*, vol. 4, no. 3, p. 031334, Mar. 2014, doi: 10.1063/1.4869095.
[120] E. C. Lins, C. F. Oliveira, O. C. C. Guimarães, C. A. de S. Costa, C. Kurachi, and V. S. Bagnato, “A Novel 785-nm Laser Diode-Based System for Standardization of Cell Culture Irradiation,” *Photomed Laser Surg*, vol. 31, no. 10, pp. 466–473, Oct. 2013, doi: 10.1089/pho.2012.3310.
[121] R. Liljemalm, T. Nyberg, and H. von Holst, “Heating during infrared neural stimulation,” *Lasers in Surgery and Medicine*, vol. 45, no. 7, pp. 469–481, 2013, doi: 10.1002/lsm.22158.
[122] F.-J. Murat, L. Poissonnier, G. Pasticier, and A. Gelet, “High-Intensity Focused Ultrasound (HIFU) for Prostate Cancer,” *Cancer Control*, vol. 14, no. 3, pp. 244–249, Jul. 2007, doi: 10.1177/107327480701400307.
[123] M. J. So *et al.*, “Does the phase of menstrual cycle affect MR-guided focused ultrasound surgery of uterine leiomyomas?,” *European Journal of Radiology*, vol. 59, no. 2, pp. 203–207, Aug. 2006, doi: 10.1016/j.ejrad.2006.05.004.
[124] J. E. Kennedy, “High-intensity focused ultrasound in the treatment of solid tumours,” *Nat Rev Cancer*, vol. 5, no. 4, pp. 321–327, Apr. 2005, doi: 10.1038/nrc1591.
[125] S. A. Sapareto, L. E. Hopwood, W. C. Dewey, M. R. Raju, and J. W. Gray, “Effects of Hyperthermia on Survival and Progression of Chinese Hamster Ovary Cells,” *Cancer Res*, vol. 38, no. 2, pp. 393–400, Feb. 1978.
[126] M. R. Horsman and J. Overgaard, “Hyperthermia: a Potent Enhancer of Radiotherapy,” *Clinical Oncology*, vol. 19, no. 6, pp. 418–426, Aug. 2007, doi: 10.1016/j.clon.2007.03.015.
[127] X. Zhang *et al.*, “Focused ultrasound radiosensitizes human cancer cells by enhancement of DNA damage,” *Strahlenther Onkol*, vol. 197, no. 8, pp. 730–743, Aug. 2021, doi: 10.1007/s00066-021-01774-5.
[128] A.-J. Mäki *et al.*, “A Portable Microscale Cell Culture System with Indirect Temperature Control,” p. 14.
[129] G. Regalia, E. Biffi, S. Achilli, G. Ferrigno, A. Menegon, and A. Pedrocchi, “Development of a bench-top device for parallel climate-controlled recordings of neuronal cultures activity with microelectrode arrays,” *Biotechnol Bioeng*, vol. 113, no. 2, pp. 403–413, Feb. 2016, doi: 10.1002/bit.25811.
[130] J.-L. Lin, M.-H. Wu, C. Y. Kuo, K.-D. Lee, and Y.-L. Shen, “Application of indium tin oxide (ITO)-based microheater chip with uniform thermal distribution for perfusion cell culture outside a cell incubator,” *Biomedical microdevices*, vol. 12, pp. 389–98, Jun. 2010, doi: 10.1007/s10544-010-9395-4.

[131] J. Vukasinovic, D. K. Cullen, M. C. LaPlaca, and A. Glezer, “A microperfused incubator for tissue mimetic 3D cultures,” *Biomed Microdevices*, vol. 11, no. 6, pp. 1155–1165, Dec. 2009, doi: 10.1007/s10544-009-9332-6.
[132] S. Petronis, M. Stangegaard, C. B. V. Christensen, and M. Dufva, “Transparent polymeric cell culture chip with integrated temperature control and uniform media perfusion,” *Biotechniques*, vol. 40, no. 3, pp. 368–376, Mar. 2006, doi: 10.2144/000112122.
[133] L. Lin, S.-S. Wang, M.-H. Wu, and C.-C. Oh-Yang, “Development of an Integrated Microfluidic Perfusion Cell Culture System for Real-Time Microscopic Observation of Biological Cells,” *Sensors (Basel)*, vol. 11, no. 9, pp. 8395–8411, Aug. 2011, doi: 10.3390/s110908395.
[134] D. Nieto, P. McGlynn, M. de la Fuente, R. Lopez-Lopez, and G. M. O’connor, “Laser microfabrication of a microheater chip for cell culture outside a cell incubator,” *Colloids and Surfaces B: Biointerfaces*, vol. 154, pp. 263–269, Jun. 2017, doi: 10.1016/j.colsurfb.2017.03.043.
[135] J.-Y. Cheng, M.-H. Yen, C.-T. Kuo, and T.-H. Young, “A transparent cell-culture microchamber with a variably controlled concentration gradient generator and flow field rectifier,” *Biomicrofluidics*, vol. 2, no. 2, p. 024105, Jun. 2008, doi: 10.1063/1.2952290.
[136] S. Halldorsson, E. Lucumi, R. Gómez-Sjöberg, and R. M. T. Fleming, “Advantages and challenges of microfluidic cell culture in polydimethylsiloxane devices,” *Biosensors and Bioelectronics*, vol. 63, pp. 218–231, Jan. 2015, doi: 10.1016/j.bios.2014.07.029.
[137] M. Mehling and S. Tay, “Microfluidic cell culture,” *Current Opinion in Biotechnology*, vol. 25, pp. 95–102, Feb. 2014, doi: 10.1016/j.copbio.2013.10.005.
[138] A. J. de Mello, M. Habgood, N. L. Lancaster, T. Welton, and R. C. R. Wootton, “Precise temperature control in microfluidic devices using Joule heating of ionic liquids,” *Lab Chip*, vol. 4, no. 5, pp. 417–419, Oct. 2004, doi: 10.1039/B405760K.
[139] C. Burke *et al.*, “Drug release kinetics of temperature sensitive liposomes measured at high-temporal resolution with a millifluidic device,” *International Journal of Hyperthermia*, vol. 34, no. 6, pp. 786–794, Aug. 2018, doi: 10.1080/02656736.2017.1412504.
[140] F. Cantoni, G. Werr, L. Barbe, A. M. Porras, and M. Tenje, “A microfluidic chip carrier including temperature control and perfusion system for long-term cell imaging,” *HardwareX*, vol. 10, p. e00245, Oct. 2021, doi: 10.1016/j.ohx.2021.e00245.
[141] D. Ross, M. Gaitan, and L. E. Locascio, “Temperature Measurement in Microfluidic Systems Using a Temperature-Dependent Fluorescent Dye,” *Anal. Chem.*, vol. 73, no. 17, pp. 4117–4123, Sep. 2001, doi: 10.1021/ac010370l.
[142] Z. Ji *et al.*, “The effect of temperature-control microwave on HELA and MG-63 cells,” *J Cancer Res Ther*, vol. 14, no. Supplement, pp. S152–S158, 2018, doi: 10.4103/0973-1482.165868.
[143] C. Guo *et al.*, “Photothermal ablation cancer therapy using homogeneous CsxWO3 nanorods with broad near-infra-red absorption,” *Nanoscale*, vol. 5, no. 14, pp. 6469–6478, Jun. 2013, doi: 10.1039/C3NR01025B.
[144] A. W. Dunn *et al.*, “Photothermal effects and toxicity of Fe3O4 nanoparticles via near infrared laser irradiation for cancer therapy,” *Mater Sci Eng C Mater Biol Appl*, vol. 46, pp. 97–102, Jan. 2015, doi: 10.1016/j.msec.2014.09.043.
[145] C.-Y. Lai, D. E. Kruse, C. F. Caskey, D. N. Stephens, P. L. Sutcliffe, and K. W. Ferrara, “Noninvasive thermometry assisted by a dual-function ultrasound transducer for mild hyperthermia,” *IEEE Trans Ultrason Ferroelectr Freq Control*, vol. 57, no. 12, pp. 2671–2684, Dec. 2010, doi: 10.1109/TUFFC.2010.1741.
[146] S. R. Heidemann, P. Lamoureux, K. Ngo, M. Reynolds, and R. E. Buxbaum, “Open-dish incubator for live cell imaging with an inverted microscope,” *BioTechniques*, vol. 35, no. 4, pp. 708–716, Oct. 2003, doi: 10.2144/03354bi01.

[147] K. M. Byers, L.-K. Lin, T. J. Moehling, L. Stanciu, and J. C. Linnes, “Versatile printed microheaters to enable low-power thermal control in paper diagnostics,” *Analyst*, vol. 145, no. 1, pp. 184–196, Dec. 2019, doi: 10.1039/C9AN01546A.
[148] J. Wu, W. Cao, W. Wen, D. C. Chang, and P. Sheng, “Polydimethylsiloxane microfluidic chip with integrated microheater and thermal sensor,” *Biomicrofluidics*, vol. 3, no. 1, p. 012005, Mar. 2009, doi: 10.1063/1.3058587.
[149] G. M. Hahn, “Hyperthermia for the Engineer: A Short Biological Primer,” *IEEE Transactions on Biomedical Engineering*, vol. BME-31, no. 1, pp. 3–8, Jan. 1984, doi: 10.1109/TBME.1984.325363.
[150] K. J. Henle and D. B. Leeper, “Interaction of Hyperthermia and Radiation in CHO Cells: Recovery Kinetics,” *Radiation Research*, vol. 66, no. 3, p. 505, Jun. 1976, doi: 10.2307/3574455.
[151] P. X. E. Mouratidis, I. Rivens, J. Civale, R. Symonds-Tayler, and G. ter Haar, “‘Relationship between thermal dose and cell death for “rapid” ablative and “slow” hyperthermic heating,’” *International Journal of Hyperthermia*, vol. 36, no. 1, pp. 228–242, Jan. 2019, doi: 10.1080/02656736.2018.1558289.
[152] Y. Miura *et al.*, “Real-time optoacoustic temperature determination on cell cultures during heat exposure: a feasibility study,” *Int J Hyperthermia*, vol. 36, no. 1, pp. 466–472, 2019, doi: 10.1080/02656736.2019.1590653.
[153] D. Haemmerich, I. dos Santos, D. J. Schutt, J. G. Webster, and D. M. Mahvi, “In vitro measurements of temperature-dependent specific heat of liver tissue,” *Medical Engineering & Physics*, vol. 28, no. 2, pp. 194–197, Mar. 2006, doi: 10.1016/j.medengphy.2005.04.020.
[154] A. R. Coombe *et al.*, “The effects of low level laser irradiation on osteoblastic cells,” *Clinical Orthodontics and Research*, vol. 4, no. 1, pp. 3–14, 2001, doi: 10.1034/j.1600-0544.2001.040102.x.
[155] J. W. Fisher *et al.*, “Photothermal Response of Human and Murine Cancer Cells to Multiwalled Carbon Nanotubes after Laser Irradiation,” *Cancer Res*, vol. 70, no. 23, pp. 9855–9864, Dec. 2010, doi: 10.1158/0008-5472.CAN-10-0250.
[156] S. I. Ertel, B. D. Ratner, A. Kaul, M. B. Schway, and T. A. Horbett, “In vitro study of the intrinsic toxicity of synthetic surfaces to cells,” *Journal of Biomedical Materials Research*, vol. 28, no. 6, pp. 667–675, 1994, doi: 10.1002/jbm.820280603.
[157] V. Chaplin and C. F. Caskey, “Multi-focal HIFU reduces cavitation in mild-hyperthermia,” *J Ther Ultrasound*, vol. 5, p. 12, 2017, doi: 10.1186/s40349-017-0089-8.
[158] A. Shanei and A. Sazgarnia, “An overview of therapeutic applications of ultrasound based on synergetic effects with gold nanoparticles and laser excitation,” *Iran J Basic Med Sci*, vol. 22, no. 8, pp. 848–855, Aug. 2019, doi: 10.22038/ijbms.2019.29584.7142.
[159] P. Li *et al.*, “Photo-thermal effect enhances the efficiency of radiotherapy using Arg-Gly-Asp peptides-conjugated gold nanorods that target αvβ3 in melanoma cancer cells,” *J Nanobiotechnol*, vol. 13, no. 1, p. 52, Aug. 2015, doi: 10.1186/s12951-015-0113-5.
[160] M. Ogawa *et al.*, “Immunogenic cancer cell death selectively induced by near infrared photoimmunotherapy initiates host tumor immunity,” *Oncotarget*, vol. 8, no. 6, pp. 10425–10436, Jan. 2017, doi: 10.18632/oncotarget.14425.
[161] “Annual Report to the Nation: Cancer deaths continue downward trend; modest improvements in survival for pancreatic cancer,” *National Institutes of Health (NIH)*, Oct. 27, 2022. https://www.nih.gov/news-events/news-releases/annual-report-nation-cancer-deaths-continue-downward-trend-modest-improvements-survival-pancreatic-cancer (accessed Nov. 10, 2022).
[162] A. Maitra and R. H. Hruban, “Pancreatic cancer,” *Annu Rev Pathol*, vol. 3, pp. 157–188, 2008, doi: 10.1146/annurev.pathmechdis.3.121806.154305.
[163] A. Adamska, A. Domenichini, and M. Falasca, “Pancreatic Ductal Adenocarcinoma: Current and Evolving Therapies,” *Int J Mol Sci*, vol. 18, no. 7, p. E1338, Jun. 2017, doi: 10.3390/ijms18071338.

[164] P. E. Oberstein and K. P. Olive, “Pancreatic cancer: why is it so hard to treat?,” *Therap Adv Gastroenterol*, vol. 6, no. 4, pp. 321–337, Jul. 2013, doi: 10.1177/1756283X13478680.
[165] G. Narayanan, D. Daye, N. M. Wilson, R. Noman, A. M. Mahendra, and M. H. Doshi, “Ablation in Pancreatic Cancer: Past, Present and Future,” *Cancers (Basel)*, vol. 13, no. 11, p. 2511, May 2021, doi: 10.3390/cancers13112511.
[166] R. C. G. Martin, “Use of irreversible electroporation in unresectable pancreatic cancer,” *Hepatobiliary Surg Nutr*, vol. 4, no. 3, pp. 211–215, Jun. 2015, doi: 10.3978/j.issn.2304-3881.2015.01.10.
[167] S. T. Tucci *et al.*, “Tumor-specific delivery of gemcitabine with activatable liposomes,” *J Control Release*, vol. 309, pp. 277–288, Sep. 2019, doi: 10.1016/j.jconrel.2019.07.014.
[168] K. Affram, O. Udofot, A. Cat, and E. Agyare, “In vitro and in vivo antitumor activity of gemcitabine loaded thermosensitive liposomal nanoparticles and mild hyperthermia in pancreatic cancer,” *Int J Adv Res (Indore)*, vol. 3, no. 10, pp. 859–874, Oct. 2015.
[169] N. Farr *et al.*, “Hyperthermia-enhanced targeted drug delivery using magnetic resonance-guided focussed ultrasound: a pre-clinical study in a genetic model of pancreatic cancer,” *Int J Hyperthermia*, vol. 34, no. 3, pp. 284–291, May 2018, doi: 10.1080/02656736.2017.1336675.
[170] Y. Cheng, S. Weng, L. Yu, N. Zhu, M. Yang, and Y. Yuan, “The Role of Hyperthermia in the Multidisciplinary Treatment of Malignant Tumors,” *Integr Cancer Ther*, vol. 18, p. 1534735419876345, Dec. 2019, doi: 10.1177/1534735419876345.
[171] L. Lutgens, J. Zee, D. K. M. De Ruysscher, P. Lambin, and J. Platt, “Combined use of hyperthermia and (chemo)radiation therapy for treating locally advanced cervix carcinoma,” *Cochrane Database Syst Rev*, vol. 2010, no. 3, p. CD006377, Mar. 2010, doi: 10.1002/14651858.CD006377.pub3.
[172] H. Fang *et al.*, “Regional hyperthermia combined with chemotherapy in advanced gastric cancer,” *Open Medicine*, vol. 14, no. 1, pp. 85–90, Jan. 2019, doi: 10.1515/med-2019-0012.
[173] P. K. Sneed *et al.*, “Survival benefit of hyperthermia in a prospective randomized trial of brachytherapy boost +/- hyperthermia for glioblastoma multiforme,” *Int J Radiat Oncol Biol Phys*, vol. 40, no. 2, pp. 287–295, Jan. 1998, doi: 10.1016/s0360-3016(97)00731-1.
[174] M. N. Rylander, Y. Feng, K. Zimmermann, and K. R. Diller, “Measurement and mathematical modeling of thermally induced injury and heat shock protein expression kinetics in normal and cancerous prostate cells,” *International Journal of Hyperthermia*, vol. 26, no. 8, pp. 748–764, Dec. 2010, doi: 10.3109/02656736.2010.486778.
[175] J. A. Pearce, “Comparative analysis of mathematical models of cell death and thermal damage processes,” *Int J Hyperthermia*, vol. 29, no. 4, pp. 262–280, Jun. 2013, doi: 10.3109/02656736.2013.786140.
[176] Y. Feng, J. Tinsley Oden, and M. N. Rylander, “A Two-State Cell Damage Model Under Hyperthermic Conditions: Theory and In Vitro Experiments,” *Journal of Biomechanical Engineering*, vol. 130, no. 4, Jun. 2008, doi: 10.1115/1.2947320.
[177] J. A. Pearce, “Improving Accuracy in Arrhenius Models of Cell Death: Adding a Temperature-Dependent Time Delay,” *J Biomech Eng*, vol. 137, no. 12, p. 121006, Dec. 2015, doi: 10.1115/1.4031851.
[178] D. P. O’Neill *et al.*, “A three-state mathematical model of hyperthermic cell death,” *Ann Biomed Eng*, vol. 39, no. 1, pp. 570–579, Jan. 2011, doi: 10.1007/s10439-010-0177-1.
[179] S. R. Hingorani *et al.*, “Trp53R172H and KrasG12D cooperate to promote chromosomal instability and widely metastatic pancreatic ductal adenocarcinoma in mice,” *Cancer Cell*, vol. 7, no. 5, pp. 469–483, May 2005, doi: 10.1016/j.ccr.2005.04.023.
[180] M. C. B. Tan *et al.*, “Disruption of CCR5-Dependent Homing of Regulatory T Cells Inhibits Tumor Growth in a Murine Model of Pancreatic Cancer,” *J Immunol*, vol. 182, no. 3, pp. 1746–1755, Feb. 2009, doi: 10.4049/jimmunol.182.3.1746.

[181] T. H. Corbett *et al.*, "Induction and chemotherapeutic response of two transplantable ductal adenocarcinomas of the pancreas in C57BL/6 mice," *Cancer Res*, vol. 44, no. 2, pp. 717–726, Feb. 1984.
[182] F. Chamani, I. Barnett, M. Pyle, T. Shrestha, and P. Prakash, "A Review of *In Vitro* Instrumentation Platforms for Evaluating Thermal Therapies in Experimental Cell Culture Models," *CRB*, vol. 50, no. 2, 2022, doi: 10.1615/CritRevBiomedEng.2022043455.
[183] N. R. Reddy, A. P. Abraham, K. Murugesan, and V. Matsa, "An Invitro Analysis of Elemental Release and Cytotoxicity of Recast Nickel–Chromium Dental Casting Alloys," *J Indian Prosthodont Soc*, vol. 11, no. 2, pp. 106–112, Jun. 2011, doi: 10.1007/s13191-011-0075-8.
[184] W. C. Dewey, "Arrhenius relationships from the molecule and cell to the clinic," *International Journal of Hyperthermia*, vol. 25, no. 1, pp. 3–20, Jan. 2009, doi: 10.1080/02656730902747919.
[185] J. A. Pearce, "Relationship between Arrhenius models of thermal damage and the CEM 43 thermal dose," presented at the SPIE BiOS: Biomedical Optics, T. P. Ryan, Ed., San Jose, CA, Feb. 2009, p. 718104. doi: 10.1117/12.807999.
[186] G. Deshazer, M. Hagmann, D. Merck, J. Sebek, K. B. Moore, and P. Prakash, "Computational modeling of 915 MHz microwave ablation: Comparative assessment of temperature-dependent tissue dielectric models," *Medical Physics*, vol. 44, no. 9, pp. 4859–4868, 2017, doi: 10.1002/mp.12359.
[187] M. J. Borrelli, L. L. Thompson, C. A. Cain, and W. C. Dewey, "Time-temperature analysis of cell killing of BHK cells heated at temperatures in the range of 43.5 degrees C to 57.0 degrees C," *Int J Radiat Oncol Biol Phys*, vol. 19, no. 2, pp. 389–399, Aug. 1990, doi: 10.1016/0360-3016(90)90548-x.
[188] M. Harris, "Criteria of viability in heat-treated cells," *Experimental Cell Research*, vol. 44, no. 2, pp. 658–661, Nov. 1966, doi: 10.1016/0014-4827(66)90479-4.
[189] S. Bhowmick, J. E. Coad, D. J. Swanlund, and J. C. Bischof, "In vitro thermal therapy of AT-1 Dunning prostate tumours," *Int J Hyperthermia*, vol. 20, no. 1, pp. 73–92, Feb. 2004, doi: 10.1080/0265673031000111932.
[190] X. He and J. C. Bischof, "The kinetics of thermal injury in human renal carcinoma cells," *Ann Biomed Eng*, vol. 33, no. 4, pp. 502–510, Apr. 2005, doi: 10.1007/s10439-005-2508-1.
[191] S. Piehler *et al.*, "Hyperthermia affects collagen fiber architecture and induces apoptosis in pancreatic and fibroblast tumor hetero-spheroids in vitro," *Nanomedicine: Nanotechnology, Biology and Medicine*, vol. 28, p. 102183, Aug. 2020, doi: 10.1016/j.nano.2020.102183.
[192] J. Palzer *et al.*, "Magnetic Fluid Hyperthermia as Treatment Option for Pancreatic Cancer Cells and Pancreatic Cancer Organoids," *Int J Nanomedicine*, vol. 16, pp. 2965–2981, 2021, doi: 10.2147/IJN.S288379.
[193] L. Beola *et al.*, "Critical Parameters to Improve Pancreatic Cancer Treatment Using Magnetic Hyperthermia: Field Conditions, Immune Response, and Particle Biodistribution," *ACS Appl. Mater. Interfaces*, vol. 13, no. 11, pp. 12982–12996, Mar. 2021, doi: 10.1021/acsami.1c02338.
[194] C. E. Maurici *et al.*, "Hyperthermia Enhances Efficacy of Chemotherapeutic Agents in Pancreatic Cancer Cell Lines," *Biomolecules*, vol. 12, no. 5, Art. no. 5, May 2022, doi: 10.3390/biom12050651.
[195] F. L. Tansi *et al.*, "Deep-tissue localization of magnetic field hyperthermia using pulse sequencing," *International Journal of Hyperthermia*, vol. 38, no. 1, pp. 743–754, Jan. 2021, doi: 10.1080/02656736.2021.1912412.
[196] R. Ludwig, F. J. Teran, U. Teichgräber, and I. Hilger, "Nanoparticle-based hyperthermia distinctly impacts production of ROS, expression of Ki-67, TOP2A, and TPX2, and induction of apoptosis in pancreatic cancer," *IJN*, vol. Volume 12, pp. 1009–1018, Feb. 2017, doi: 10.2147/IJN.S108577.
[197] F. L. Tansi *et al.*, "Effect of Matrix-Modulating Enzymes on the Cellular Uptake of Magnetic Nanoparticles and on Magnetic Hyperthermia Treatment of Pancreatic Cancer Models In Vivo," *Nanomaterials*, vol. 11, no. 2, p. 438, Feb. 2021, doi: 10.3390/nano11020438.

[198] K. W. Baumann, J. M. Baust, K. K. Snyder, J. G. Baust, and R. G. Van Buskirk, “Characterization of Pancreatic Cancer Cell Thermal Response to Heat Ablation or Cryoablation,” *Technol Cancer Res Treat*, vol. 16, no. 4, pp. 393–405, Aug. 2017, doi: 10.1177/1533034616655658.
[199] H. Lage, A. Jordan, R. Scholz, and M. Dietel, “Thermosensitivity of multidrug-resistant human gastric and pancreatic carcinoma cells,” *International Journal of Hyperthermia*, vol. 16, no. 4, pp. 291–303, Jan. 2000, doi: 10.1080/02656730050074069.
[200] J. A. Pearce, “Models for thermal damage in tissues: processes and applications,” *Crit Rev Biomed Eng*, vol. 38, no. 1, pp. 1–20, 2010, doi: 10.1615/critrevbiomedeng.v38.i1.20.
[201] D. Tang *et al.*, “Expression of heat shock proteins and heat shock protein messenger ribonucleic acid in human prostate carcinoma in vitro and in tumors in vivo,” *Cell Stress Chaperones*, vol. 10, no. 1, pp. 46–58, 2005, doi: 10.1379/csc-44r.1.
[202] S. Bhowmick, N. E. Hoffmann, and J. C. Bischof, “Thermal Therapy of Prostate Tumor Tissue in the Dorsal Skin Flap Chamber,” *Microvascular Research*, vol. 64, no. 1, pp. 170–173, Jul. 2002, doi: 10.1006/mvre.2002.2408.
[203] J. Cros, J. Raffenne, A. Couvelard, and N. Poté, “Tumor Heterogeneity in Pancreatic Adenocarcinoma,” *PAT*, vol. 85, no. 1–2, pp. 64–71, 2018, doi: 10.1159/000477773.
[204] M. W. Dewhirst, J. R. Oleson, J. Kirkpatrick, and T. W. Secomb, “Accurate Three-Dimensional Thermal Dosimetry and Assessment of Physiologic Response Are Essential for Optimizing Thermoradiotherapy,” *Cancers*, vol. 14, no. 7, Art. no. 7, Jan. 2022, doi: 10.3390/cancers14071701.
[205] J. G. Kiang and G. C. Tsokos, “Heat shock protein 70 kDa: molecular biology, biochemistry, and physiology,” *Pharmacol Ther*, vol. 80, no. 2, pp. 183–201, Nov. 1998, doi: 10.1016/s0163-7258(98)00028-x.
[206] J. Martin, A. L. Horwich, and F. U. Hartl, “Prevention of protein denaturation under heat stress by the chaperonin Hsp60,” *Science*, vol. 258, no. 5084, pp. 995–998, Nov. 1992, doi: 10.1126/science.1359644.
[207] S. Madersbacher, M. Gröbl, G. Kramer, S. Dirnhofer, G. E. Steiner, and M. Marberger, “Regulation of heat shock protein 27 expression of prostatic cells in response to heat treatment,” *The Prostate*, vol. 37, no. 3, pp. 174–181, 1998, doi: 10.1002/(SICI)1097-0045(19981101)37:3<174::AID-PROS6>3.0.CO;2-4.
[208] M. N. Rylander, Y. Feng, J. Bass, and K. R. Diller, “Heat shock protein expression and injury optimization for laser therapy design,” *Lasers in Surgery and Medicine*, vol. 39, no. 9, pp. 731–746, 2007, doi: 10.1002/lsm.20546.
[209] N. b. Gibbons, R. w. g. Watson, R. n. t. Coffey, H. p. Brady, and J. m. Fitzpatrick, “Heat-shock proteins inhibit induction of prostate cancer cell apoptosis,” *The Prostate*, vol. 45, no. 1, pp. 58–65, 2000, doi: 10.1002/1097-0045(20000915)45:1<58::AID-PROS7>3.0.CO;2-#.
[210] Z. Albakova and Y. Mangasarova, “The HSP Immune Network in Cancer,” *Frontiers in Immunology*, vol. 12, 2021, Accessed: Apr. 11, 2023. [Online]. Available: https://www.frontiersin.org/articles/10.3389/fimmu.2021.796493
[211] E. A. Repasky, S. S. Evans, and M. W. Dewhirst, “Temperature Matters! And Why it Should Matter to Tumor Immunologists,” *Cancer Immunol Res*, vol. 1, no. 4, pp. 210–216, Oct. 2013, doi: 10.1158/2326-6066.CIR-13-0118.
[212] A. Adnan, N. M. Muñoz, P. Prakash, P. Habibollahi, E. N. K. Cressman, and R. A. Sheth, “Hyperthermia and Tumor Immunity,” *Cancers (Basel)*, vol. 13, no. 11, p. 2507, May 2021, doi: 10.3390/cancers13112507.
[213] Y. Wang *et al.*, “Genomic sequencing of key genes in mouse pancreatic cancer cells,” *Curr Mol Med*, vol. 12, no. 3, pp. 331–341, Mar. 2012, doi: 10.2174/156652412799218868.

[214] T. H. Corbett *et al.*, "Induction and chemotherapeutic response of two transplantable ductal adenocarcinomas of the pancreas in C57BL/6 mice," *Cancer Res*, vol. 44, no. 2, pp. 717–726, Feb. 1984.
[215] "Heat Shock Protein 70 Expression Patterns in Dermal Explants in Response to Ablative Fractional Phothothermolysis, Microneedle, or Scalpel Wounding," *Wounds*, vol. 23, no. 3, Mar. 2011, Accessed: Apr. 11, 2023. [Online]. Available: https://www.hmpgloballearningnetwork.com/site/wounds/article/heat-shock-protein-70-expression-patterns-dermal-explants-response-ablative-fractional-photh
[216] E. Y. Komarova *et al.*, "Hsp70-containing extracellular vesicles are capable of activating of adaptive immunity in models of mouse melanoma and colon carcinoma," *Sci Rep*, vol. 11, no. 1, Art. no. 1, Oct. 2021, doi: 10.1038/s41598-021-00734-4.
[217] M. Alhajj and A. Farhana, "Enzyme Linked Immunosorbent Assay," in *StatPearls*, Treasure Island (FL): StatPearls Publishing, 2023. Accessed: Apr. 11, 2023. [Online]. Available: http://www.ncbi.nlm.nih.gov/books/NBK555922/
[218] H. Fallahi, D. Clausing, A. Shahzad, M. O'Halloran, M. C. Dennedy, and P. Prakash, "Microwave antennas for thermal ablation of benign adrenal adenomas," *Biomed. Phys. Eng. Express*, vol. 5, no. 2, p. 025044, Feb. 2019, doi: 10.1088/2057-1976/ab068b.
[219] J. Sebek, R. Bortel, and P. Prakash, "Broadband lung dielectric properties over the ablative temperature range: experimental measurements and parametric models," *Med Phys*, vol. 46, no. 10, pp. 4291–4303, Oct. 2019, doi: 10.1002/mp.13704.
[220] H. Fallahi, J. Sebek, and P. Prakash, "Broadband Dielectric Properties of Ex Vivo Bovine Liver Tissue Characterized at Ablative Temperatures," *IEEE Trans Biomed Eng*, vol. 68, no. 1, pp. 90–98, Jan. 2021, doi: 10.1109/TBME.2020.2996825.
[221] M. Matthaiou, S. Koulouridis, and S. Kotsopoulos, "A Novel Dual-Band Implantable Antenna for Pancreas Telemetry Sensor Applications," *Telecom*, vol. 3, no. 1, Art. no. 1, Mar. 2022, doi: 10.3390/telecom3010001.
[222] A. Mohammadi, L. Bianchi, S. Asadi, and P. Saccomandi, "Measurement of Ex Vivo Liver, Brain and Pancreas Thermal Properties as Function of Temperature," *Sensors*, vol. 21, no. 12, Art. no. 12, Jan. 2021, doi: 10.3390/s21124236.
[223] IT'IS Foundation, "Tissue Properties Database V4.0." IT'IS Foundation, 2018. doi: 10.13099/VIP21000-04-0.
[224] D. J. Schutt and D. Haemmerich, "Effects of variation in perfusion rates and of perfusion models in computational models of radio frequency tumor ablation," *Medical Physics*, vol. 35, no. 8, pp. 3462–3470, 2008, doi: 10.1118/1.2948388.
[225] A. Burke *et al.*, "Long-term survival following a single treatment of kidney tumors with multiwalled carbon nanotubes and near-infrared radiation," *Proceedings of the National Academy of Sciences of the United States of America*, vol. 106, no. 31, p. 12897, Aug. 2009, doi: 10.1073/pnas.0905195106.
[226] T. C. Moloney, D. B. Hoban, F. P. Barry, L. Howard, and E. Dowd, "Kinetics of thermally induced heat shock protein 27 and 70 expression by bone marrow-derived mesenchymal stem cells," *Protein Sci*, vol. 21, no. 6, pp. 904–909, Jun. 2012, doi: 10.1002/pro.2077.
[227] D. Ciocca, S. Fuqua, S. Lock-Lim, D. Toft, W. Welch, and W. McGuire, "Response of human breast cancer cells to heat shock and chemotherapeutic drugs.," *Cancer research*, Jul. 1992, Accessed: Apr. 12, 2023. [Online]. Available: https://www.semanticscholar.org/paper/Response-of-human-breast-cancer-cells-to-heat-shock-Ciocca-Fuqua/4de7fba1951fda2c44cd1f1621ce331914a389b0
[228] B. Giri *et al.*, "Hsp70 modulates immune response in pancreatic cancer through dendritic cells," *OncoImmunology*, vol. 10, no. 1, p. 1976952, Jan. 2021, doi: 10.1080/2162402X.2021.1976952.

[229] G. Forika, E. Kiss, G. Petovari, T. Danko, A. B. Gellert, and T. Krenacs, “Modulated Electro-Hyperthermia Supports the Effect of Gemcitabine Both in Sensitive and Resistant Pancreas Adenocarcinoma Cell Lines,” *Pathol Oncol Res*, vol. 27, p. 1610048, Dec. 2021, doi: 10.3389/pore.2021.1610048.
[230] J. T. Beckham *et al.*, “Assessment of cellular response to thermal laser injury through bioluminescence imaging of heat shock protein 70,” *Photochem Photobiol*, vol. 79, no. 1, pp. 76–85, Jan. 2004.
[231] C. E. O’Connell-Rodwell *et al.*, “In vivo analysis of heat-shock-protein-70 induction following pulsed laser irradiation in a transgenic reporter mouse,” *J Biomed Opt*, vol. 13, no. 3, p. 030501, 2008, doi: 10.1117/1.2904665.
[232] Z. Albakova, M. K. S. Siam, P. K. Sacitharan, R. H. Ziganshin, D. Y. Ryazantsev, and A. M. Sapozhnikov, “Extracellular heat shock proteins and cancer: New perspectives,” *Transl Oncol*, vol. 14, no. 2, p. 100995, Dec. 2020, doi: 10.1016/j.tranon.2020.100995.
[233] Y. Li, D. Wang, and X. Li, “The blood cells in NSCLC and the changes after RFA,” *International Journal of Hyperthermia*, vol. 37, pp. 753–762, Jan. 2020, doi: 10.1080/02656736.2020.1782486.
[234] G. Zhou, X. Kan, F. Zhang, H. Ji, J. Sun, and X. Yang, “Interventional Oncolytic Immunotherapy with LTX-315 for Residual Tumor after Incomplete Radiofrequency Ablation of Liver Cancer,” *Cancers (Basel)*, vol. 14, no. 24, p. 6093, Dec. 2022, doi: 10.3390/cancers14246093.
[235] J. Sebek *et al.*, “System for delivering microwave ablation to subcutaneous tumors in small-animals under high-field MRI thermometry guidance,” *International Journal of Hyperthermia*, vol. 39, no. 1, pp. 584–594, Dec. 2022, doi: 10.1080/02656736.2022.2061727.
[236] M. Savage *et al.*, “A computational model of radiofrequency ablation in the stomach, an emerging therapy for gastric dysrhythmias,” in *2021 43rd Annual International Conference of the IEEE Engineering in Medicine & Biology Society (EMBC)*, Nov. 2021, pp. 1495–1498. doi: 10.1109/EMBC46164.2021.9630633.
[237] F. Chamani, “Experiments and computational models to characterize a radiofrequency ablation device for the treatment of rhinitis,” Report, 2019. Accessed: Sep. 08, 2020. [Online]. Available: https://krex.k-state.edu/dspace/handle/2097/40014
[238] M. R. S. Ramu and K. Arunachalam, “Microstrip C patch antenna for hyperthermia treatment: A comparative numerical study with cavity backed C patch antennas,” in *2022 3rd URSI Atlantic and Asia Pacific Radio Science Meeting (AT-AP-RASC)*, May 2022, pp. 1–4. doi: 10.23919/AT-AP-RASC54737.2022.9814180.
[239] E. A. Gelvich and V. N. Mazokhin, “Contact flexible microstrip applicators (CFMA) in a range from microwaves up to short waves,” *IEEE Transactions on Biomedical Engineering*, vol. 49, no. 9, pp. 1015–1023, Sep. 2002, doi: 10.1109/TBME.2002.802053.
[240] M. M. Paulides, J. F. Bakker, N. Chavannes, and G. C. Van Rhoon, “A patch antenna design for application in a phased-array head and neck hyperthermia applicator,” *IEEE Trans Biomed Eng*, vol. 54, no. 11, pp. 2057–2063, Nov. 2007, doi: 10.1109/TBME.2007.895111.
[241] S. Curto, P. McEvoy, Xiulong Bao, and M. J. Ammann, “Compact Patch Antenna for Electromagnetic Interaction With Human Tissue at 434 MHz,” *IEEE Trans. Antennas Propagat.*, vol. 57, no. 9, pp. 2564–2571, Sep. 2009, doi: 10.1109/TAP.2009.2027040.
[242] A. F. Alsager, “Design and Analysis of Microstrip Patch Antenna Arrays”.
[243] I. Gharbi, R. Barrak, M. Menif, and H. Ragad, “Design of patch array antennas for future 5G applications,” in *2017 18th International Conference on Sciences and Techniques of Automatic Control and Computer Engineering (STA)*, Dec. 2017, pp. 674–678. doi: 10.1109/STA.2017.8314954.
[244] S. D. Mendgudle, S. A. Chakraborty, J. Y. Bhanushali, M. Bhatia, and S. B. Umbarkar, “Design and Comparison of Electromagnetically Coupled Patch Antenna Arrays at 30 GHz,” in *Progress in Advanced Computing and Intelligent Engineering*, K. Saeed, N. Chaki, B. Pati, S. Bakshi, and D. P.

Mohapatra, Eds., in Advances in Intelligent Systems and Computing. Singapore: Springer, 2018, pp. 619–628. doi: 10.1007/978-981-10-6875-1_61.

[245] G. Chakaravarthi and K. Arunachalam, “A compact microwave patch applicator for hyperthermia treatment of cancer,” in *2014 36th Annual International Conference of the IEEE Engineering in Medicine and Biology Society*, Aug. 2014, pp. 5320–5322. doi: 10.1109/EMBC.2014.6944827.